Stressed Erythrophagocytosis as a Modifier of the Innate Immune Response to *Klebsiella pneumoniae*

by

Tolani Folajimi Olonisakin

BA, Fisk University, 2012

Submitted to the Graduate Faculty of

the School of Medicine in partial fulfillment

of the requirements for the degree of

Doctor of Philosophy

University of Pittsburgh

2020

UNIVERSITY OF PITTSBURGH

SCHOOL OF MEDICINE

This dissertation was prepared

by

Tolani Folajimi Olonisakin

It was defended on

March 17, 2020

and approved by

Wendy M. Mars, Associate Professor, Department of Pathology

Sally E. Wenzel, Professor, Department of Occupational & Environmental Health

Grant C. Bullock, Assistant Professor, Department of Pathology

Saumendra N. Sarkar, Associate Professor, Department of Microbiology & Molecular Genetics

Dissertation Director: Janet S. Lee, Professor, Department of Medicine

Stressed Erythrophagocytosis as a Modifier of the Innate Immune Response to *Klebsiella pneumoniae*

Tolani Folajimi Olonisakin, PhD

University of Pittsburgh, 2020

Macrophages are main effectors of heme metabolism, increasing transiently in the liver during heightened disposal of damaged or senescent red cells (sRBC). Macrophages are also essential in defense against microbial threats, but pathologic states of heme excess may be immunosuppressive. Here, we uncover a novel mechanism whereby an acute rise in sRBC disposal by macrophages leads to an immunosuppressive phenotype following intrapulmonary *Klebsiella pneumoniae* infection characterized by increased extrapulmonary dissemination and reduced survival in mice. The impaired immunity to *K. pneumoniae* during heightened sRBC disposal is independent of iron acquisition by bacterial siderophores, as *K. pneumoniae* mutant lacking siderophore function recapitulates findings observed with wildtype strain. Rather, we show that sRBC disposal induces a liver transcriptomic profile notable for suppression of *Stat1* and interferon-related responses during *K. pneumoniae* infection. Excess heme handling by macrophages recapitulates STAT1 suppression during infection that requires synergistic NRF1 and NRF2 activation but is independent of heme oxygenase-1 induction. Whereas iron is dispensable, the porphyrin moiety of heme is sufficient to mediate suppression of STAT1-dependent responses in human and mouse macrophages and promote liver dissemination of *K. pneumoniae* in vivo. Thus, dysfunction in cellular heme metabolism negatively regulates the STAT1 pathway with implications in host defense.

Table of Contents

List of Tables

List of Figures

Preface

To my late father, who laid the foundation for the love of learning and who I so desperately wish I could've gotten to know as an adult.

"A New Determination of Molecular Dimensions," a doctoral thesis published in 1905, sought to estimate Avogadro's number. Measurements by Jean Baptiste Perrin four years later determined the estimation to be markedly inaccurate[1], by a factor of nearly three. The author of the mistaken dissertation? Albert Einstein, Ph.D. Of course, a correction to the thesis was published in 1911, and Dr. Einstein went on to transform our world of physics and the philosophy of science. The point is, while this has been quite an undertaking for me and I'm oh so glad that it's coming to a close, this is the *beginning* of a lifetime of discoveries—and for that, I am stoked!

If I could choose again, I'd still choose Dr. Janet Lee as my dissertation advisor. Dr. Lee is an incredibly thorough scientist with a million and one creative ideas—the variety of projects that I have undertaken under her tutelage is proof of this. It has been a privilege to train under Dr. Lee and I have grown so much as a scientist and have become somewhat confident of my own capabilities as a critical thinker, all thanks to her! While Dr. Lee is an exceptional scientist, she is an even better person and her relationships with me and other members of our laboratory are exemplary. To said members of the laboratory: *Will*, thank you so much for allowing me to use your office to write my dissertation; *Ms. Mei*, thank you for saying "yes" to every crazy experimental mouse work; *Dr. Z*, nearly half of this dissertation is as a result of your hard work;

[1] Norbert Straumann. "On Einstein's Doctoral Thesis." Talk given at the joint colloquium of ETH and the University of Zürich, 27 April 2005.

Tomeka, thank you for reassuring me that there's a light at the end of this tunnel and for nominating me for "Rising Stars"; *Lauren*, thank you for always inviting me to hang out and giving me a little bit of a social life; *Rick*, thank you for your contributions to this project, my fellow PhD comrade; *Hernan*, thank you for our debates filled with friendly fire and an endless supply of almonds; *Jill*, thank you for filling me in on what to expect on the wards.

I am greatly indebted to my mother, without whom I'd be in debt, literally—she singlehandedly funded my first two years of medical school, which, considering the exchange rate, is no small feat. I have watched you crush barriers in your career, so I have no excuses for mine. I cannot assure you that your investments will pay off (sorry, haha), but I will try. I promise. To my siblings, *Ibitoye* and *Opeyemi*, thank you for being an unwavering source of support for nearly all my life! To my dear friends—*Sarah*, *Tracy*, *Rukky*, *Sola*, *the "Microsoft crew*," *the "Fisk-Pittsburgh transplants*," *Mariam*, *Shahin*—thank you for bolstering my sanity, for all of the laughter and fun trips (even those yet to come!). To *Ray*, thank you for making my life richer in every way possible. Your doggedness, your desire to know what is true, and your resolution to live by the truth are nothing short of inspirational.

1.0 Introduction

1.1 Erythrocyte disposal under homeostasis

Approximately 2 x 10^{11} red blood cells (RBC) are synthesized each day in the healthy adult human[1–3]. Physiologic senescence—characterized by loss of surface sialic acid[4], externalization of phosphatidylserine[5], band 3 clustering with subsequent antibody and complement binding[6,7], and reduced flexibility[4]—results in RBC trapping in the cords of Billroth in splenic red pulp[8] at about 120 days post-synthesis. A distinct set of *Spic*-expressing macrophages[9] found in the splenic red pulp (red pulp macrophages, RPM) recognize and ingest senescent RBC via Fcγ receptor-mediated and scavenger receptor-mediated phagocytosis[10]. Hydrolysis of RBC in the phagolysosome of RPM liberates heme, which is further catabolized into biliverdin, carbon monoxide, and ferrous iron[8]. Iron is then either stored intracellularly by ferritin[11] or excreted from the macrophage via the transmembrane receptor ferroportin-1 (FPN1)[12]. Plasma iron content is sensed by hepatocytes, which synthesize transferrin and hepcidin—the former binds ferric iron in the circulation to minimize free ionic iron and distribute bound iron[10] and the latter restrains macrophage iron efflux via FPN1 degradation[13,14]. Because dietary nonheme-iron is poorly absorbed[15], the vast majority of iron required for erythropoiesis is obtained from recycling of iron following ingestion of damaged or senescent RBC (sRBC) by the mononuclear phagocyte system within the bone marrow, liver, and spleen[3,10]. This recycling of heme-iron from sRBC is tightly regulated in the healthy individual as perturbations in heme-iron recycling efficiency can yield free labile heme or non-transferrin bound iron[16] that is potentially toxic to host tissue[17] and can also be a source of nutrition for opportunistic extracellular pathogens[18]. Though RBC recycling also occurs in the

healthy liver, it is thought that the spleen is the predominant organ tasked with eliminating senescent RBC in steady state[10].

1.2 Stressed erythrophagocytosis

Heightened RBC disposal, herein termed *stressed erythrophagocytosis*, occurs as a consequence of several pathologies—including sepsis, inherited and acquired defects in RBC stability[19,20]—and interventions such as transfusion of storage-damaged RBC[10,19]. In sepsis, there is marked reduction in the sialic acid content of the RBC membrane[21] and decreased RBC flexibility[22], akin to the senescent RBC. Ineffective erythropoiesis in the hemoglobinopathies results in rigid, damaged RBC that precipitates mononuclear phagocytic uptake well before the physiologic 120-day lifespan[23,24]. And multiple, frequent transfusions of RBC damaged by extended storage results in an acute increase in delivery of aged, damaged RBC to mononuclear phagocytes for disposal and a resultant rise in iron recycling[25]. Stressed erythrophagocytosis in these aforementioned pathologies overwhelms physiologic RBC removal by RPM and Kupffer cells in the liver, and may result in an oxidative, iron-dependent cell death known as ferroptosis[26]. In response to RBC damage requiring on-demand RBC disposal and restoration of iron homeostasis, mammals have evolved mechanisms to adapt to fluctuations in RBC integrity[19]. Ly-6C^{high} monocytes are shuttled to the liver and spleen in response to CCL2 and CCL3, and differentiate into iron-recycling Tim-4^{neg}FPN1^{+} macrophages in the liver—but not the spleen—in a CSF1 and NRF2-dependent manner[19]. While this transient on-demand mechanism restores iron homeostasis and prevents organ damage[19], the impact of this adaptive responsive to increased circulating damaged RBC during ongoing bacterial infection remains poorly defined.

1.3 *Klebsiella pneumoniae*

In the late 19th century, German pathologist and microbiologist, Carl Friedländer, identified a Gram-negative encapsulated bacillus as the causative agent of pneumonia in deceased patients[27,28]. Originally called Friedländer's bacillus, *Klebsiella pneumoniae* became quickly recognized as an important cause of acute lower respiratory tract infections and sepsis worldwide[29,30]. Though *K. pneumoniae* is an opportunistic bacterial pathogen that often colonizes mucosal surfaces of the oropharynx and gastrointestinal tracts[31,32], a diagnosis of Klebsiella pneumonia typically portends a grim prognosis in the critically ill, with mortality rates approaching 50%[27]. The rise in multidrug-resistant, carbapenemase-producing strains of *K. pneumoniae* has further compounded the severity of Klebsiella infections globally[33] and is often associated with increased costs, prolonged hospitalization, and significant morbidity and mortality[34]. With the lack of effective antimicrobial therapies, a robust innate host defense is essential for containment of *K. pneumoniae* infection and prompts the question of whether acquired host factors or modifiers can enhance the pathogenicity of opportunistic *K. pneumoniae*.

1.3.1 Virulence mechanisms of *K. pneumoniae*

Perhaps its most important virulence factor, *K. pneumoniae* expresses a double-layered polysaccharide capsule (Fig. 1) that enables its ability to evade phagocytosis[35], escape complement-mediated killing[36] and enhance pathogenicity in both mice and men[37–39]. To date, a total of 79 different capsular serotypes of *K. pneumoniae* have been identified[40]. Interestingly, the abundance of mannose-α-2/3-mannose or rhamnose-α-2/3-rhamnose sequences within the polysaccharide capsule appears to correlate with virulence of the pathogen[32]. Well-described

virulent strains such as *K. pneumoniae* serotype K2 do not express any mannose sugars in their capsules and are lethal in mice[41] whereas less virulent strains such as *K. pneumoniae* serotype K21a contain repetitive mannose structures in their capsules and are rapidly cleared from circulation in infected mice[42].

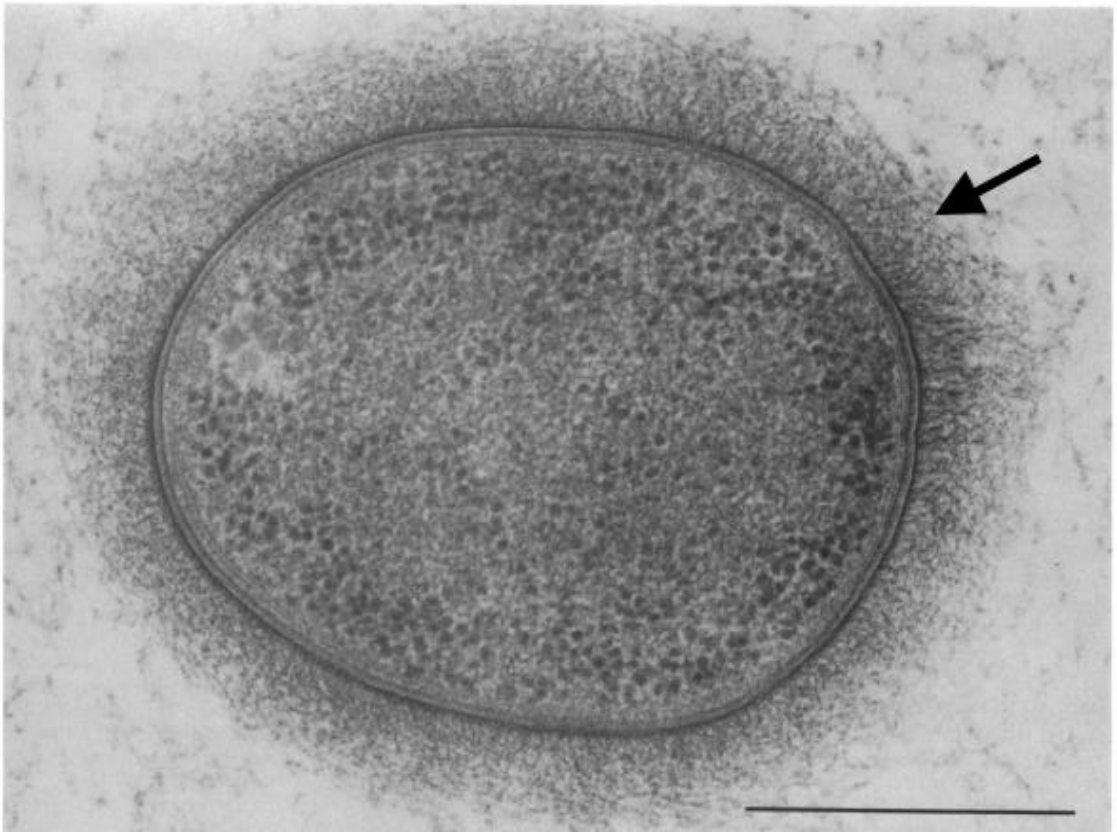

Figure 1: Electron micrograph of *K. pneumoniae*.

Arrow indicates thick double-layered capsule consisting of fibrillous structures. Capsular structure is approximately 160 nm wide. Scale bar = 0.5 μm. Reprinted from Amako K et al. *J Bacteriol* 1988 with permission under Creative Commons Attribution 4.0 International License.

As a Gram-negative bacterial pathogen, *K. pneumoniae* expresses lipopolysaccharide (LPS) that consists of three structural domains; (1) an immune-activating lipid A domain, (2) a core oligosaccharide, and (3) an outermost polysaccharide O side chain (O antigen)[43]. Though the overall structure of the hydrophobic lipid A domain is highly conserved among Gram-negative bacteria, modifications in extracytoplasmic enzymatic biosynthesis can yield lipid A that varies from organism to organism, sometimes even within the same species[44]. Indeed, *K. pneumoniae*

has been shown to remodel its lipid A in vivo in response to environmental cues, thus counteracting innate immune defenses and promoting pathogenesis in mice[45]. On the other hand, the O antigen of *K. pneumoniae* shows limited serotype diversity, with majority of clinical isolates belonging to one of four serogroups—O1, O2, O3, and O5[46]—highlighting the potential of O antigens as targets for vaccine design[46,47]. Though Regué M et al. suggest that a second type of core oligosaccharide contributes to virulence in *K. pneumoniae*[48], it remains unclear whether or not the core oligosaccharide directly modulates virulent gene or protein expression in *K. pneumoniae* and there do not appear to be any associations between core oligosaccharide expression and disease outcomes with *K. pneumoniae* infection[47].

Iron is an essential growth factor for nearly all forms of life[49,50]. The bulk of iron in the mammalian host exists complexed to hemoglobin, myoglobin, and ferritin, hence diminishing free iron available to bacterial pathogens in the host milieu. To circumvent this and like several *Enterobacteriaceae*, *K. pneumoniae* scavenges iron from its host by secreting siderophores—low-molecular weight, high-affinity iron-chelating compounds[32]. Indeed, siderophores such as enterobactin (Ent) exhibit higher affinity for ferric iron (Fe^{3+}) than transferrin and lactoferrin and can theoretically outcompete host-iron binding proteins[51]. Other siderophore systems employed by *K. pneumoniae* include glycosylated-enterobactin (also known as Salmochelin, gly-Ent) and yersiniabactin (Ybt)[52,53]. Unlike Ent, gly-Ent and Ybt are resistant to capture by lipocalin 2 (Lcn2, also referred to as neutrophil gelatinase-associated lipocalin (NGAL), siderochelin or 24p3), an innate host defense protein that prevents pathogen ability to acquire iron from host environment[54]. Thus, *K. pneumoniae* strains expressing gly-Ent and Ybt are able to cause disease even in sites where Lcn2 is prevalent[53].

1.3.2 Innate immune response to *K. pneumoniae*

Mechanical defenses such as mucociliary clearance in the respiratory tract or urine flow in the genitourinary tract are often the first barriers that opportunistic pathogens like *K. pneumoniae* encounter in the host[55]. Once these barriers have been breached, however, tissue-resident macrophages are essential for the recognition, ingestion, and destruction of invading pathogens. Pathogen-associated molecular patterns (PAMPs) such as lipoprotein/LPS and capsular polysaccharide expressed by *K. pneumoniae* are recognized by innate pattern recognition receptors (PRRs) on macrophages, such as toll-like receptors (TLRs) and lectin receptors, respectively[56]. Mannose/*N*-acetylglucosamine-specific lectin receptors expressed by macrophages recognize repeating mannose sequences found on some *K. pneumoniae* capsular strains, resulting in direct non-opsonic bacterial internalization in a process termed lectinophagocytosis[57], and may account for the divergence in virulence among capsular serotypes[42,57]. TLR4 sensing of LPS, together with myeloid differentiation factor 2 (MD2), recruits toll/IL-1R homology (TIR) domain-containing adaptors, activates a distinct set of transcription factors—including NF-κB, activator protein 1 (AP-1), interferon regulatory factors (IRFs), CCAAT/enhancer-binding protein β (C/EBPβ)— and ultimately results in transcriptional upregulation of hundreds of genes in macrophages[56]. While TLR4-mediated microbial recognition and signaling are crucial for optimal host defense[56], macrophages appear to show no defects in phagocytosis of pathogenic Gram-negative bacteria in the absence of TLR4[58,59], suggesting that bacterial recognition and bacterial internalization are not necessarily coupled events in the macrophage.

Chemical defenses such as collectins, antimicrobial peptides/proteins, and the complement system are another important arm of innate defense against *K. pneumoniae*[55]. Collectins are a

family of humoral collagenous calcium-dependent defense lectins that recognize PAMPs[60]. They include mannan-binding lectin (MBL), secreted by hepatocytes, and surfactant proteins A & D, secreted primarily by alveolar type II cells and non-ciliated bronchial epithelial cells[60,61]. Collectins act as opsonins and enhance phagocytosis of microbial pathogens. They also induce agglutination of bacteria, due to formation of bridges between carbohydrate ligands on pathogen surfaces, that may enhance mucociliary clearance by the respiratory tract[60,61]. Antimicrobial peptides and proteins such as defensins and serine proteases are found primarily in the granules of Paneth cells and polymorphonuclear cells, respectively[62]. Fusion of defensin/serine protease-rich primary granules with phagocytic vacuoles containing bacteria results in permeabilization of bacterial cell membrane and bacterial cell death. Indeed, we have shown that enhanced catalytic activity of neutrophil serine proteases, neutrophil elastase and cathepsin G, limits bacterial dissemination and enhances murine survival following intrapulmonary infection with *K. pneumoniae*[63].

Lastly, complement activation involves a series of cleavage reactions that culminate in formation of enzymatic C3 convertase activity, deposition of C3b fragments on pathogen surface, generation of C5 convertase activity, and assembly of the membrane-attack complex that destroys bacterial cell membrane[64]. The deposition of C3b on *K. pneumoniae* is dependent on capsular thickness and we and others have shown that multi-drug resistant *K. pneumoniae* strains that colonize and infect hospitalized patients express predominantly non-K1, K2 capsular antigens (non-hypermucoviscous phenotypes) and are susceptible to complement-mediated killing in the healthy host[37,65]. Paradoxically, these relatively avirulent strains often cause mortality in critically ill patients—suggesting that while targeting the infectious agent has traditionally been a successful

strategy in combating infection, alternative approaches that boost/enhance the host immune response to infection may be paramount in this era of antimicrobial resistance.

1.4 Macrophages and heme-iron metabolism in immunity

At least 80% of the adult human's total iron supply is contained in the RBC[66]. While other mammalian cells acquire iron predominantly in the form of diferric transferrin, macrophages are the primary cells that recognize and phagocytose sRBC to extract heme and eventually iron[1]. Hence, macrophages function as central regulators of heme-iron homeostasis in the mammal[67]. As iron is an essential growth factor for most pathogens, the host employs several mechanisms to limit iron availability to pathogenic organisms through macrophage retention of heme-associated iron and non-heme-associated iron[68]. Pathogen sensing via PRR stimulates IL-6 secretion that subsequently induces synthesis of the iron regulatory hormone, hepcidin[69], through Janus kinase 2 (JAK2)/ Signal Transducer and Activator of Transcription 3 (STAT3) activation[70,71]. Hepcidin binds directly to FPN1 (also known as solute carrier family 40, subfamily A1, SLC40A1), causing internalization and lysosomal degradation of FPN1/SLC40A1, and resulting in ablation of cellular iron export[72]. Furthermore, infected macrophages secrete the antimicrobial peptide, Lcn2, that captures iron-laden bacterial siderophores and subverts pathogen iron acquisition[73]. Intracellularly, natural resistance-associated macrophage protein 1 (NRAMP1, also known as solute carrier family 11 subfamily A1, SLC11A1) restricts microbial access to iron[74]. All of these mechanisms exerted by and on the macrophage work in concert to decrease plasma iron levels within hours after the onset of an infection (Fig. 2)[75].

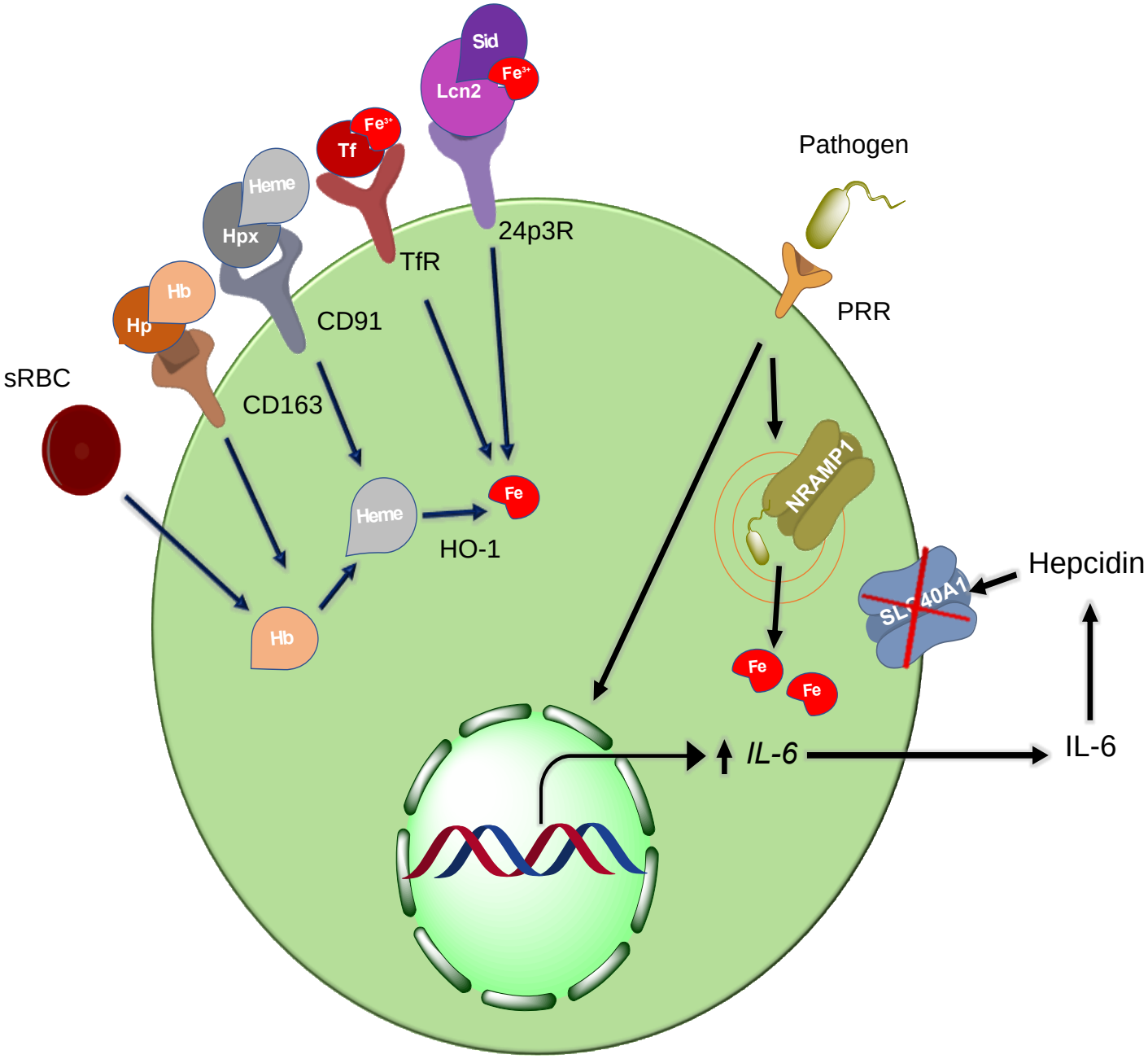

Figure 2: Macrophages and heme-iron metabolism in immunity.

Multiple pathways for macrophage iron uptake: (1) Erythrophagocytosis of damaged/senescent RBC (sRBC) yields hemoglobin (Hb) that is degraded to heme. Heme is catabolized by heme-oxygenase 1 (HO-1) to yield iron (Fe), biliverdin and carbon monoxide (not shown); (2) Haptoglobin (Hp)-Hb complexes are taken up by the CD163

receptor; (3) Hemopexin (Hpx)-Heme complexes are taken up by the CD91 receptor; (3) Transferrin receptor (TfR) recognizes transferrin (Tf)-bound ferric iron (Fe^{3+}); (4) Lipocalin 2 (Lcn2) captures iron-laden bacterial siderophore and is taken up by the Lcn2 receptor (24p3R). Natural resistance-associated macrophage protein 1 (NRAMP1) restricts iron availability to pathogens within the phagolysosome. Pathogen sensing via pattern recognition receptors (PRR) stimulates IL-6 secretion that subsequently induces synthesis of hepcidin (from hepatocytes, not shown). Hepcidin binds to ferroportin-1 (SLC40A1) resulting in SLC40A1 lysosomal degradation and ablation of cellular iron export.

In healthy adults, cell-free unbound hemoglobin and heme are virtually undetectable in plasma[76], as they are typically found bound to haptoglobin and hemopexin, respectively. Excess hemoglobin or heme resulting from saturation of haptoglobin, hemopexin, or inundated mononuclear phagocytic capacity has been shown to alter the course of bacterial infection[77,78]. Though iron acquisition from host hemoglobin/heme has been regarded as an important mechanism of enhanced pathogenicity in severe infection, growing evidence suggests that hemoglobin and heme have immunomodulatory properties beyond mere bacterial iron provision. Hemoglobin has been shown to form complexes with LPS leading to probable enhanced biological activity of LPS and amplification of the inflammatory response[79,80]. Heme has been shown to both amplify the innate immune response to microbial stimuli[81,82] and elicit anti-inflammatory responses during bacterial infection[83]. It is worth noting that experimental findings depicting heme's potent proinflammatory capacity in macrophages are observed only in protein-free culture media[82] and that these findings are not readily observed in protein-replete culture media or in the whole organism[84]. Thus, the precise mechanisms underlying distinct host-pathogen interplay in states of heme and iron excess remain poorly understood and necessitates extensive investigation.

2.0 Stressed erythrophagocytosis impairs host defense to *Klebsiella pneumoniae*

2.1 Rationale

Whereas healthy, freshly isolated RBC (denoted young RBC, yRBC) persist in circulation for at least 24 h in mice, RBC damaged by extended storage (denoted stressed RBC, sRBC) are rapidly cleared from circulation as early as 2 h post-transfusion (Fig. 3).

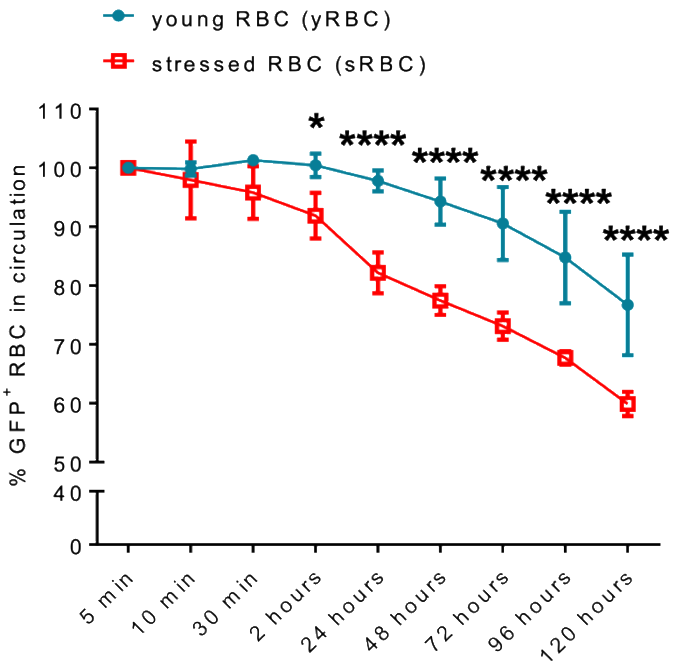

Figure 3: Kinetics of sRBC disposal.

Freshly isolated, young GFP$^+$ RBC (yRBC) or stressed GFP$^+$ RBC (sRBC) were transfused into C57BL/6 mice. The ratio of GFP$^+$ cells at 5 min was set as 100% and all time points were normalized to 5 min. Data is presented as mean ± SEM, n = 4 mice per group. *p<0.05, ****p<0.0001 by two-way ANOVA with Sidak's multiple comparisons test.

The precipitous decline in sRBC post-transfusion survival is distinct from spontaneous RBC lysis (intravascular hemolysis), as deletion of a single scavenger receptor implicated in sRBC uptake, macrophage scavenger receptor 1 (MSR1)[19], leads to a significant reversal in sRBC disposal (Fig. 4)—emphasizing the role of the mononuclear phagocyte system in sRBC clearance. While erythrophagocytosis under homeostatic conditions is largely an immunologically silent event, enhanced sRBC delivery to the macrophage during infection provides a competing stressor that may alter integration of signals when the macrophage is also tasked to sense, elaborate mediators, engulf, and destroy invading pathogens. How the macrophage is able to process competing signals, respond and prioritize function is largely unknown.

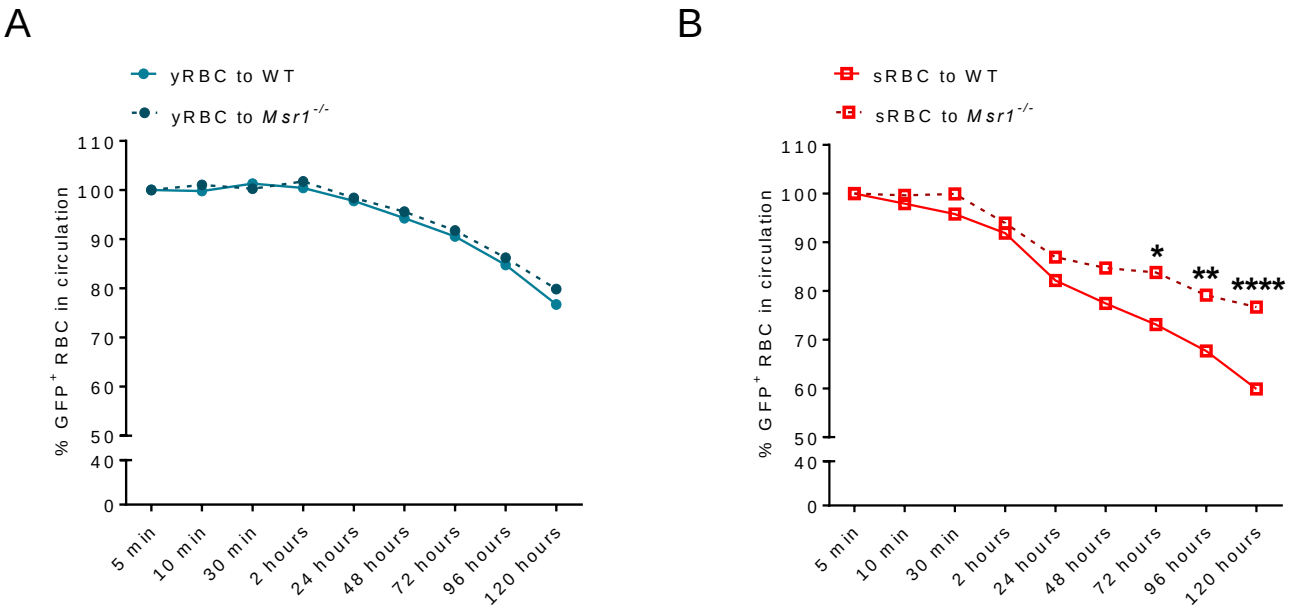

Figure 4: sRBC persist in circulation in *Msr1*$^{-/-}$ mice.

(A) yRBC or (B) sRBC were transfused into C57BL/6 or *Msr1*$^{-/-}$ recipient mice. The ratio of GFP^{+} cells at 5 min was set as 100% and all time points were normalized to 5 min. Data is presented as mean, n = 4 mice per group. *p<0.05, **p<0.01, ****p<0.0001 by two-way ANOVA with Sidak's multiple comparisons test.

2.2 Results

2.2.1 Stressed erythrophagocytosis enhances bacterial dissemination and worsens survival following *K. pneumoniae* intrapulmonary infection.

To examine the effect of sRBC disposal on host outcome during acute bacterial infection in vivo, mice initially underwent intratracheal inoculation with *K. pneumoniae* and were challenged 1 h later with 200 µL of yRBC or sRBC. This volume approximates one packed red blood cell unit in humans[25]. Mice challenged with sRBC following acute intrapulmonary *K. pneumoniae* infection showed increased mortality compared to mice challenged with yRBC from the same pool of donor mice blood (Fig. 5A). The median survival following *K. pneumoniae* infection was 9.5 days for the yRBC-challenged group and 2.5 days for the sRBC-challenged group over a 2-week observational period (Log-rank Mantel-Cox test, p=0.005).

To determine whether increased mortality observed in mice challenged with sRBC is due to impaired host defense, we evaluated lung bacterial burden and extrapulmonary dissemination. As the initial mortality was observed by 48 h, we examined mice prior to this time point to minimize survivor bias. Although mice challenged with sRBC showed increased bacterial burden in the lungs compared with mice challenged with yRBC at 4 h, the lung bacterial burden by 24 h was comparable in both groups (Fig. 5B). In contrast, mice challenged with sRBC showed increased splenic dissemination by 4 and 24 h (Fig. 5C). Consistent with the spleen data, liver and blood colony-forming units (CFU) burden were increased at 24 h (Fig. 5D-E). Thus, in a *K. pneumoniae* model of acute bacterial pneumonia, sRBC disposal impairs the ability of mice to control pathogen replication following breach of the lung mucosal barrier, resulting in enhanced extrapulmonary dissemination and worsened survival.

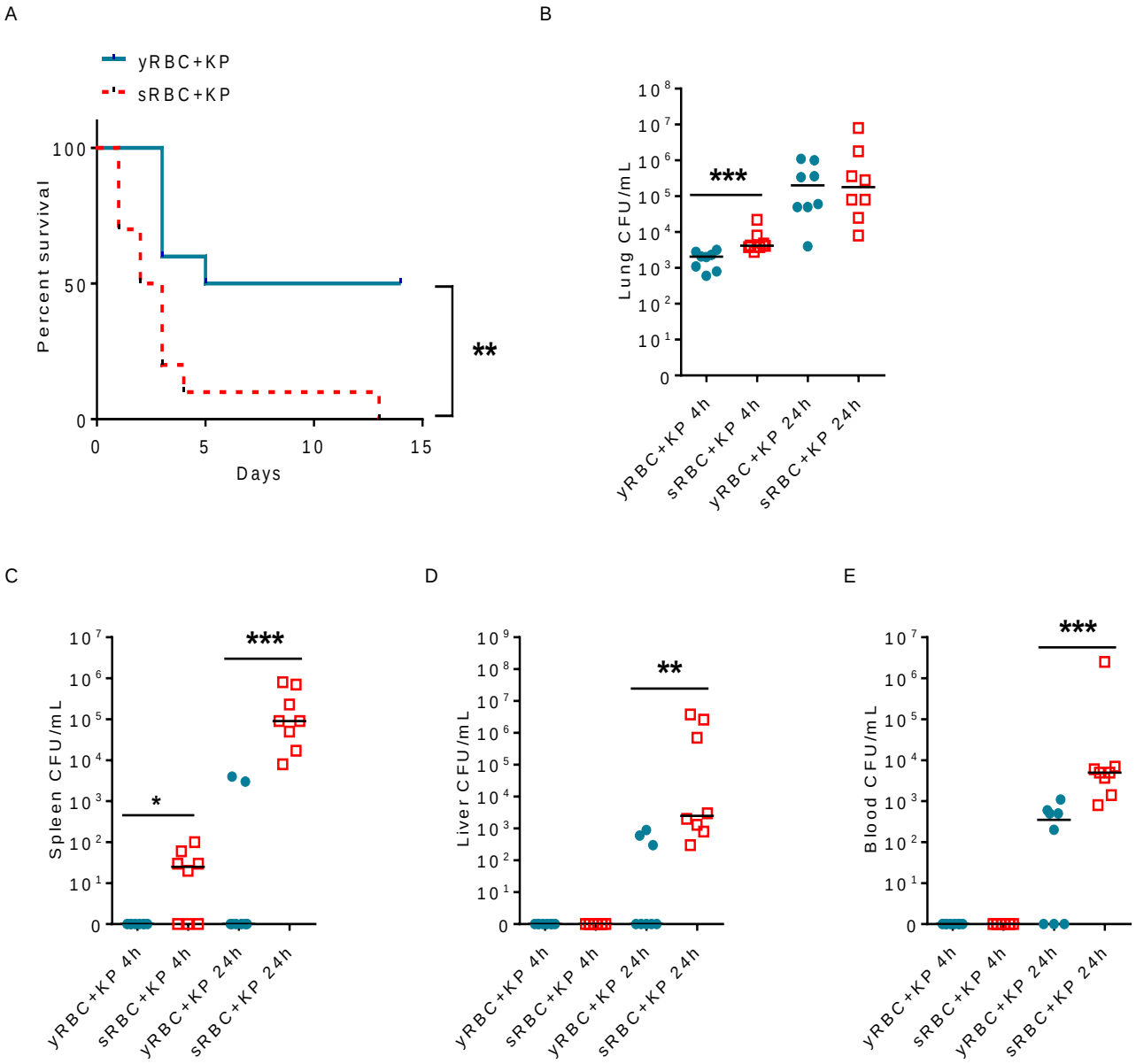

Figure 5: Stressed erythrophagocytosis enhances bacterial dissemination and worsens survival following *K. pneumoniae* intrapulmonary infection.

(A) *K. pneumoniae* was instilled intratracheally into C57BL/6 mice and followed by challenge with yRBC or sRBC. n=10 mice per group, Log-rank test **p=0.005. (B) Lung bacterial burden was estimated by colony forming units (CFU) count/mL of tissue homogenates. (C) Spleen CFU/mL, (D) Liver CFU/mL, (E) Blood CFU/mL. (C-E) Each point indicates individual mice, n=7-8 mice/group, line indicates the median. *p<0.05, **p<0.01, ***p<0.001 by Mann-Whitney U two-tailed test.

2.2.2 Stressed erythrophagocytosis heightens systemic inflammatory response to *K. pneumoniae* intrapulmonary infection.

Inability to control bacterial replication and extrapulmonary dissemination can be accompanied by a robust systemic inflammatory response. Conversely, systemic immunoparalysis may underlie the profound extrapulmonary *K. pneumoniae* dissemination observed with stressed erythrophagocytosis. Therefore, to delineate the systemic inflammatory response following sRBC delivery, we measured plasma cytokines at 4 h and 24 h in mice challenged with yRBC or sRBC during acute bacterial pneumonia. Mice challenged with sRBC showed elevated plasma inflammatory cytokine production of C5a, CXCL10, IFNγ, IL-1β, IL-6, IL-10, and acute-phase protein, mannose binding lectin (MBL2) at 4 h (Fig. 6A–G). Plasma CXCL10, IL-10, and TNFα remained elevated in infected mice challenged with sRBC at 24 h compared to mice challenged with yRBC (Fig. 6B, F, H). Collectively, these findings indicate that during *K. pneumoniae* intrapulmonary infection, heightened disposal of sRBC results in a dysregulated hyperinflammatory sepsis phenotype.

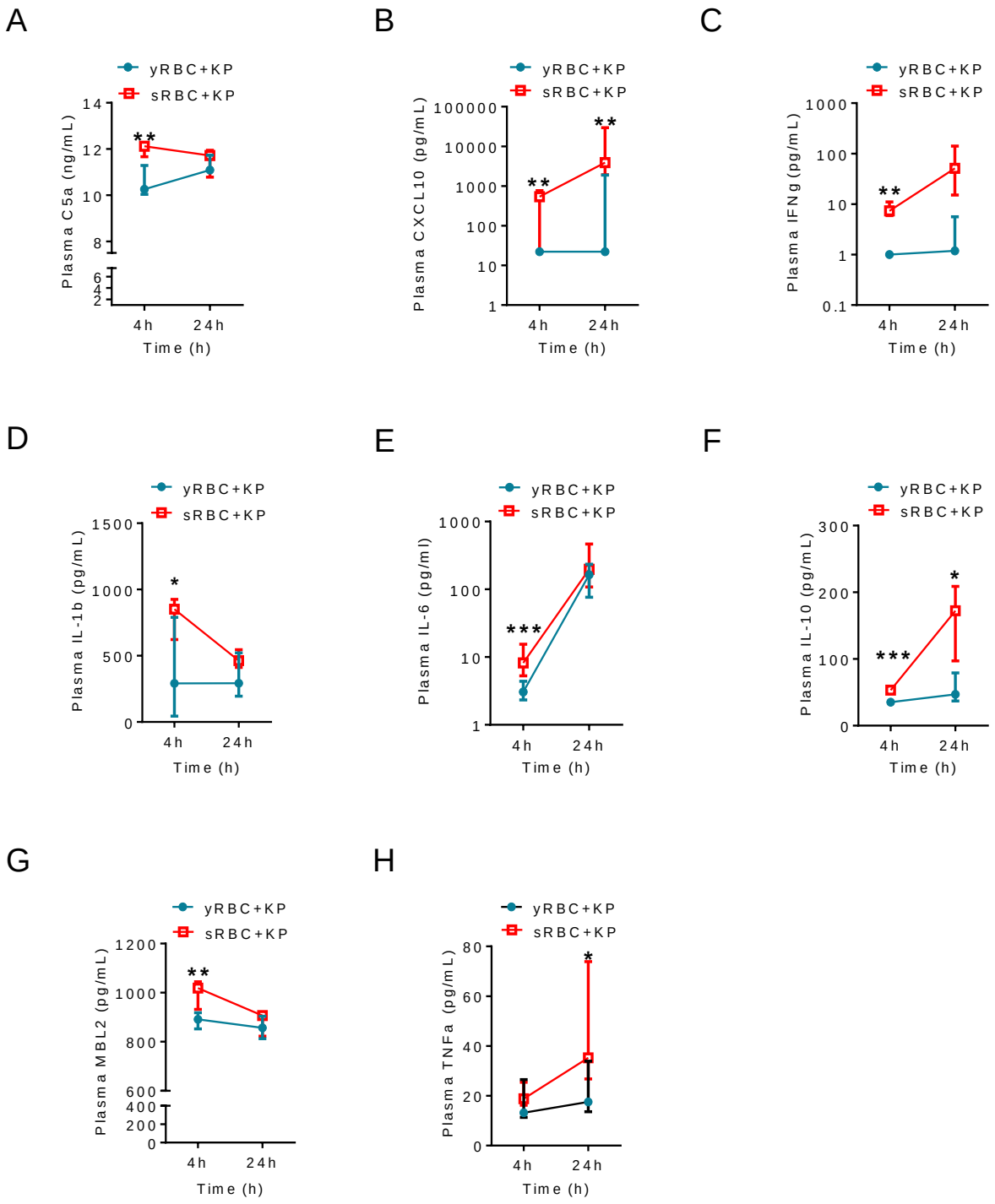

Figure 6: Stressed erythrophagocytosis heightens systemic inflammatory response to *K. pneumoniae* intrapulmonary infection.

K. pneumoniae was instilled intratracheally into C57BL/6 mice followed by challenge with either yRBC or sRBC. Mice were euthanized at pre-determined specified time points as indicated. Mouse plasma cytokines were measured

by ELISA. (A) C5a, (B) CXCL10, (C) IFNγ, (D) IL-1β, (E) IL-6, (F) IL-10, (G) MBL2, and (H) TNFα. Each point indicates median with error bars, n=4-8 mice/group. *p<0.05, **p<0.01, ***p<0.001 by Mann-Whitney U two-tailed test.

2.2.3 Inflammatory response in the lungs is relatively unperturbed with stressed erythrophagocytosis during *K. pneumoniae* intrapulmonary infection.

As the lungs were the initial site of infection, we evaluated the lung inflammatory response following yRBC or sRBC challenge in *K. pneumoniae*-infected mice. We observed no differences in total airspace leukocyte numbers in the bronchoalveolar lavage (BAL) fluid, total BAL neutrophils or total BAL mononuclear cell counts obtained at 4 h from infected mice challenged with yRBC or sRBC (Fig. 7A-C). At 24 h post-*K. pneumoniae* infection, total BAL leukocyte cell counts were decreased in mice challenged with sRBC (Fig. 7A), with a more marked reduction in mononuclear cell recruitment (Fig. 7C) compared to neutrophil recruitment to the airspaces (Fig. 7B). Though leukocyte recruitment to the airspaces appeared to be inhibited with sRBC disposal during *K. pneumoniae* infection at 24 h, cytokine responses in the entire lungs were not altered with sRBC challenge as no differences in production of C5a, IFNγ, IL-1β, IL-6, IL-10, and TNFα were observed between the two mouse groups (Fig. 7D-I). These findings are in contrast to the exuberant systemic inflammatory response observed with sRBC disposal and suggest a modest effect in the lungs following sRBC delivery.

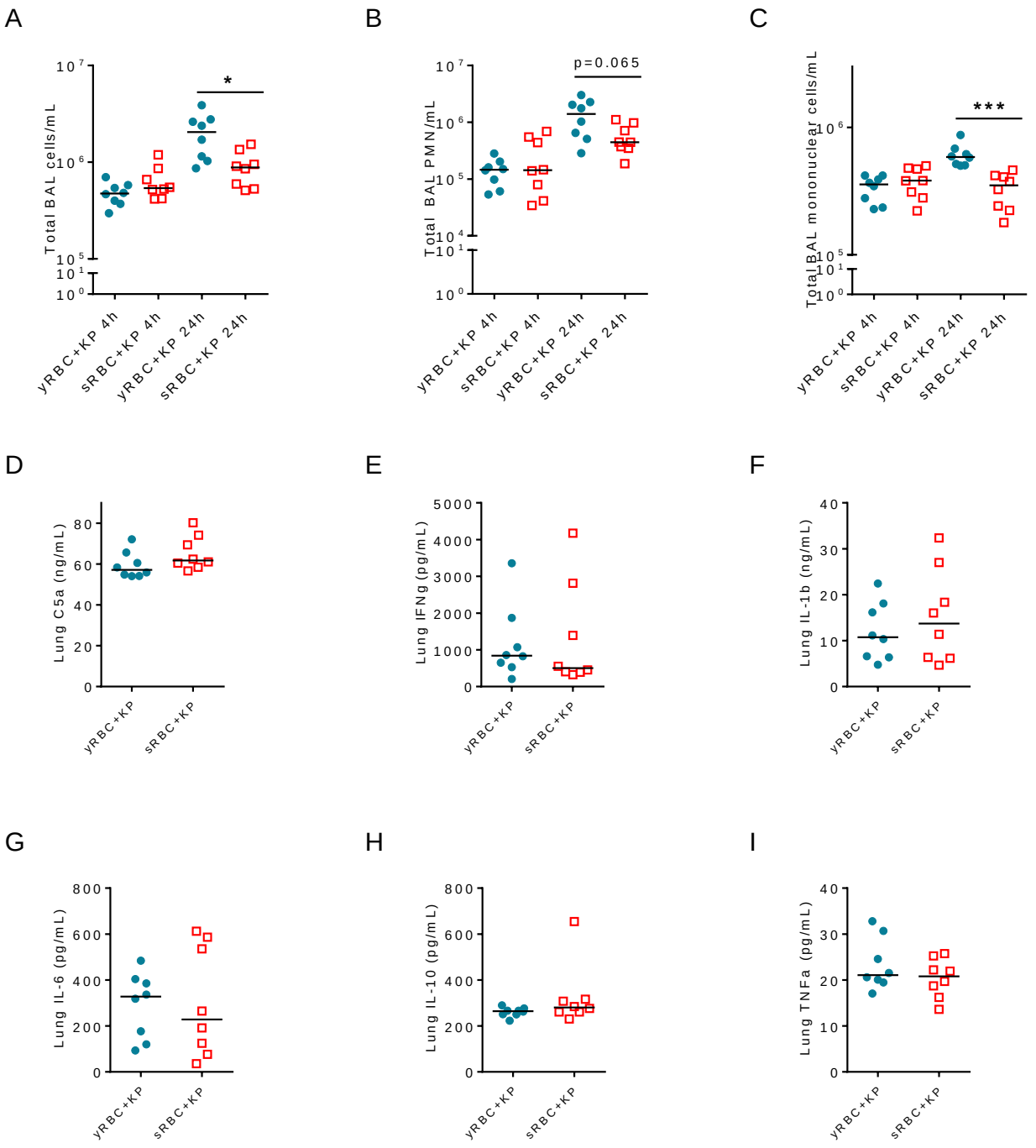

Figure 7: Inflammatory response in the lungs is relatively unperturbed with stressed erythrophagocytosis during *K. pneumoniae* intrapulmonary infection.

K. pneumoniae was instilled intratracheally into C57BL/6 mice followed by challenge with either yRBC or sRBC. Mice were euthanized at pre-determined specified time points as indicated. (A) Total BAL cell count/mL, (B) Total BAL PMN count/mL and (C) Total BAL mononuclear cell count/mL. n=7-8 mice/group, line indicates the median.

**p<0.01, ***p<0.001 by Mann-Whitney U two-tailed test. (D-I) Cytokines in the lung were measured by ELISA at 24 h post-infection and normalized to 50 μg of total protein. (D) C5a, (E) IFNγ, (F) IL-1β, (G) IL-6, (H) IL-10, and (I) TNFα. Each point indicates individual mice. Line indicates median, n=8 mice per group. *p<0.05, ***p<0.001 by Mann-Whitney U two-tailed test.

2.2.4 Enhanced bacterial dissemination observed with stressed erythrophagocytosis is independent of iron acquisition by bacterial siderophores.

sRBC challenge enhances plasma transferrin-bound iron when compared with mice challenged with yRBC or untreated mice by electron paramagnetic resonance spectroscopy (Fig. 8A). Others have also reported a rise in non-transferrin bound iron following challenge with damaged RBC in humans[16] and mice[25]. As *K. pneumoniae* utilizes siderophores enterobactin (Ent), glycosylated enterobactin (gly-Ent), and yersiniabactin (Ybt) as virulence mechanisms to scavenge iron in iron-restricted environments such as the lung, we utilized *entB ybtS* isogenic *K. pneumoniae* mutant lacking ability to produce all three siderophores Ent, gly-Ent, and Ybt to assess whether sRBC delivery enhances the pathogenicity of this *K. pneumoniae* isolate. We show in vitro growth of *entB ybtS K. pneumoniae* mutant is similar when compared to wild-type parent strain (Fig. 8B). However, in the absence of these siderophores, *entB ybtS K. pneumoniae* mutant exhibits poor growth in iron-rich plasma obtained from mice challenged with sRBC when compared to parent strain (Fig. 8C). In addition, *entB ybtS K. pneumoniae* mutant shows reduced bacterial burden in the lung when compared to wild-type *K. pneumoniae*[52] (Fig. 8D) and shows reduced dissemination to the spleen, liver, and blood compartments (Fig. 8E-G). Following challenge with sRBC, mice infected with *entB ybtS K. pneumoniae* mutant showed no difference in lung bacterial burden when

compared with mice challenged with either vehicle (PBS) or yRBC (Fig. 8H). However, challenge with sRBC resulted in enhanced extrapulmonary dissemination of the less virulent *entB ybtS K. pneumoniae* mutant (Fig. 8I-K). Collectively, these findings suggest that, while bacterial siderophores are key virulence factors that enhance microbial dissemination within the host, sRBC delivery enhances *K. pneumoniae* dissemination through an alternative mechanism that is independent of pathogen siderophore function.

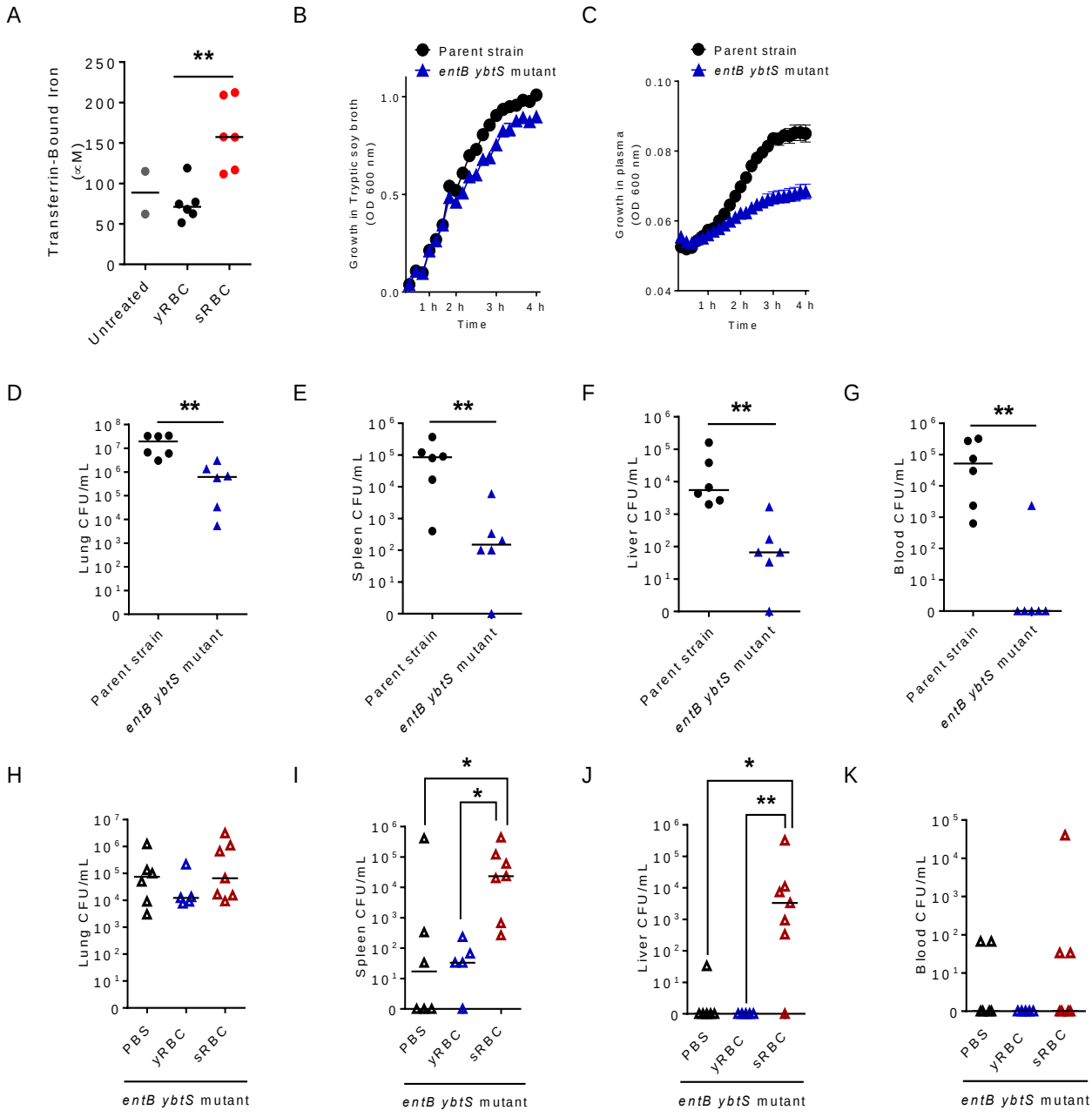
A
B
C
D
E
F
G
H
I
J
K
Transferrin-Bound Iron (∝M)
Untreated
yRBC
sRBC
Parent strain
entB ybtS mutant
Growth in Tryptic soy broth (OD 600 nm)
Growth in plasma (OD 600 nm)
Time
Lung CFU/mL
Spleen CFU/mL
Liver CFU/mL
Blood CFU/mL
PBS
entB ybtS mutant

Figure 8: Enhanced bacterial dissemination observed with stressed erythrophagocytosis is independent of iron acquisition by bacterial siderophores.

(A) Plasma transferrin bound iron from mice 2 h following challenge with either yRBC or sRBC, with unchallenged mice serving as baseline control. Growth curve of *entB ybtS* isogenic *K. pneumoniae* mutant and wild-type parent strain in (B) tryptic soy broth and (C) plasma obtained from mice challenged with sRBC. (D-G) *EntB ybtS* isogenic *K. pneumoniae* mutant and parent strain were instilled intratracheally into C57BL/6 mice (10^4 CFU inoculum each). Bacterial burden was obtained from homogenates of (D) lung, (E) spleen, (F) liver and (G) blood as CFU/mL at 24 h post-infection. Each point indicates individual mice, n=6 mice per group, line indicates median, **p<0.01 by Mann-Whitney U two-tailed test. (H-K) *EntB ybtS* isogenic *K. pneumoniae* mutant was instilled into C57BL/6 mice (10^3 CFU inoculum), followed by challenge with either PBS, yRBC or sRBC. Bacterial burden was obtained from (H) lung, (I) spleen, (J) liver tissue homogenates and (K) blood as CFU/mL at 24 h. Each point indicates individual mice, n=5-7 mice per group, line indicates median. *p <0.05, **p<0.01 by Kruskal-Wallis test with Dunn's multiple comparisons.

2.2.5 Enhanced bacterial dissemination observed with stressed erythrophagocytosis is independent of macrophage scavenger receptor A function.

Evasion of host phagocytic function is a major mechanism of *K. pneumoniae* pathogenicity[85,86] and surface receptors on phagocytes are critical for recognition and elimination of the pathogen independent of opsonization[87]. Scavenger receptors, in particular, have been shown to play important roles in uptake and clearance of pathogenic bacteria, and modulate the immune response to infection[88,89]. As the scavenger receptor MSR1 is involved in phagocytic clearance of sRBC, we tested whether acute increase in sRBC disposal co-opts MSR1 function in host defense. Compared to mice challenged with yRBC, sRBC delivery selectively reduced MSR1

expression, a class A scavenger receptor—but not MARCO, another class A scavenger receptor or CD36, a class B scavenger receptor (Fig. 9A).

MSR1 is a known pattern recognition receptor that can mediate direct non-opsonic phagocytosis of pathogenic bacteria[90–92]. We observed that F4/80^{+} splenic macrophages of *Msr1*$^{-/-}$ mice show impaired phagocytosis of *K. pneumoniae* in vivo compared to WT mice (Fig. 9B, C), suggesting that compromised MSR1 function during *K. pneumoniae* infection may underlie the worsened phenotype observed with stressed erythrophagocytosis. We utilized nonselective pharmacologic inhibitor of class A scavenger receptor, polyinosinic acid (poly(I))[93,94], to determine whether blocking class A scavenger receptor function recapitulates findings observed with stressed erythrophagocytosis during *EntB ybtS K. pneumoniae* infection. There were no differences in lung bacterial burden in infected mice receiving either PBS, sRBC or poly(I) following bacterial inoculation (Fig. 9D). However, poly(I) administration failed to reproduce the enhanced extrapulmonary dissemination of *entB ybtS K. pneumoniae* to the spleen and liver observed with sRBC delivery (Fig. 9E-F). No significant differences were observed in the blood compartment among the three groups (Fig. 9G). Furthermore, deletion of MSR1 did not alter murine susceptibility to *K. pneumoniae* intrapulmonary infection (Fig. 9H) and median survival for both mice groups was 4 days over a nearly 3-week observational period (Log-rank Mantel-Cox test, p=0.98). Moreover, no differences in lung, spleen, liver or blood bacterial CFU were observed between WT and *Msr1*$^{-/-}$ mice following *K. pneumoniae* intrapulmonary infection (Fig. 9I-L). Taken together, these findings indicate that although sRBC delivery appears to modulate MSR1 expression, the enhanced *K. pneumoniae* pathogenicity observed with stressed erythrophagocytosis is independent of MSR1 function.

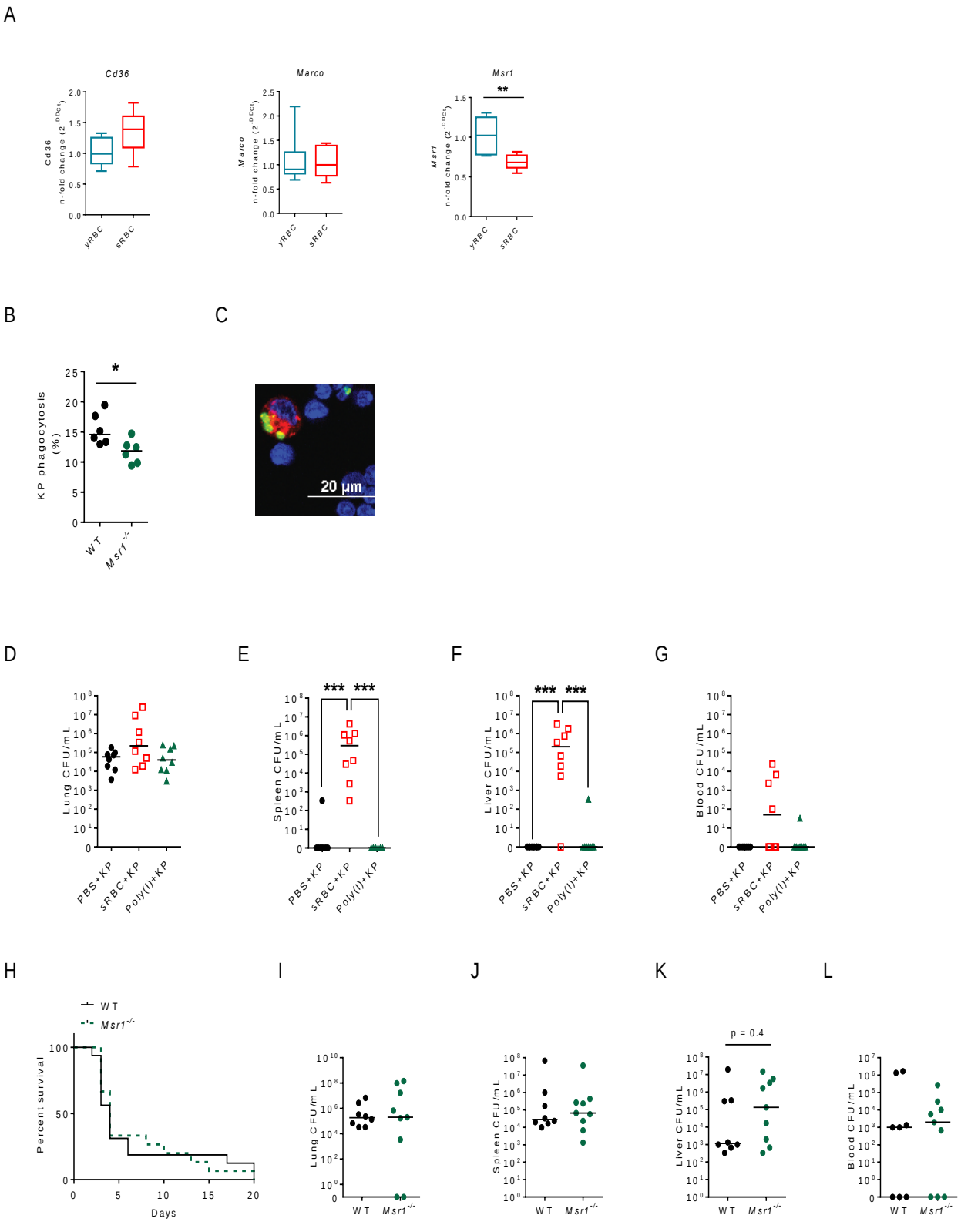
A
Cd36
Marco
Msr1
**
yRBC
sRBC
B
C
*
KP phagocytosis (%)
WT
Msr1-/-
20 µm
D
E
F
G
Lung CFU/mL
Spleen CFU/mL
Liver CFU/mL
Blood CFU/mL
*** ***
PBS+KP
sRBC+KP
Poly(I)+KP
H
I
J
K
L
WT
Msr1-/-
Percent survival
Days
p = 0.4

Figure 9: Enhanced bacterial dissemination observed with stressed erythrophagocytosis is independent of macrophage scavenger receptor A function.

(A) Gene expression of scavenger receptors in mouse liver 2 hours following either yRBC or sRBC challenge. Mouse liver gene expression was evaluated by qPCR with fold-change normalized to 18S. Box and whisker plot indicates median and 25-75%, n = 6 mice per group. **p<0.01 by Mann-Whitney U two-tailed test. (B) C57BL/6 mice were transfused with yRBC or sRBC, followed by retro-orbital injection of CFSE-labeled *K. pneumoniae* 1 h post-transfusion. Mouse splenic macrophages were gated as $F4/80^+$ and percentage of $CFSE^+$ cells was obtained by flow cytometry. *p<0.05 by Mann-Whitney U two-tailed test. Line indicates median, n = 6 mice per group. (C) Representative image of phagocytosed *K. pneumoniae* (green) within F4/80+ macrophages (red). Nuclei = blue. (D-G) *EntB ybtS K. pneumoniae* mutant was instilled into C57BL/6 mice (10^3 CFU inoculum), followed by challenge with either PBS, sRBC or 250 μg polyinosinic acid (poly(I)). Bacterial burden was obtained from (D) lung, (E) spleen, (F) liver tissue homogenates and (G) blood as CFU/mL at 24 h. Each point indicates individual mice, n=6-8 mice per group, line indicates median. ***p<0.001 by Kruskal-Wallis test with Dunn's multiple comparisons. (H) Kaplan-Meier survival curve of WT (n=16) and *Msr1*$^{-/-}$ (n=15) mice following *K. pneumoniae* instillation (7000 CFU inoculum). CFU obtained from (I) lung, (J) spleen, (K) liver, and (L) blood of WT and *Msr1*$^{-/-}$ mice 48 h following *K. pneumoniae* instillation (10^3 CFU). Line indicates median, n = 8-9 mice per group.

2.3 Discussion

We demonstrate that heightened disposal of sRBC enhances pathogenicity of the opportunistic Gram-negative pathogen *Klebsiella pneumoniae*. Mice challenged with sRBC following intratracheal *K. pneumoniae* instillation show impaired ability to control bacterial replication once *K. pneumoniae* breached the lung mucosal barrier. This is evidenced by enhanced extrapulmonary dissemination, increased systemic inflammatory cytokine response, and worsened survival compared to infected yRBC-challenged mice. The enhanced *K. pneumoniae*

dissemination observed with sRBC delivery is independent of iron acquisition by bacterial siderophores, as *K. pneumoniae* mutant lacking production of all 3 major siderophore systems (enterobactin, glycosylated enterobactin, and yersiniabactin) show increased dissemination in mice challenged with sRBC compared to yRBC or PBS-challenged mice. Furthermore, we demonstrate that enhanced *K. pneumoniae* pathogenicity during sRBC disposal is independent of macrophage scavenger receptor function and points to an alternative mechanism of defective host immunity.

An acute increase in circulating sRBC overwhelms physiologic capacity to process iron released from catabolism of sRBC and results in transferrin saturation and appearance of circulating nontransferrin-bound iron in mice[25] and humans[16,95]. This increase in iron availability may stimulate extracellular bacterial growth in mammalian tissue environments where free ionic iron is typically about 10^{-18} M and too low to support normal bacterial proliferation[96]. Indeed, introduction of exogenous iron into plasma enhances growth of *K. pneumoniae* and abolishes bactericidal properties of plasma in vitro[96]. However, in vivo, we demonstrate that despite increased circulating iron, sRBC disposal impairs host immunity in a mechanism independent of enhanced nutritional iron availability to the pathogen. This is consistent with more recent findings showing that bacterial heme-iron acquisition does not account for increased bacterial burden triggered by excess heme[97].

Besides elaboration of iron acquisition systems, *K. pneumoniae* virulence determinants include the ability to evade phagocytosis and complement-mediated killing that is dictated primarily by the polysaccharide capsular structure[85] and LPS O-antigen polysaccharide chain[36]. Both factors contribute to bacteremia and lethality in murine models of experimental pneumonia[85,98]. As in host defense against pneumococcal pneumonia, direct uptake of *K.*

pneumoniae by phagocytes can occur in the absence of circulating and local opsonins[87]. Scavenger receptors, initially identified for their ability to internalize oxidized low-density lipoprotein, recognize conserved microbial structures such as LPS and LTA, and have been shown to mediate direct uptake of pathogenic bacteria[91,99–101]. Though there exist eight classes of scavenger receptors with at least fifteen distinct members, direct uptake of bacteria with subsequent roles in host defense have largely been ascribed to a subset of receptors including MSR1 (also known as scavenger receptor A), MARCO (macrophage receptor with collagenous structure), and CD36[88,100]. While increased RBC disposal selectively suppresses MSR1 in the liver and MSR1 deficiency impairs *K. pneumoniae* uptake, we demonstrate—using both pharmacologic inhibition and genetic deletion of MSR1—that MSR1 does not significantly alter immune defense against *K. pneumoniae* intrapulmonary infection and enhanced *K. pneumoniae* pathogenicity observed with sRBC delivery is independent of MSR1 function. Our findings expand our understanding of the impact of acute sRBC disposal on host defense against *K. pneumoniae* and propose a role for sRBC-mediated injury beyond bacterial iron provision and macrophage scavenger receptor function.

2.4 Methods

Animals

C57BL/6J (#000664) mice were obtained from the Jackson Laboratory (Bar Harbor, ME). 8-12-week-old, male and female mice were utilized in experiments conducted with age-matched, sex-matched groups. In select experiments, *Msr1*$^{-/-}$ mice (B6.Cg-*Msr1*^{tm1Csk}/J, #006096) were obtained from the Jackson Laboratory. These mutant mice were originally backcrossed to

C57BL/6JIco for 12 generations before acquisition by the Jackson Laboratory. We subsequently backcrossed *Msr1*$^{-/-}$ mice to the C57BL/6J mice once and utilized wildtype littermates as controls for post-transfusion recovery studies. The animals were housed and maintained in a specific pathogen-free environment and studies were conducted in accordance with the Institutional Animal Care and Use Committee at the University of Pittsburgh.

Mouse RBC preparation and storage

C57BL/6J (#000664) or C57BL/6-Tg (UBC-GFP)30Scha/J (#004353) mice expressing green fluorescent protein under the control of the human ubiquitin C promoter were euthanized and blood obtained aseptically via cardiac puncture using citrate dextrose phosphate anticoagulant. The method of red cell storage using Citrate Phosphate Dextrose Adenine (CPDA-1) solution has been previously reported[25]. Briefly, whole blood was collected from donor mice, pooled and leukoreduced through a Neonatal High-Efficiency Leukocyte Reduction Filter (Purecell Neo; Pall Corporation). The pooled blood was centrifuged at 400 *g* for 15 minutes, and the volume reduced to a final hemoglobin level ranging from 17.0 to 17.5 g/dL. The final CPDA-1 concentration in the red cell concentrate was 14% and stored in the dark at 4°C for up to 13 days. For mouse red cells, 14 days corresponds to the limits of storage duration[25,102].

Experimental Bacterial Pneumonia model with RBC delivery

Klebsiella pneumoniae (KP) strain 43816, serotype 2 (American Type Culture Collection, Manassas, VA) was utilized for the bacterial pneumonia studies. *entB ybtS* mutant mice lacking production of siderophores enterobactin, glycosylated enterobactin, and yersiniabactin[53,54] and its parent wildtype strain were used in select experiments. The method of bacterial growth and

suspension for inoculation has been previously reported[63]. Following overnight culture in tryptic soy broth, a 1 mL inoculum of the *K. pneumoniae* culture was grown in fresh tryptic soy broth for 2 hours. Initial experiments indicated that an OD_{600} = 0.2 represents the mid-log phase of growth and subsequent experiments prepared the inoculum at the absorbance measurement. The actual inoculum concentration measured in colony forming units (CFU) was also determined by serial bacterial plating on tryptic soy agar plates (Sigma, St. Louis, MO). Bacteria were harvested, washed and resuspended in PBS just prior to use. Mice were anesthetized with isoflurane and 10^3 CFU of *K. pneumoniae* in a total volume of 100 μL was administered intratracheally under direct visualization using a sterile 200 μL pipet with filtered tip positioned just above the vocal cords. One hour following *K. pneumoniae* inoculation, 200 μl of freshly isolated yRBC (0–1 day old) or sRBC (11-13 days old) was transfused via retro-orbital vein.

RBC recovery rate after transfusion

GFP^+ yRBC or sRBC were transfused into WT or *Msr1*$^{-/-}$ mice as we have previously described[102]. 10 μL of fresh whole blood was collected from the mouse tail vein at each time point and transfused GFP signal quantified by flow cytometeric analysis. GFP^+ and GFP^- cells were gated respectively. The ratio of GFP^+ RBC to total RBC was calculated at each time point for each individual mouse. The ratio of GFP^+ cells at 5 min was set as 100%, and all other time points were normalized to 5 min in each mouse.

Bronchoalveloar Lavage fluid collection

A closed container system was used to euthanize animals at pre-specified times using isoflurane. A laparotomy was immediately performed, and mice were exsanguinated via the

inferior vena cava using citrate as the anticoagulant. The trachea was cannulated using a 20-gauge catheter, secured with silk suture. The left hilum was identified, secured with a second silk suture, and the left lung was removed for immediate tissue homogenization. Bronchoalveloar lavage (BAL) was performed by instilling 0.6 mL 0.9% NS into the R lung, followed by 0.5 mL x 3 washes. Total cell counts in BAL were determined using a hemocytometer. Cytospins were prepared from BAL fluid and stained with Diff-Quick (Siemens Healthcare Diagnosis Inc., Newark, DE). Differential cell counts were determined by counting a total of 200 cells from each slide.

Polyinosinic acid administration

Polyinosinic acid potassium salt (Poly(I) Cat# P4154, MilliporeSigma, Burlington MA) was dissolved in PBS prior to administration. *EntB ybtS K. pneumoniae* mutant was resuspended in PBS following culture in tryptic soy broth containing rifampin and instilled intratracheally at an inoculum of 7500 CFU in 100 μL PBS. 1 hour post-bacterial instillation, 200 μL sRBC (hematocrit 55%), 200 μL vehicle (PBS) or 250 μg of poly(I) in 200 μL PBS were administered retro-orbitally. Mice were sacrificed 24 h post-bacterial instillation.

Measurements of lung, spleen, liver and blood bacterial burden

The left lung, spleen, and right medial lobe of the liver were removed following euthanasia at pre-determined time points. For enumerating bacterial CFUs in the lung, spleen and liver, tissue was homogenized in 1 mL of sterile ddH_2O. Bacterial CFU was also measured from whole blood obtained from the inferior vena cava as described above. 10 μL of tissue homogenates or whole

blood in triplicates was plated by 10-fold serial dilution on tryptic soy agar plates. Bacterial plates were counted following an overnight incubation at 37°C and CFU/mL determined.

Measurement of lung and plasma cytokines

Total protein in lung tissue homogenates were quantified using the Pierce BCA Protein Assay Kit (Thermo Scientific, Rockford, IL). The volume of lung tissue homogenate corresponding to 50 µg total protein from each sample was used to perform ELISA. Plasma from mouse was diluted at 1:1 to 1:5 for measurement of cytokines in half-area ELISA plates, and the values in pg/mL were calculated based on dilution. ELISA duoset antibodies for measuring TNFα, IL-6, IL-10, C5a, MBL2, IL-1ß, CXCL10 and IFNγ were obtained from R&D Systems (Minneapolis, MN).

Measurement of transferrin-bound iron

Transferrin-bound iron was measured by electron paramagnetic spectroscopy. Plasma (~400 µL) was transferred to quartz tubes (Wilmad, Vineland, NJ) for freezing in liquid nitrogen. Measurements of the samples were carried out at 5-8 K using an EMX 10/12 spectrometer (Bruker Biospin Corp., Billerica, MA) cooled by liquid helium and operated at microwave power of 0.1 mW, microwave frequency 9.387 GHz, modulation amplitude 15 G, with a sweep width of 1500 G, center field of 1250 G, sweep time of 42 s and time constant of 81.92 ms. Transferrin-bound iron concentrations in the samples were obtained by fitting (least squares fit) to basis spectra of standard of known concentration.

In vivo phagocytosis of K. pneumoniae by mouse splenic macrophages

K. pneumoniae serotype 2 was washed with cold 0.9% saline 3 times, and then heat-killed at 65°C for 1 hour. *K. pneumoniae* was labeled with CFSE in the dark. Mice were transfused with 200 µL of sterile PBS, yRBC or sRBC via the retro-orbital vein. One hour later, CFSE labeled *K. pneumoniae* at 1×10^8 was injected via the other retro-orbital vein. At 1 h 45 minutes post-RBC transfusion, mice were euthanized and spleens were harvested. Single cell suspensions were obtained by grinding spleen between 2 frosted slides that were subsequently filtered through a cell strainer. Mouse splenocytes were immunostained with F4/80 antibody conjugated with APC. Flow cytometric data were acquired from BD biosciences FACSCalibur (BD biosciences, San Jose, CA). F4/80+ macrophages were analyzed by gating for F4/80 and CFSE double positive events. Representative images of phagocytosed *K. pneumoniae* within F4/80+ macrophages with DAPI nuclear staining were obtained by confocal microscope.

Immunofluorescent image by confocal microscopy

For immunofluorescence staining, mouse splenocytes were immobilized on glass slides by cytospin. The cells were fixed with 2% paraformaldehyde and then permeabilized by 0.1% Triton X-100 in PBS. 20% goat serum (obtained from Center for Biologic Imaging CBI, University of Pittsburgh) in 0.5% PBS was used to block nonspecific binding for 1 hour. The slides were incubated with 10 µg/mL of anti-F4/80 antibody (Abcam #ab6640, UK) overnight at 4oC. After washing, Cy3-labeled goat anti-rat secondary antibody (CBI, University of Pittsburgh) was added to the slides and incubated at room temperature for 1 hour. Nuclei was stained with DAPI for 1 min before slides were covered with gelvatol. For confocal microscopy, z-stack images of the immunofluorescence in each slide were obtained using the Nikon A1 Confocal Microscope (CBI, University of Pittsburgh) at 60 X magnification with Nyquist XY setting to optimize resolution.

The z-stack images were processed by Nikon NIS-Element software to visualize *K. pneumoniae* phagocytosis. CFSE-labeled *K. pneumoniae* and Cy-3 antibody-bound F4/80 macrophage actin co-localization indicates phagocytosed *K. pneumoniae* (yellow).

Quantification and statistical analysis

Results are reported as the median unless otherwise indicated. Log-rank test was performed to generate the Kaplan-Meier survival curve. For in vivo comparisons between two groups, a nonparametric Mann-Whitney test was undertaken. For in vivo comparisons of multiple groups, Kruskal-Wallis with Dunn's multiple comparisons test was undertaken. GraphPad Prism software version 5.0 and 6.0 were used for statistical analysis (La Jolla, CA). A *p*- value less than 0.05 was considered significant.

3.0 Stressed erythrophagocytosis suppresses STAT1 and interferon-related responses in the liver during *Klebsiella pneumoniae* infection

3.1 Rationale

The innate immune transcriptional responses in the lungs and livers of *K. pneumoniae*-infected mice following yRBC or sRBC challenge were initially evaluated using PCR Array to profile 87 antibacterial response genes (Fig. 10A). In contrast to the lungs where minimal differences in gene expression were noted between lungs of *K. pneumoniae*-infected mice challenged with yRBC versus sRBC (Fig. 10A, B), a significant reduction in innate immune gene expression (approximately 96% of statistically significant differential gene expression between the two groups) was observed in the livers of infected sRBC-challenged mice (Fig. 10A, C). This observation suggests that sRBC delivery during intrapulmonary *K. pneumoniae* infection induces a suppressive transcriptional response in the liver that may be detrimental to the host and prompted an extensive evaluation of the liver transcriptome.

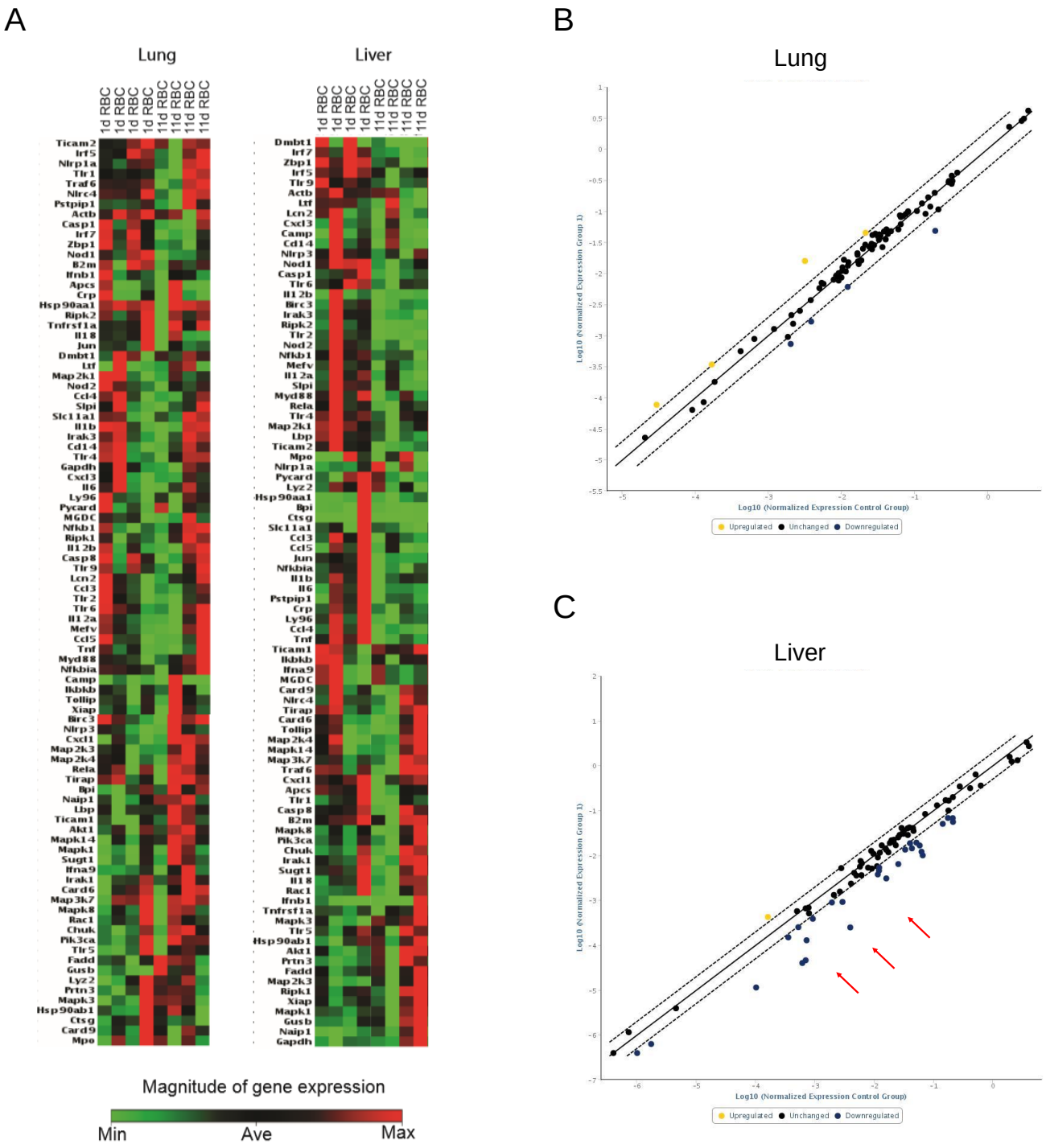

Figure 10: Differentially regulated genes in the lungs and livers of *K. pneumoniae*-infected mice challenged with yRBC (1d RBC) or sRBC (11d RBC) at 24 h.

(A) Heat map depicting 87 genes examined by PCR-Array for alterations in mouse antibacterial response in lungs and livers of mice challenged with yRBC or sRBC 24 hours post-*K. pneumoniae* infection. Scatter plot of lung (B) and (C) liver depicting differentially expressed genes with >2-fold change. Yellow = upregulated. Blue = downregulated. n = 4 mice per group. Red arrows highlight marked downregulation of antibacterial gene expression in the liver following sRBC delivery.

3.2 Results

3.2.1 RNA-Seq of the liver in mice following sRBC delivery reveals unique transcriptomic profile notable for suppression of *Stat1* and interferon-related responses during *K. pneumoniae* infection.

Prior studies have highlighted the important role of the liver in the innate immune response to acute bacterial pneumonia. Indeed, hepatocyte-specific *RelA* and *Stat3* control the production of acute phase reactants and shape the blood proteome during the innate host response to *S. pneumoniae* bacterial infection[103]. Moreover, in response to RBC damage requiring heightened or on-demand RBC disposal, the liver is the primary organ that responds to fluctuations in RBC integrity and restores iron homeostasis[19]. To obtain a comprehensive view of the transcriptome during sRBC disposal, we evaluated gene expression profile by RNA-Seq 24 h following acute intrapulmonary *K. pneumoniae* infection in mice challenged with either yRBC or sRBC (KP + yRBC vs KP + sRBC). We observed excellent separation between these two groups in terms of global transcriptomic profile and detected 4891 differentially expressed genes (threshold 1.5-fold change, FDR adjusted p-value ≤ 0.05) between livers of *K. pneumoniae*-infected mice challenged with yRBC and the livers of *K. pneumoniae*-infected mice challenged with sRBC (Fig. 11A).

Given impaired immunity in the acute infection model, we focused on innate immune gene expression (Appendix A). Although *Nfκb* related genes *Rela*, *Relb*, *Nfκbia*, *Nfκbib*, *Nfκbiz* and *Stat3* were increased in KP + sRBC group, the data was notable for suppression of Signal Transducer and Activator of Transcription 1 *Stat1* (-3.2 fold-change, FDR p-value=0) and interferon regulatory factors such as *Irf1*, *Irf2*, *Irf3*, *Irf5*, *Irf8* (Fig. 11B). Suppression of interferon responses was supported by upregulation of Suppressor of Cytokine Signaling *Socs3* (2.76 fold-change, FDR p-value=1.5 x 10^{-12}) and *Socs1* (7.6 fold-change, FDR p-value=0) gene expression (Fig. 11B). Notably, heme-oxygenase 1 (*Hmox1*), the enzyme catalyzing the rate-limiting step of heme catabolism, was also increased (3.46 fold-change, FDR p-value=0). Reduced *Irf1*, *Irf3*, *Irf8*, *Stat1* and increased *Rela*, *Socs1*, *Socs3*, *Stat3*, and *Hmox1* gene expression were confirmed by qRT-PCR (Fig. 11C).

STAT1 is essential for transducing IFNα and IFNγ responses[104] and is required for optimal defense against *K. pneumoniae*[105]. We evaluated STAT1 protein expression, and one of its key downstream effectors IRF1, in liver tissue homogenates of *K. pneumoniae*-infected mice challenged with either yRBC or sRBC. *K. pneumoniae*-infected mice challenged with sRBC showed impaired activation of STAT1 (Fig. 11D) and reduction of IRF1 expression in the liver compared to *K. pneumoniae*-infected mice challenged with yRBC (Fig. 11E), supporting the findings of RNA-Seq. Taken together, these results indicate that delivery of sRBC to the infected host suppresses STAT1, a critical regulator of interferon response and antimicrobial immune defense.

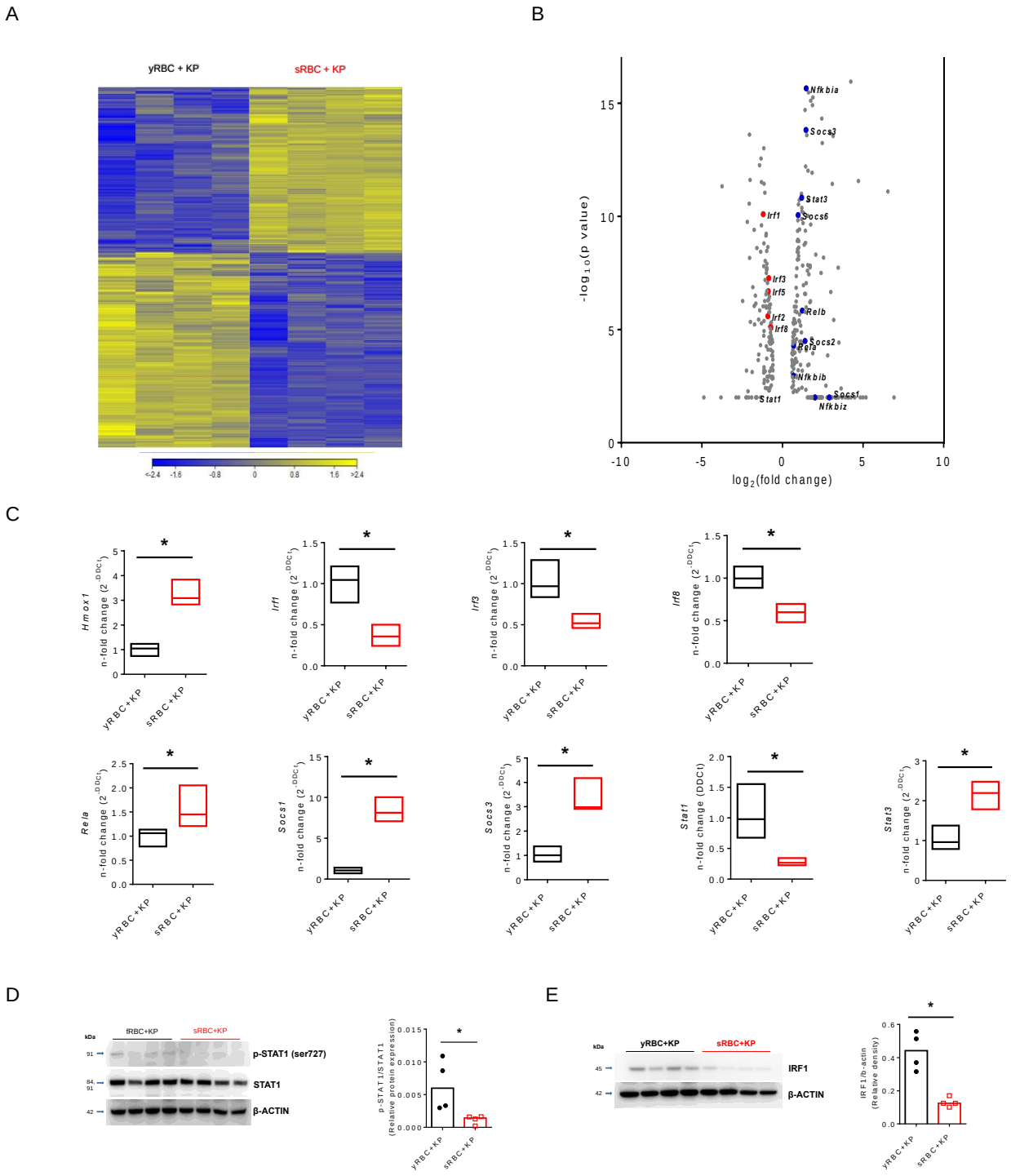

Figure 11: RNA-Seq of the liver in mice following sRBC delivery reveals unique transcriptomic profile notable for suppression of *Stat1* and interferon responses during *K. pneumoniae* infection.

K. pneumoniae was instilled intratracheally into C57BL/6 mice and followed by challenge with either yRBC or sRBC. Mice were euthanized at 24 h. (A) Heat map depicting differentially expressed genes in the livers of mice challenged with either yRBC or sRBC 24 h post-*K. pneumoniae* infection. Threshold 1.5-fold change, FDR adjusted p-value ≤ 0.05. n=4 mice per group. (B) Volcano plot of innate immune genes. Red depicts downregulated genes. Blue depicts upregulated genes. (C) qPCR validation of RNA-sequencing data. Box plot indicates median and 25-75%. n=4 mice per group, *p<0.05 by Mann-Whitney U two-tailed test. Fold change relative to yRBC + KP. (D) p-STAT1 (ser 727), STAT1, and (E) IRF1 immunoblot in livers of *K. pneumoniae*-infected mice challenged with either yRBC or sRBC. *Left*, immunoblot. *Right*, relative density of blot depicted on left. n=4 mice per group, line indicates the median *p<0.05 by Mann-Whitney U two-tailed test.

3.2.2 Plasma transaminase concentrations and liver histology following sRBC delivery in the acute *K. pneumoniae* infection model.

Next, we evaluated plasma transaminase concentrations and liver tissue architecture in mice following yRBC or sRBC delivery to determine the impact of liver damage caused by heightened sRBC disposal during infection. Though we observed elevated plasma alanine transaminase and aspartate transaminase levels in mice challenged with sRBC 24 h post-*K. pneumoniae* infection (Fig. 12A-B), we did not observe gross differences in liver tissue architecture between *K. pneumoniae*-infected mice challenged with yRBC or sRBC in our model (Fig. 12 C-D). Moreover, evaluation of inflammatory foci (Fig. 12E) and necrotic regions (Fig. 12F) in the livers of *K. pneumoniae*-infected mice following yRBC or sRBC yielded no differences between the two mouse groups (Fig. 12G-H), suggesting that injury to the liver is relatively modest in this model.

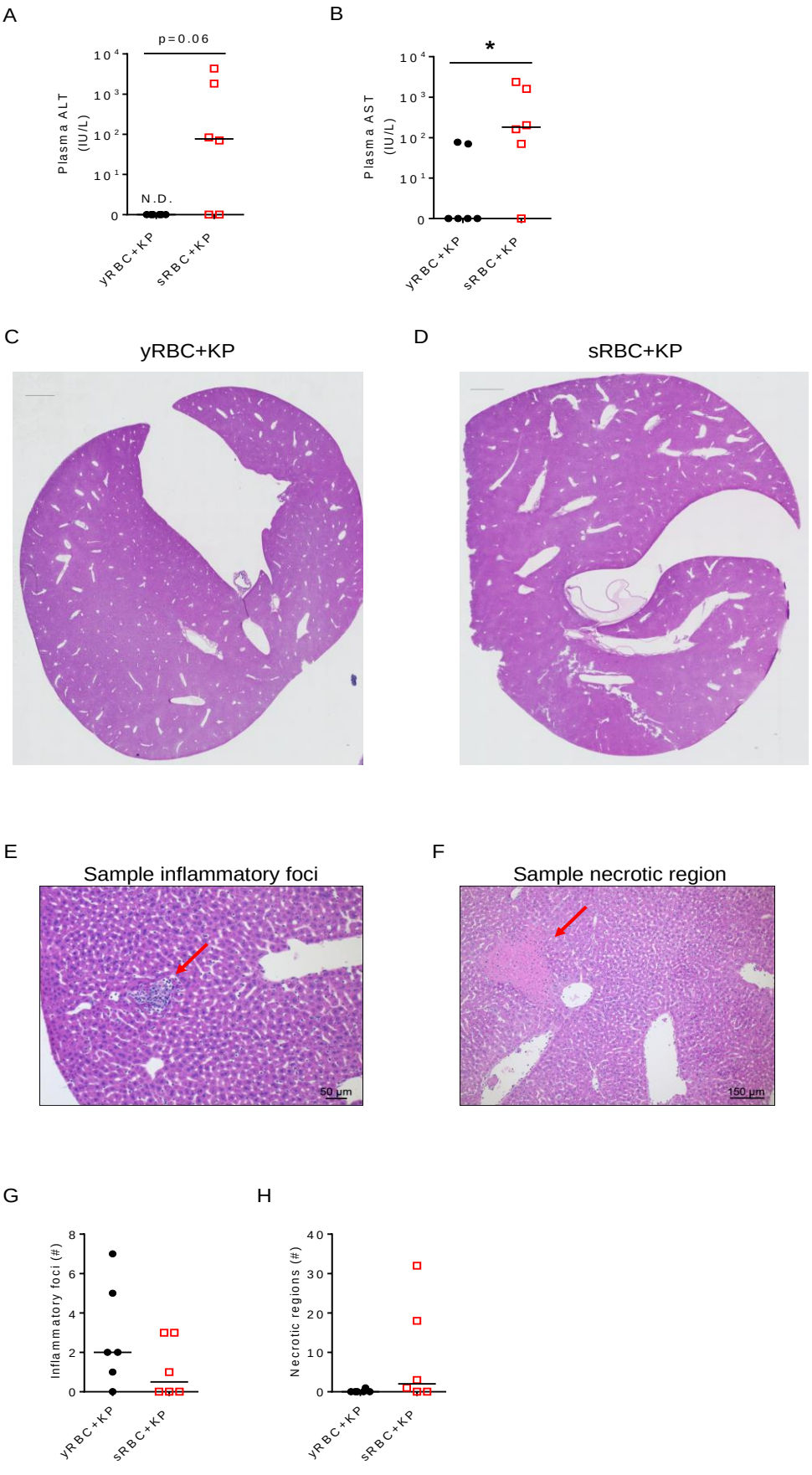
A
p=0.06
Plasma ALT (IU/L)
N.D.
yRBC+KP
sRBC+KP
B
*
Plasma AST (IU/L)
yRBC+KP
sRBC+KP
C
yRBC+KP
D
sRBC+KP
E
Sample inflammatory foci
50 μm
F
Sample necrotic region
150 μm
G
Inflammatory foci (#)
yRBC+KP
sRBC+KP
H
Necrotic regions (#)
yRBC+KP
sRBC+KP

Figure 12: Plasma transaminase concentrations and liver histology following sRBC delivery in the acute *K. pneumoniae* infection model.

(A) Alanine transaminase (ALT) and Aspartate transaminase (AST) (B) were obtained in plasma of mice challenged with yRBC or sRBC 24 h post-*K. pneumoniae* infection. Line indicates median, n = 6 mice per group. *p<0.05 by Mann-Whitney U test. (C-D) Representative liver tissue section of mice challenged with yRBC or sRBC 24 h post-*K. pneumoniae* infection, n = 6 mice per group. Scale bar = 1 mm. (E) Sample inflammatory foci and (F) Sample necrotic regions in liver histology following yRBC or sRBC delivery 24 h post-*K. pneumoniae* infection as determined in (G) and (H), respectively. n = 6 mice per group.

3.2.3 Assessment of oxygenated phosphatidylethanolamine species in mouse liver following sRBC delivery.

Others have reported induction of ferroptosis in splenic red pulp macrophages following sRBC delivery, as determined by enhanced lipid peroxidation and reactive oxygen species production[106]. As ferroptotic cell death in the liver may account for the suppressed innate immune signaling observed following acute delivery of sRBC during infection, we evaluated pro-ferroptotic oxygenated phospholipids in mouse livers 24 h following *K. pneumoniae* infection and yRBC or sRBC challenge. Whereas two highly oxygenated polyunsaturated phosphatidylethanolamine (PE) species—PE(40:7) and PE(40:8)—were significantly elevated in the liver following sRBC delivery (Fig. 13B-C), neither of these species containing three oxygens has been previously identified as a pro-ferroptotic predictive biomarker[107] and we did not observe significant differences in oxidized PE levels in livers of *K. pneumoniae*-infected mice challenged with yRBC or sRBC for majority of the molecular species evaluated (Fig. 13D). Hence, while

sRBC delivery causes changes in PE oxidation in the liver, these changes are most likely distinct from execution of the ferroptotic cell death program.

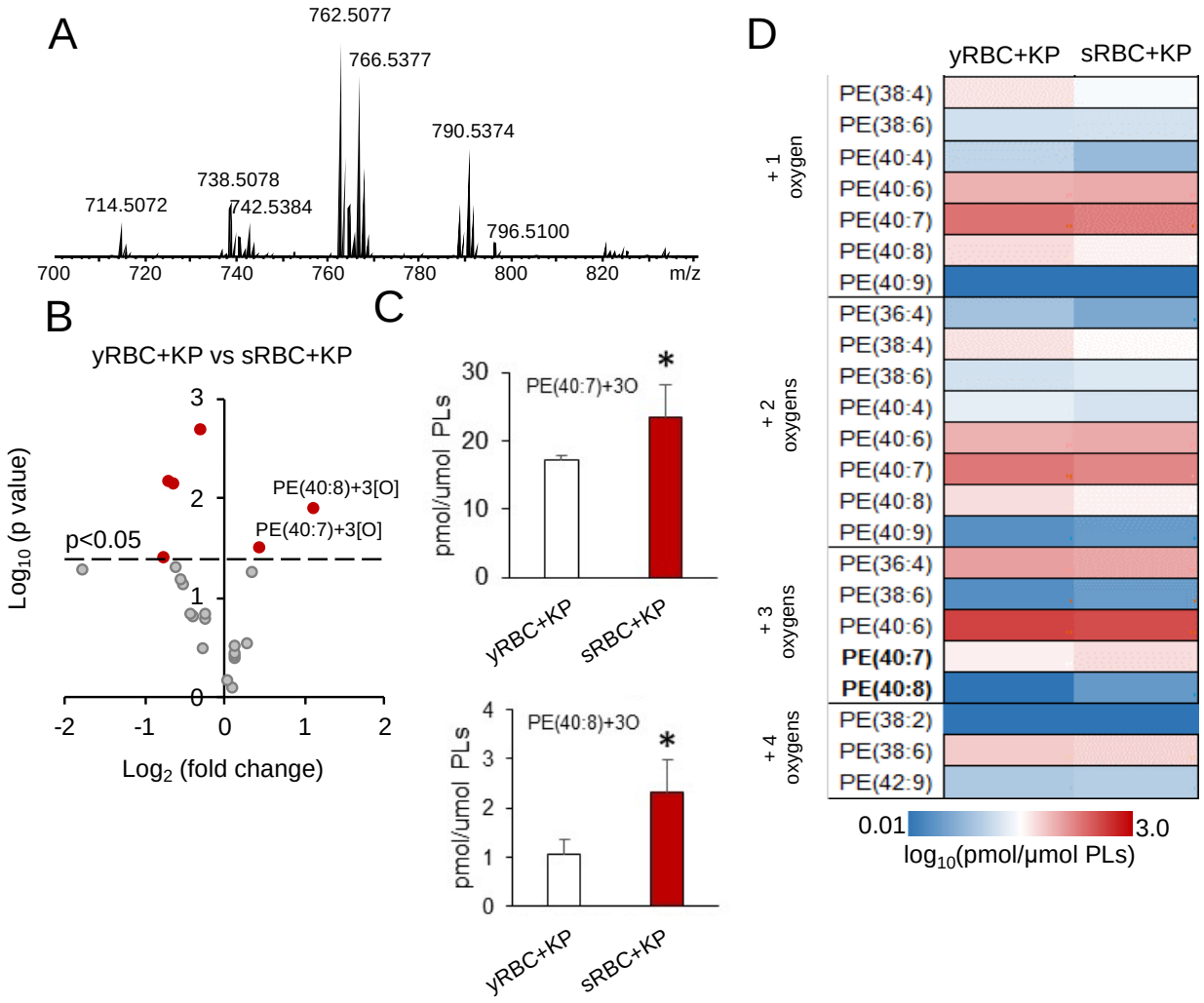

Figure 13: Assessment of oxygenated phosphatidylethanolamine species in mouse liver following sRBC delivery.

(A) Typical mass spectrum of phosphatidylethanolamine (PE) from mouse liver. (B) Differences in the level of oxygenated PE (PEox) species in livers from *K. pneumoniae*-infected mice challenged with yRBC or sRBC. (C) Quantitative LC/MS assessment of PEox. n= 4 mice per group. (D) Heat map of PEox.

3.2.4 *K. pneumoniae* enhances erythrophagocytosis in a TLR4-dependent manner.

Macrophages are the main effector cells of heme catabolism and iron recycling, and heightened RBC disposal occurs through transient accumulation of macrophages in the liver that enable restoration of iron homeostasis[19]. Macrophages are also the initial effector cells of host defense in tissue, but how the macrophage can process competing signals, respond and prioritize function during infection is less known. We challenged RAW 264.7 macrophages with live *K. pneumoniae* to evaluate the effect on downstream innate immune signaling in the presence or absence of a competing stressor such as senescent, damaged RBC (sRBC, generated by heating at 48^{o}C and continuous agitation[19]). Others have previously shown that RBC stressed by either aging or heating show no differences in clearance from circulation in mouse models[19]. We demonstrate uptake of sRBC following delivery to macrophages (Fig. 14A-B). Bacterial infection with *K. pneumoniae* potentiated uptake of sRBC by macrophages (Fig. 14C). As TLR stimulation may underlie accelerated erythrophagocytosis observed with bacterial infection[108], we tested whether TLR4 deficiency blunts sRBC uptake in *K. pneumoniae*-infected macrophages. In the absence of TLR4, sRBC uptake was significantly decreased in *K. pneumoniae*-infected macrophages (Fig. 14D). However, the increased erythrophagocytosis did not significantly alter macrophage uptake of *K. pneumoniae* (Fig. 14E), indicating that macrophages are capable of ingesting sRBC and *K. pneumoniae* concurrently.

A

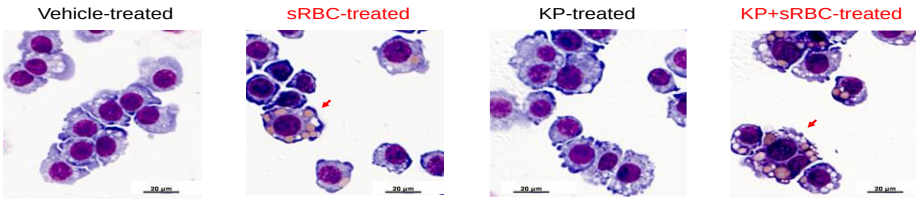
Vehicle-treated
sRBC-treated
KP-treated
KP+sRBC-treated

B

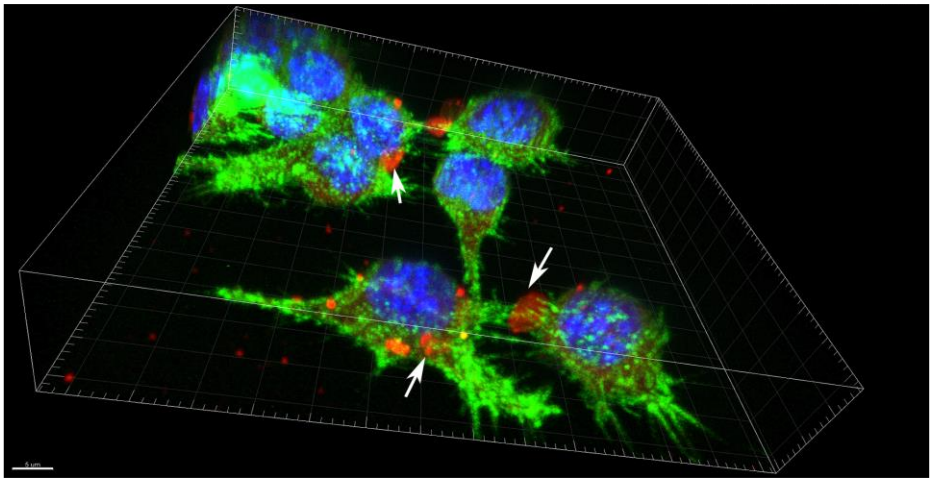

C

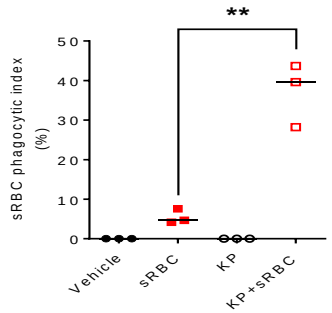
**
sRBC phagocytic index (%)
50
40
30
20
10
0
Vehicle
sRBC
KP
KP+sRBC

D

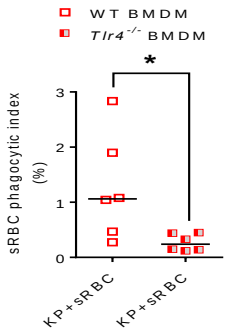
WT BMDM
Tlr4-/- BMDM
*
sRBC phagocytic index (%)
3
2
1
0
KP+sRBC
KP+sRBC

E

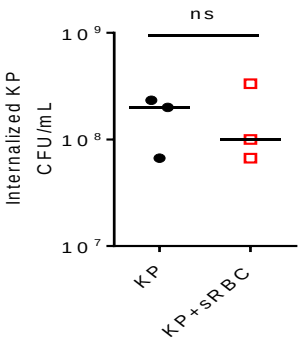
ns
Internalized KP CFU/mL
10 9
10 8
10 7
KP
KP+sRBC

Figure 14: *K. pneumoniae* enhances erythrophagocytosis in a TLR4-dependent manner.

(A) Evidence of stressed RBC (sRBC) internalization in experimental model. RAW 264.7 cells were incubated with vehicle (sterile PBS), sRBC (50 sRBC:1 Mφ), *K. pneumoniae* (KP, MOI 10:1) or KP + sRBC for 90 min. Following incubation, phagocytes were washed with PBS and non-internalized RBCs were lysed with hypotonic lysis buffer. Red arrow indicates internalized sRBC. (B) Three-dimensional visualization of sRBC uptake in RAW 264.7 cells. Arrow indicates internalized CD235a-labeled sRBC (red), nuclei are stained with Hoechst (blue), and macrophages are labeled with F4/80. Scale bar = 5 μM (C) Quantification of sRBC uptake shown in (A). n=3 technical replicates per group and is indicative of two independent experiments. **p<0.01 by two-tailed t test. (D) Bone marrow-derived macrophages (BMDM) obtained from wildtype (WT) and *Tlr4*$^{-/-}$ mice were challenged with KP + sRBC (10 sRBC:1 Mφ) for 2 h. Data is indicative of 2 independent experiments. n=3 technical replicates per group. Line indicates median. (E) RAW cells were challenged with KP or KP + sRBC for 90 min. Following incubation, phagocytes were washed with HBSS containing 100 μg/mL gentamicin to kill extracellular, attached bacteria and subsequently lysed to reveal intracellular colony forming units (CFU) per mL.

3.2.5 Stressed erythrophagocytosis upregulates heme-iron transcriptional responses and suppresses STAT1 in macrophages during *K. pneumoniae* infection.

Heme accumulation following erythrophagocytosis induces transcription of heme oxygenase-1 (*Hmox1*)[109] and ferroportin-1 (*Slc40a1*)[110]. Indeed, we observed increased *Hmox1* and *Slc40a1* gene expression in *K. pneumoniae*-infected macrophages challenged with sRBC (Fig. 15A). As observed in vivo, we noted suppression of *Stat1* in *K. pneumoniae*-infected macrophages challenged with sRBC (Fig. 15B). STAT1 regulates transcription of critical immune effectors such as complement component 3 (*C3*), complement factor b (*Cfb*), IRF1 (*Irf1*), and inducible nitric oxide synthase (iNOS or *Nos2*) in macrophages in response to interferon stimulation[104]. Following

sRBC delivery to *K. pneumoniae*-infected macrophages, *C3*, *Cfb*, *Irf1*, and *Nos2* gene expression were also impaired (Fig. 15B).

We next investigated STAT1 protein expression and showed sRBC delivery to macrophages dose-dependently reduced both phosphorylated STAT1 and total STAT1 expression during *K. pneumoniae* infection (Fig. 15C). sRBC delivery to *K. pneumoniae*-infected macrophages also dose-dependently inhibited IRF1, a downstream target of STAT1 (Fig. 15C). Though hepatocytes constitute ~80% of liver volume and have been shown to recognize and respond directly to microbial products[111–113], we demonstrate in our model that hepatocytes do not regulate the interferon response to *K. pneumoniae* and sRBC delivery has no effect on IRF1 expression in hepatocytes (Fig. 15D).

To determine whether sRBC-mediated suppression of STAT1 and IRF1 induction resulted in impaired macrophage cytokine responses, we evaluated CCL5, CXCL10, and TNFα secretion in *K. pneumoniae*-infected macrophages challenged with sRBC. We observed that sRBC delivery markedly reduced production of interferon-related cytokines CCL5 and CXCL10 to *K. pneumoniae* (Fig. 15E). In contrast, sRBC delivery did not alter TNFα secretion in *K. pneumoniae*-infected macrophages (Fig. 15E). Moreover, *Stat1*$^{-/-}$ BMDMs showed impaired *C3, Cfb, Irf1, Nos2* but not *Rela* transcriptional responses following *K. pneumoniae* infection and CXCL10 but not TNFα secretion was STAT-1 dependent (Fig. 15F-G). Taken together, these findings indicate that *K. pneumoniae* infection heightens erythrophagocytosis resulting in selective transcriptional responses notable for heme-iron metabolism and suppression of STAT1 and its downstream targets.

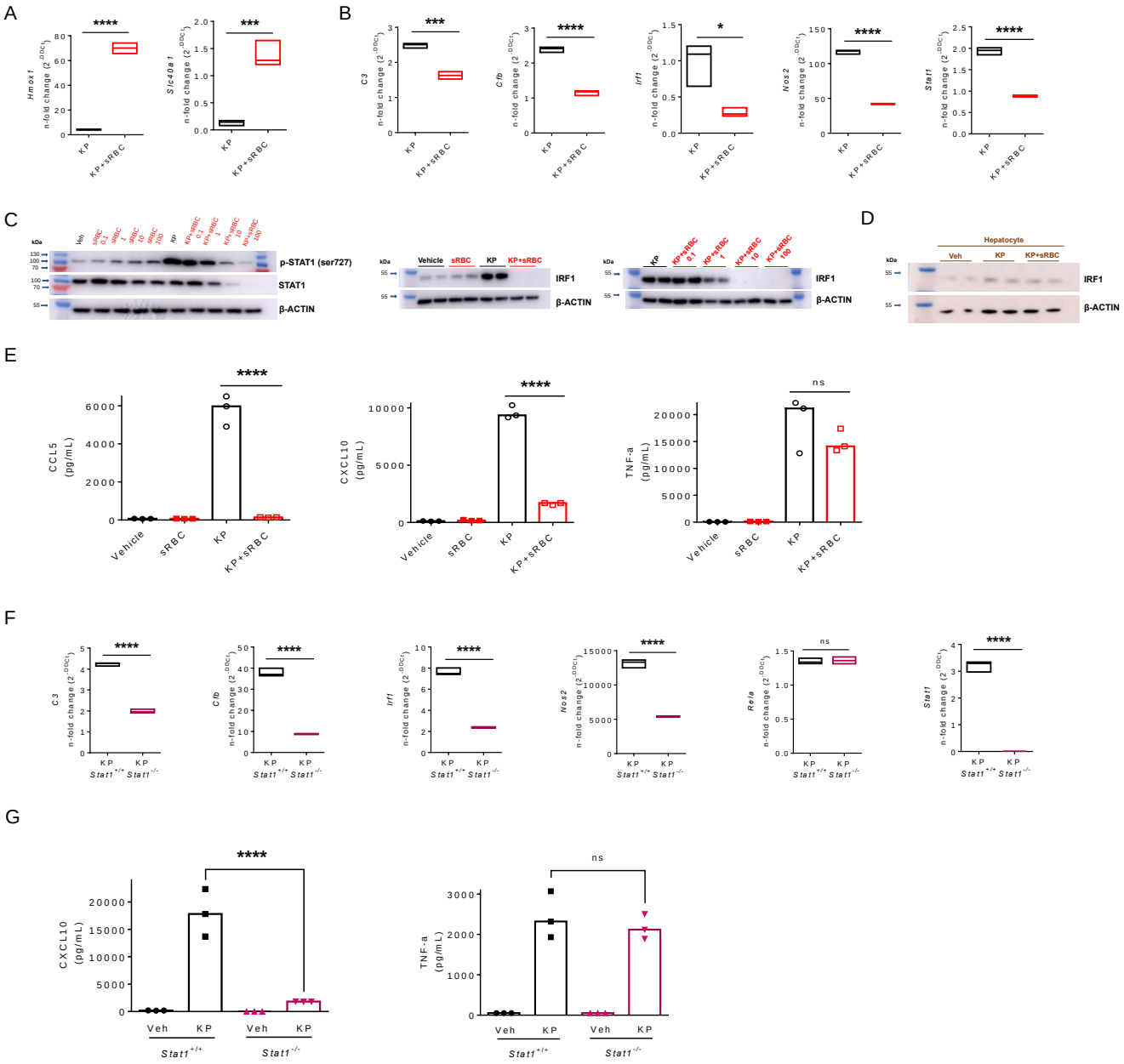

Figure 15: Stressed erythrophagocytosis upregulates heme-iron transcriptional responses and suppresses STAT1 in macrophages during *K. pneumoniae* infection.

(A) Heme-iron transcriptional genes *Hmox1* and *Scl40a1* and (B) STAT1 target genes *C3*, *Cfb*, *Irf1*, *Nos2* and *Stat1* transcripts in RAW cells challenged with *K. pneumoniae* (KP) or KP + sRBC for 4 h. Gene expression was evaluated by qPCR analysis. (A-B) Fold change relative to vehicle (PBS)-treated macrophages. Box plot indicates median and 25-75%, n=3 technical replicates per group and is indicative of at least 2 independent experiments. *p<0.05, ***p<0.001, ****p<0.0001 by two-tailed t test. (C) STAT1 and IRF1 immunoblots in RAW cells challenged with

vehicle (PBS), sRBC, KP or KP + sRBC for 4 h. Blots are indicative of at least 3 independent experiments. (D) IRF1 immunoblots in primary hepatocytes obtained following collagenase perfusion of murine liver and challenged with vehicle, KP or KP + sRBC for 4 h. Blot is indicative of two independent experiments. (E) CCL5, CXCL10, and TNF-α were measured in cell culture supernatant by ELISA 4 h post-infection. n=3 technical replicates per group and is indicative of 3 independent experiments. *p<0.05, **p<0.01, ****p<0.0001 by two-tailed t test. (F) *C3*, *Cfb*, *Irf1*, *Nos2*, *Rela*, and *Stat1* in $Stat1^{+/+}$ and $Stat1^{-/-}$ bone marrow-derived macrophages (BMDM) challenged with KP or KP + sRBC for 4 h. Gene expression was evaluated by qPCR analysis. Fold change relative to vehicle (PBS)-treated $Stat1^{+/+}$ BMDMs. Box plot indicates median and 25-75%, n=3 technical replicates per group. ****p<0.0001 by two-tailed t test. (G) CXCL10 and TNF-α were measured in cell culture supernatant by ELISA 4 h post-infection. n=3 technical replicates per group. ****p<0.0001 by one-way ANOVA with Tukey's multiple comparisons test.

3.3 Discussion

Although acute bacterial lower respiratory tract infections are exceedingly common occurrences, remarkably little is known about innate host defense mechanisms that go awry leading to a relatively immunosuppressed state. Increased circulation of sRBC—either from intrinsic causes such as hemolytic anemias, severe sepsis or extrinsic causes such as transfusion of storage-damaged RBC—precipitates mononuclear phagocytic uptake, disrupts heme-iron homeostasis, and may predispose affected individuals to opportunistic bacterial infections. Here, we present the novel finding that an acute rise in RBC disposal during bacterial infection suppresses STAT1 expression in the liver, the primary site of RBC removal during stress. STAT1 is a critical transcription factor as STAT1 deficiency renders mice[104] and humans[114] unresponsive to type I or II interferons and impairs ability to clear pathogenic microbes and viruses. We further show that *K. pneumoniae* infection intensifies sRBC uptake by macrophages in a TLR4-dependent manner, resulting in upregulation of heme-iron transcriptional responses and suppression of

STAT1 and its downstream effectors. Collectively, our findings demonstrate that an increased demand for erythrophagocytosis during bacterial infection results in macrophage dysfunction characterized by defects in the STAT1 pathway.

Ferroptosis is an iron-dependent form of regulated cell death that involves lethal, iron-catalyzed lipid damage and whose execution lies at the intersection of amino acid, lipid, and iron metabolism[26,115]. sRBC delivery to macrophages acutely increases intracellular iron availability that may predispose erythrophagocytic macrophages to pathologic accumulation of lipid peroxides and execution of ferroptosis[67,106]. Decreased cell viability, as a consequence, may underlie impaired immune response to bacterial infection following sRBC challenge. However, we demonstrate that immunosuppressive effects observed in the liver in our acute bacterial infection model are most likely not due to ferroptosis, as accumulation of proferroptotic oxygenated phospholipids were not observed following sRBC delivery. Furthermore, injury to the liver, as determined by plasma aminotransferase levels and pathologic scoring, was relatively modest in our model, suggesting that direct cellular insult triggering cell death is an unlikely mechanism for immunosuppression in this context.

Though virtually all mammalian cell types are equipped to ingest and process circulating iron, the macrophage is the primary cell responsible for engulfing and processing aged or damaged RBC to maintain suitable plasma iron levels[17]. While enhanced delivery of effete RBC to macrophages may increase pathogen virulence by boosting nutritional iron source to the pathogen, heightened erythrophagocytosis may weaken immunity through dysregulated heme-iron metabolism in the host cell. We show here that stressed erythrophagocytosis selectively disrupts STAT1 signaling in macrophages during *K. pneumoniae* infection. Our findings highlight a

potential mechanism underlying the acquired immunosuppressive phenotype observed in some patients following critical illness.

3.4 Methods

Animals

C57BL/6J, (#000664), *Tlr4*$^{-/-}$ (#029015), and *Stat1*$^{-/+}$ (#012606) mice were obtained from the Jackson Laboratory and respective breeding colonies were established at our facilities. Resulting progeny (*Tlr4*$^{-/-}$, *Stat1*$^{-/-}$ and *Stat1*$^{+/+}$) were utilized in select experiments. All mice were fed the same chow within the same room of the vivarium for at least 4 weeks prior to experimentation and animals were housed and maintained in a specific pathogen-free environment and studies were conducted in accordance with the Institutional Animal Care and Use Committee at the University of Pittsburgh.

PCR-Array

Total RNA extracted from tissues were reverse transcribed to cDNA using the RT^2 First Strand kit according to the manufacturer's instructions (SABiosciences, Frederick, MD, USA). The amplified cDNA was diluted in nuclease-free water and added to the RT^2 qPCR SYBR green Master Mix (SA Biosciences, Frederick MD). The above mixtures were added to RT² Profiler™ PCR Array Mouse Antibacterial Response 384-well plates (330231 PAMM-148ZA, SA Biosciences, Frederick MD). Amplification was performed with ABI 7900HT Real-Time PCR System in accordance with the manufacturer's guidelines. Data were analyzed by online analysis tool at Qiagen Data Analysis Center (http://www.qiagen.com/us/shop/data-interpretation-

systems/biological-data-tools/geneglobe-data-analysis-center). Two housekeeping genes, beta-actin (*Actb*) and Glyceraldehyde-3-phosphate dehydrogenase (*Gapdh*) were used for normalization. The cycle threshold (CT) was determined for each sample and normalized to the average CT of the two housekeeping genes. The difference in ΔCt values between experimental and control samples are calculated (ΔΔCt). This allowed for the calculation of the Fold-Change (2^(- ΔΔCT)), or the normalized gene expression (2^(- ΔCT)) in the test Sample divided by the normalized gene expression (2^(- ΔCT)) in the control Sample. The p values are calculated based on a Student's t-test of the replicate 2^(- ΔCT) values for each gene in the control group and test sample groups, and p values less than 0.05 are considered statistically significant.

RNA-Seq

Livers were obtained from *K. pneumoniae*-infected mice challenged with yRBC or sRBC 24 h post-*K. pneumoniae* infection. RNA was purified from liver tissue using RNeasy Plus Universal Mini kit (Cat # 73407) according to the manufacturer's instructions (Qiagen, Germany) and concentration of isolated RNA was determined by NanoDrop. Purified RNA was sequenced using NextSeq 500 System (Illumina, San Diego, CA) at high output and paired-end read (2 x 150 cycles) by the Health Sciences Sequencing Core at Children's Hospital of Pittsburgh. The sequencing data was analyzed with CLC Genomics Workbench (Qiagen). Briefly, the sequencing data quality was assessed and low quality reads (Phred Quality Score<20) and adaptor sequences were trimmed for downstream analysis. The RNA-Seq data were mapped against mouse genomic sequence, gene sequence and mRNA sequence. Expression difference between treatment groups was considered significant when absolute fold change>=1.5, maximum group mean>=1, FDR p value <0.05.

Quantitative PCR

Tissues were frozen in cold Qiazol lysis reagent and homogenized using a hand-held homogenizer. Following centrifugation at 12,000 *g* for 10 min, the supernatants were used for total RNA extraction using RNeasy Plus Universal Mini kit. For in vitro studies, cells were lysed in Qiazol lysis reagent and RNA was also extracted using RNeasy Plus Universal Mini kit. RNA samples were reverse transcribed into cDNA using SuperScript III Reverse Transcriptase or MultiScribe Reverse Transcriptase (Moloney murine leukemia virus reverse transcriptase; Invitrogen). Quantitative PCR was performed according to the manufacturer's protocol (Applied Biosystems, Foster City, CA) by incubating cDNA samples with specified probes and primers of interest and TaqMan Universal PCR Master Mix II and measuring PCR amplification using the 7900HT Real-Time PCR System. Probes and primers for heme oxygenase 1 (*Hmox1*; Mm00516004_m1), NF-κB subunit p65 (Rela; Mm00501346_m1), suppressor of cytokine signaling 1 (*Socs1*; Mm01342740_g1), suppressor of cytokine signaling 3 (*Socs3*; Mm00545913_s1), signal transducer and activator of transcription 3 (*Stat3*; Mm01219775_m1), signal transducer and activator of transcription 1 (*Stat1*; Mm01257286_m1), inducible nitric oxide synthase (*Nos2*; Mm00440502_m1), interferon regulatory factor 1 (*Irf1*; Mm01288580_m1), interferon regulatory factor 3 (*Irf3*; Mm00516784_m1), interferon regulatory factor 8 (*Irf8*; Mm00492567_m1), ferroportin-1 (*Slc40a1*; Mm01254822_m1), complement component 3 (*C3*; Mm01232779_m1), complement factor b (*Cfb*; Mm00433909_m1), glyceraldedyde 3-phosphate dehydrogenase (*Gapdh*; Mm99999915_g1), and 18S (*18S*; Hs99999901_s1) were commercially available at Applied Biosystems. Gene expression was analyzed by the ΔΔ-threshold

cycle (ΔΔCt) method, with 18S rRNA or Gapdh as the endogenous control, and average ΔCt of unstimulated wild-type controls served as the calibrator.

Immunoblot

Macrophages were lysed with Pierce IP lysis buffer (Thermo Scientific, Pittsburgh, PA) with complete mini-protease inhibitor and phosphatase inhibitor (Roche, Indianapolis, IN). After brief sonication on ice, samples were centrifuged at 10,000 *g* at 4°C for 10 min and supernatants were saved for Western blotting. 5–30 µg protein was loaded per well onto a NuPAGE 4-12% Bis-Tris Gel (Life Technologies, Grand Island, NY). After protein transfer, membranes were incubated with 1:1000 dilution of specific antibodies to phospho-STAT1 (ser 727, #9177), phospho-STAT1 (tyr 701, #9167), STAT1 (#14994) and IRF1 (#8478) obtained from Cell Signaling Technology (Danvers, MA). Membranes also were incubated with 1:2000 dilution of antibody to β-ACTIN (#4970) obtained from Cell Signaling Technology (Danvers, MA).

Phagocytosis assays

For sRBC uptake, macrophages were seeded at a density of 1 x 10^6 cells per well of a 6-well tissue culture plate in DMEM supplemented with 10% bovine serum 24 h prior to assay. Macrophages were then incubated with vehicle (PBS), sRBC (50:1), *K. pneumoniae* (KP; 10:1) or KP + sRBC for 90 min or 2 h. Following incubation, macrophages were washed with PBS, unengulfed sRBC were lysed, and macrophages were washed again with PBS. Macrophages were then incubated briefly (< 5 min) in 0.5% trypsin-EDTA at 37ºC to allow cell detachment prior to cytospin. Suspended cells were immobilized onto glass slides by centrifugation at 450 RPM for 3

min and slides were stained using Diff-Quik. Phagocytic index was determined as previously described [116]:

$$\frac{Number\ of\ engulfed\ sRBC}{Number\ of\ M\varphi\ counted} \times \frac{Number\ of\ M\varphi\ containing\ engulfed\ sRBC}{Number\ of\ M\varphi\ counted} \times 100$$

For KP uptake, macrophages were seeded at a density of 2.5 x 10^5 cells per well of a 24-well tissue culture plate 24 h prior to assay and subsequently incubated with KP (MOI 10:1) or KP + sRBC 90 min or 2 h. Following incubation, phagocytes were incubated in HBSS containing 100 µg/mL gentamicin for 1 h to kill extracellular, attached bacteria, subsequently lysed with 100 µL HBSS containing 0.1% Triton-X, and lysates were plated on tryptic soy agar to reveal intracellular colony forming units (CFU) per mL.

In vitro K. pneumoniae stimulation

RAW cells or BMDMs were seeded at a density of 1 x 10^6 cells per well of a 6-well tissue culture plate or at a density of 5 x 10^5 cells per well of a 12-well tissue culture plate in DMEM containing 10% bovine serum 24 h prior to stimulation. Media was replaced and opsonized live *K. pneumoniae* serotype 2 (MOI 10:1, log phase) was introduced. *K. pneumoniae* was opsonized by incubating with 20% bovine serum for 30 minutes at 4°C. Leukoreduced sRBC was resuspended in sterile PBS. At indicated time (usually 4 h post-KP infection), media was collected, spun at 10,000 *g* for 10 min at 4°C, and cytokine release was evaluated in resulting supernatant. Macrophages were washed with PBS and incubated in 800 µL–1 mL of RBC lysis buffer (eBioscience, Invitrogen Cat# 00-4333) for 30–60 seconds at room temperature with continuous swirling to lyse unengulfed RBC. Macrophages were washed again with PBS and lysed to examine gene and protein expression via qRT-PCR and western blot, respectively.

Liver histology

The median lobe of the liver was fixed in 2% paraformaldehyde for 4 hours. Subsequently, the lobes were embedded in paraffin and processed for sectioning and H&E staining. Whole section images of the median lobes at 100x magnification were obtained using a TissueFAXS PLUS system (Tissuegnostics, Vienna, Austria). Using the overview images, the total number of inflammatory foci and necrotic regions in each liver section was assessed by an investigator blinded to the experimental groups.

Quantification and statistical analysis

Results are reported as the median unless otherwise indicated. For in vivo comparisons, a nonparametric Mann-Whitney test was undertaken. For in vitro comparisons between two groups, a two-tailed t test was undertaken. For in vitro comparisons of multiple groups, a one-way ANOVA with Tukey's multiple comparisons test was undertaken. GraphPad Prism software version 6.0 was used for statistical analysis (La Jolla, CA). A *p*- value less than 0.05 was considered significant.

Data availability

Data files for RNA-Seq reported in this chapter have been deposited at NCBI GEO, GEO accession number: GSE144902.

4.0 STAT1 suppression requires NRF1 and NRF2 activation but is independent of heme oxygenase-1 induction

4.1 Rationale

Acute sRBC disposal marks the host for an immunosuppressive fate during *K. pneumoniae* infection characterized by increased extrapulmonary dissemination, reduced murine survival, and impaired macrophage STAT1 responses. To understand how sRBC disposal alters interferon signaling during infection, we sought to (1) delineate macrophage STAT1 response to *K. pneumoniae* under homeostasis and (2) identify mechanisms by which sRBC or its breakdown products halt STAT1 response to *K. pneumoniae*.

Infected cells secrete proteins that "interfere" with pathogen proliferation and subsequent infections, known as interferons[117]. Though originally discovered in the context of viral infections, interferons have been shown to be critical for host defense against *K pneumoniae* infections[118–120]. Ligand engagement of the interferon α/β receptor or interferon γ receptor on macrophages activates STAT1 and interferon stimulated gene transcription in canonical JAK-STAT signaling[121] (Fig. 16). STAT1 propagates interferon signaling and in the absence of STAT1, macrophages are unresponsive to type I or II interferons[104,114]. LPS stimulation triggers autocrine macrophage IFNβ production that has been shown to mediate STAT1α/β phosphorylation and subsequent induction of STAT1-dependent gene expression[122,123]. The conundrum, however, lies in the fact that IFNβ is not secreted by macrophages until at least two to four hours post-LPS stimulation[124], yet STAT1 is rapidly phosphorylated within minutes following LPS stimulation in macrophages[125]. This suggests that other interferon-independent mechanisms mediate STAT1 activation to microbial

stimuli and prompts an investigation of this seemingly basic lapse in our knowledge of interferon signaling.

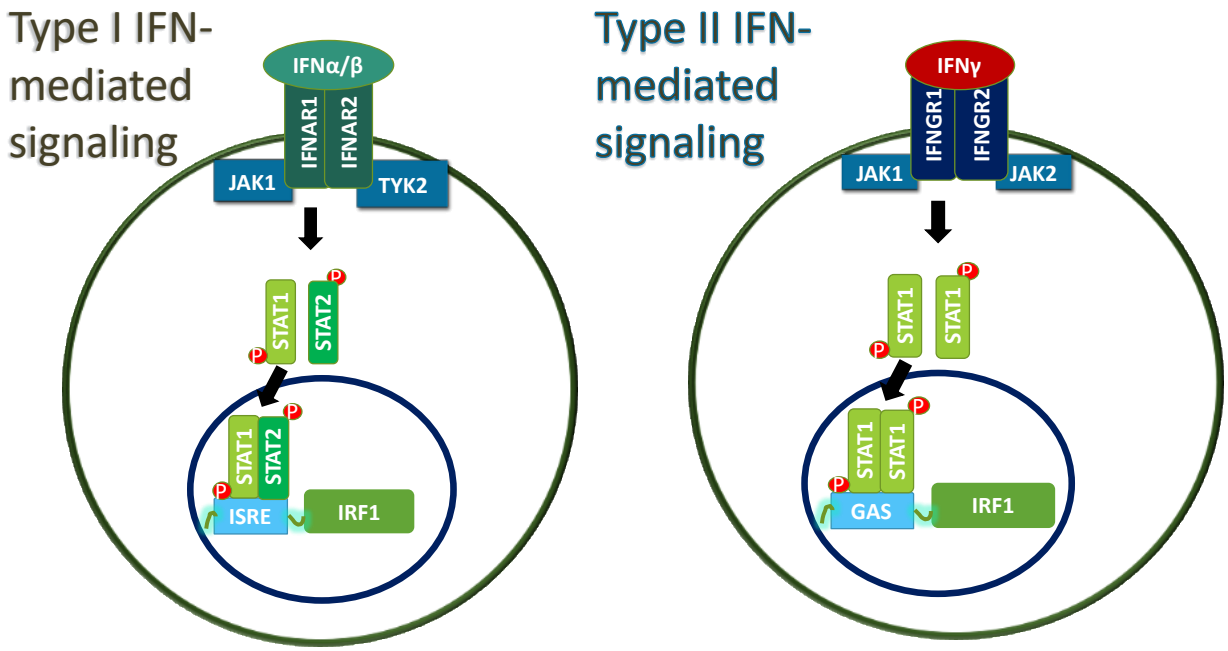

Figure 16: Canonical interferon receptor signaling.

Left, binding of type I interferon (IFN) to heterodimeric interferon α/β receptors (IFNAR) activates receptor-associated tyrosine kinases, janus kinase 1 (JAK1) and tyrosine kinase 2 (TYK2), resulting in phosphorylation of STAT1 and STAT2, formation of the heterotrimeric complex IFN-stimulated gene factor 3 (ISGF3) with IRF9 (not shown), subsequent binding to interferon-sensitive response elements (ISRE) and activation of interferon-stimulated genes (ISGs) such as IRF1[121]. *Right*, binding of sole type II IFN, IFNγ, to heterodimeric interferon gamma receptors 1 & 2 (IFNGR) activates JAK1 and JAK2, resulting in phosphorylation of STAT1, formation of STAT1 homodimers, subsequent binding to gamma-activated site (GAS) and activation of ISGs, notably CXCL10 and IRF1.

4.2 Results

4.2.1 Interferon response to *K. pneumoniae* is independent of autocrine type I or II interferon signaling in macrophages but may require NF-κB activation.

As STAT1 activation is typically downstream of type I or II interferon receptor engagement in canonical interferon signaling (Fig. 16), we evaluated the interferon response in macrophages deficient in type I or II interferon receptor (*Ifnar1*$^{-/-}$ or *Ifngr1*$^{-/-}$) following infection with *K. pneumoniae*. IRF1 expression was utilized as a STAT1 target readout. As expected, *K. pneumoniae* infection induced robust IRF1 expression in macrophages and sRBC delivery abrogated IRF1 induction (Fig. 17A). To our surprise, IRF1 expression following *K. pneumoniae* stimulation remained intact even in the absence of type I or II interferon receptors (Fig. 17A-B), indicating that macrophage interferon response during *K. pneumoniae* infection is independent of autocrine type I or II interferon signaling. Though not as extensively studied, inhibitory κB kinase ε (IKKε/IKKi), a member of the NF-κB cascade, has been shown to directly activate STAT1[126,127], suggesting that NF-κB may regulate the macrophage interferon response during *K. pneumoniae* infection. Thus, we utilized small molecular inhibitor of IKK, BAY 11-7082, to test whether disrupting NF-κB activation impairs interferon response to *K. pneumoniae* in macrophages. IKK inhibition recapitulated IRF1 suppression observed with *K. pneumoniae*-infected macrophages challenged with sRBC (Fig. 17C). Taken together, these findings suggest that during *K. pneumoniae* infection in macrophages, induction of STAT1-dependent interferon-regulated protein expression is independent of autocrine type I or II interferon signaling but may require NF-κB activation.

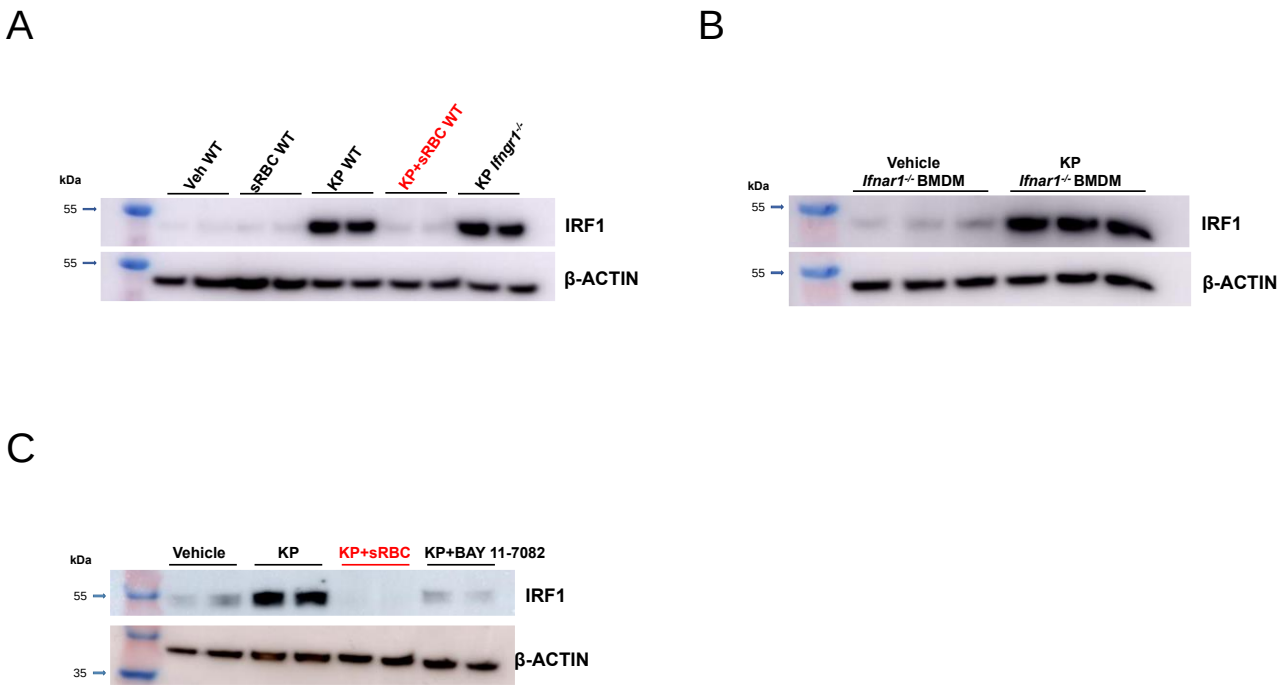

Figure 17: Interferon response to *K. pneumoniae* is independent of autocrine type I or II interferon signaling in macrophages but may require NF-κB activation.

(A-B) IRF1 immunoblots in bone marrow-derived macrophages (BMDM) obtained from *Ifngr1*$^{-/-}$, *Ifnar1*$^{-/-}$, and wildtype (WT) mice challenged with vehicle (PBS), sRBC, *K. pneumoniae* (KP) or KP + sRBC for 4 h. (C) IRF1 immunoblot in RAW cells challenged with vehicle (1% DMSO), KP, KP + sRBC or KP + BAY 11-7082 10 μM for 4 h. (A-C) Blots are indicative of two independent experiments.

4.2.2 sRBC-mediated STAT1 suppression during *K. pneumoniae* infection is not due to STAT3 activation.

Activation of JAK2, through binding of hepcidin to ferroportin-1 in conditions of iron surplus, may result in STAT3-mediaated transcriptional activation of SOCS3 and subsequent dampening of inflammatory cytokine production[128]. As we observed in the liver, we show that

sRBC delivery upregulated *Stat3* and *Socs3* gene expression in *K. pneumoniae*-infected macrophages (Fig. 18A-B). We tested whether inhibition of STAT3 using FDA-approved tyrosine kinase inhibitor, Sunitinib, reverses IRF1 suppression observed in *K. pneumoniae*-infected macrophages challenged with sRBC. Though we observed *Stat3* upregulation following sRBC delivery, STAT3 activation, as determined by tyrosine phosphorylation, was impaired in *K. pneumoniae*-infected macrophages challenged with sRBC (Fig. 18C). Moreover, dose-dependent inhibition of STAT3 with sunitinib failed to rescue IRF1 in *K. pneumoniae*-infected macrophages challenged with sRBC (Fig. 18C). Thus, sRBC-mediated STAT1 suppression observed during *K. pneumoniae* infection is not due to enhanced STAT3 activation.

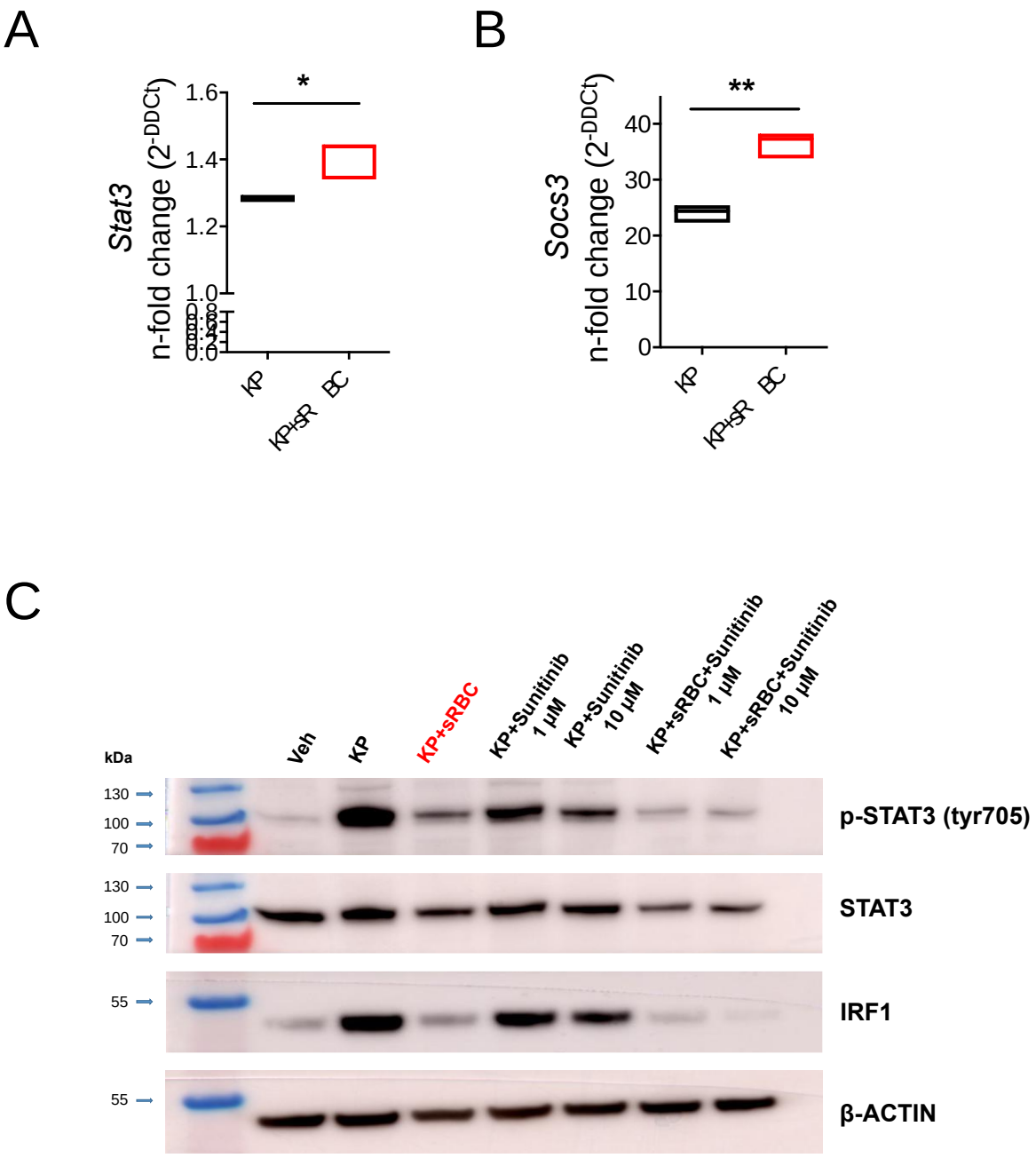

Figure 18: sRBC-mediated STAT1 suppression during *K. pneumoniae* infection is not due to STAT3 activation.

(A) *Stat3* and (B) *Socs3* gene expression in RAW cells challenged with *K. pneumoniae* (KP) or KP + sRBC for 2 h. Gene expression was evaluated by qPCR analysis. (A-B) Fold change relative to vehicle (PBS)-treated macrophages. Box plot indicates median and 25-75%, n=3 technical replicates per group. *p<0.05, **p<0.01 by two-tailed t test.

(C) p-STAT3, STAT3 and IRF1 in RAW macrophages challenged with vehicle (PBS), KP, KP + sRBC or KP + indicated concentrations of sunitinib for 4 h.

4.2.3 sRBC-mediated STAT1 suppression during *K. pneumoniae* infection is independent of BACH1 degradation and HO-1 induction.

Heme accumulation following erythrophagocytosis induces proteasome-dependent degradation of the transcriptional repressor BTB (bric-a-brac, tramtrack, broad complex) Domain and CNC (cap'n'collar) Homolog 1 (BACH1)[129,130] that results in de-repression of *Hmox1*[130] (Fig. 19A). As expected, we observed reduction in BACH1 expression in *K. pneumoniae*-infected macrophages following sRBC delivery (Fig. 19B). *Bach1* silencing enhanced *Hmox1* (Fig. 19C) but not *Stat1* transcription in response to *K. pneumoniae* (Fig. 19C). Moreover, *Bach1* silencing induced HO-1 expression but did not alter STAT1 protein expression in *K. pneumoniae*-infected macrophages (Fig. 19D). Based upon these findings, we concluded that BACH1 does not contribute to STAT1 suppression following *K. pneumoniae* + sRBC delivery.

HO-1 is the rate-limiting enzyme in heme catabolism yielding ferrous iron, carbon monoxide, and biliverdin. These biologically active end products, carbon monoxide and biliverdin, have been implicated as anti-inflammatory[131–133]. To determine whether sRBC-mediated STAT1 suppression in *K. pneumoniae*-infected macrophages is due to increased HO-1 induction, we silenced *Hmox1* in *K. pneumoniae*-infected macrophages challenged with sRBC. We achieved, on average, approximately 60% *Hmox1* knockdown in *K. pneumoniae*-infected macrophages with or without sRBC delivery (Fig. 19E). *Hmox1* silencing resulted in further suppression rather than increase in *Stat1* expression in *K. pneumoniae*-infected macrophages with sRBC delivery (Fig.

19E). This suggests that HO-1 induction does not mediate STAT1 suppression following sRBC delivery and may instead be vital for augmenting STAT1 expression during *K. pneumoniae* infection.

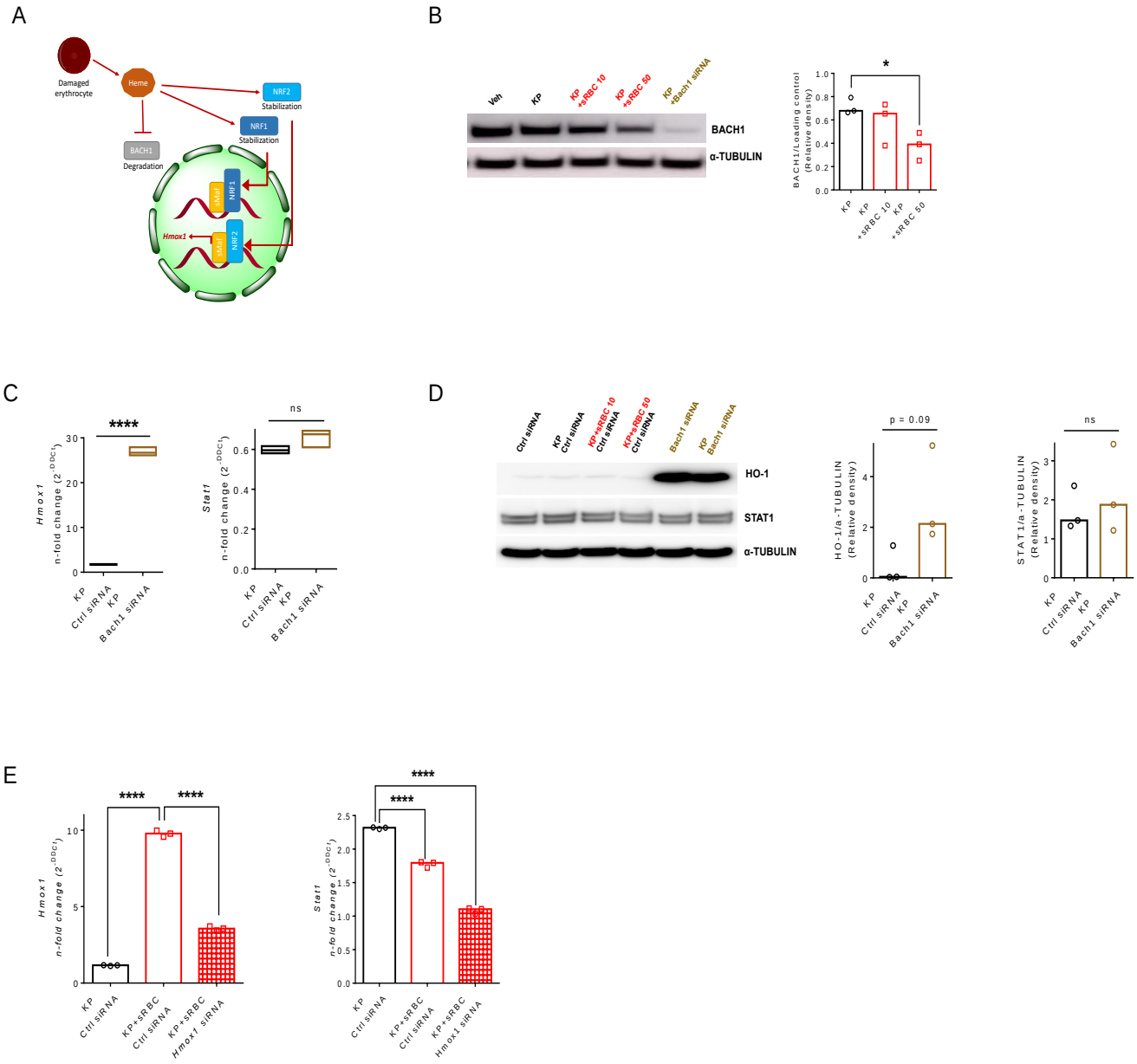

Figure 19: sRBC-mediated STAT1 suppression during *K. pneumoniae* infection is independent of BACH1 and HO-1 induction.

A) Schematic depicting Heme-BACH1-NRF1/2 interaction. Heme accumulation following erythrophagocytosis induces degradation of BACH1, stabilization of NRF1 and NRF2, with nuclear translocation of NRF2 resulting in *Hmox1* transcription. (B) BACH1 immunoblot in RAW cells challenged with vehicle (PBS), KP or KP + sRBC (50:1)

for 4 h. Blot is indicative of three independent experiments. *Left*, immunoblot. *Right*, relative density of three independent experiments. *p<0.05 by one-way ANOVA with Tukey's multiple comparisons test. (C) *Hmox1* and *Stat1* expression in RAW cells transfected with scrambled siRNA (control siRNA) or *Bach1* siRNA and subsequently challenged with KP for 4 h. n = 3 technical replicates per group, ****p<0.0001 by two-tailed t test. (D) HO-1, STAT1 immunoblot in RAW cells transfected with control siRNA or Bach1 siRNA and challenged with KP or KP + sRBC for 4 h. Blot is indicative of three independent experiments. *Left*, immunoblot. *Right*, relative density of three independent experiments. p=0.09 by two-tailed t test. (E) *Hmox1* and *Stat1* gene expression in RAW cells transfected with scrambled siRNA (control) or *Hmox1* siRNA and subsequently challenged with KP or KP+sRBC for 4 h. n = 3 technical replicates per group, ***p<0.001, ****p<0.0001 by one-way ANOVA with Tukey's multiple comparisons test. Data is average of 3 independent experiments. (C, E) Fold change relative to uninfected control siRNA-transfected RAW cells.

4.2.4 sRBC activates NRF2 during *K. pneumoniae* infection

Next, we examined the effect of cycloheximide on sRBC-induced transcriptional suppression during *K. pneumoniae* infection to determine whether transcriptional changes mediated by sRBC required novel protein synthesis. We show, as expected, that cycloheximide halts novel protein synthesis during *K. pneumoniae* infection (Fig. 20A). Remarkably, introduction of cycloheximide did not alter sRBC-mediated transcriptional changes during *K. pneumoniae* infection (Fig. 20B), indicating that effects induced by sRBC delivery do not require synthesis of a protein mediator but may instead involve mobilization of basally synthesized factors.

Heme accumulation following sRBC ingestion evokes nuclear translocation of nuclear factor erythroid 2-related factor 2 (NFE2L2, NRF2)[134] and activation of NRF2 is required for heme-iron transcriptional response following heme stimulation in macrophages[110,134]. In addition, NRF2 has been shown to regulate the innate immune response to microbial stimuli[135] and can

inhibit proinflammatory cytokine gene transcription possibly through direct DNA binding[136] or repress STING-dependent interferon response[137]—highlighting a potential link between heme-iron transcriptional response and the innate immune response. We demonstrate that sRBC delivery activates NRF2 as assessed by upregulation of NRF2 target genes NAD(P)H quinone oxidoreductase 1 (*Nqo1*)[138] and *Hmox1* in *K. pneumoniae*-infected macrophages challenged with sRBC (Fig. 20C), suggesting that NRF2 activation during bacterial infection may underlie the immunosuppressive effects of acute sRBC disposal.

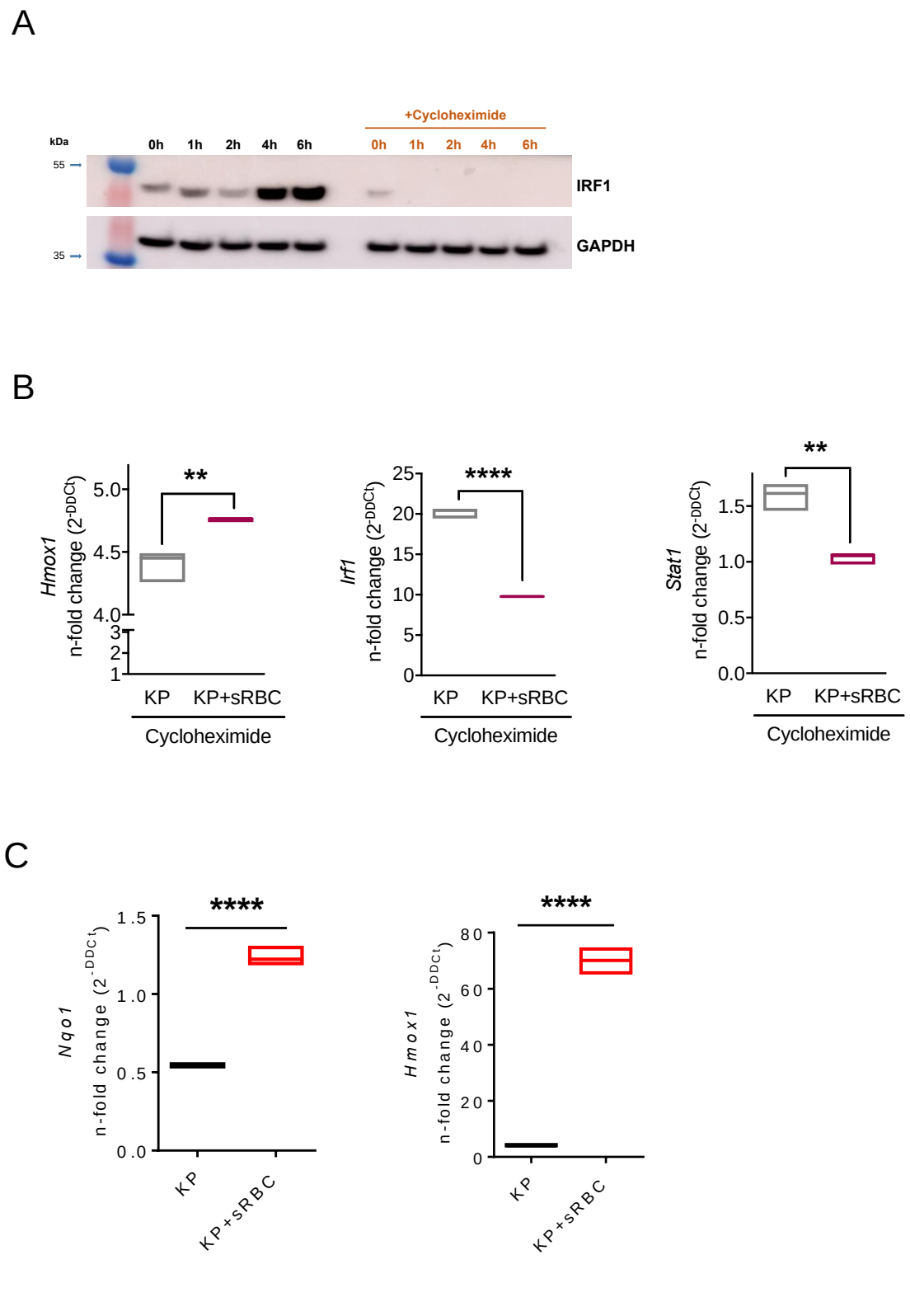

Figure 20: sRBC activates NRF2 during *K. pneumoniae* infection

(A) IRF1 in RAW cells stimulated with *K. pneumoniae* (KP) at indicated time points with or without cycloheximide. (B) *Hmox1, Irf1, Stat1* transcripts in RAW cells pre-incubated with cycloheximide and subsequently challenged with KP or KP + sRBC for 4 h. (C) NRF2 target genes, *Nqo1* and *Hmox1*, in RAW cells challenged with KP or KP + sRBC for 4 h. n = 3 technical replicates per group, ****p<0.001 by two-tailed t test. Data is indicative of 2 independent experiments.

4.2.5 Sulforaphane phenocopies the effect of heightened RBC disposal in macrophages during *K. pneumoniae* infection even in the absence of NRF2.

To determine whether NRF2 activation accounts for the effect of acute sRBC disposal on macrophages during bacterial infection, we utilized known NRF2 activator, isothiocyanate sulforaphane (SFN)[139], in *K. pneumoniae*-infected macrophages. As others have demonstrated, SFN dose-dependently increased NRF2 target genes *Hmox1*, *Nqo1*, and *Slc40a1* in macrophages during *K. pneumoniae* infection (Fig. 21A). Furthermore, treatment with SFN recapitulated *Irf1* and *Stat1* suppression observed with sRBC delivery in *K. pneumoniae*-infected macrophages (Fig. 21B). Immunoblot analyses of NRF2 and IRF1 corroborated transcript findings and revealed that dose-dependent increase in NRF2 stability correlated with dose-dependent reduction in IRF1 expression in SFN-treated macrophages during *K. pneumoniae* infection (Fig. 21C-D). As observed with sRBC delivery, interferon-related cytokine production, CCL5 and CXCL10—but not TNFα—was impaired in SFN-treated macrophages during *K. pneumoniae* infection (Fig. 21E). However, suppression of STAT1 target gene *Nos2* (Fig. 21F) and protein IRF1 (Fig. 21G) expression persisted even in the absence of NRF2, suggesting that NRF2 is necessary but not sufficient for sRBC-mediated STAT1 suppression.

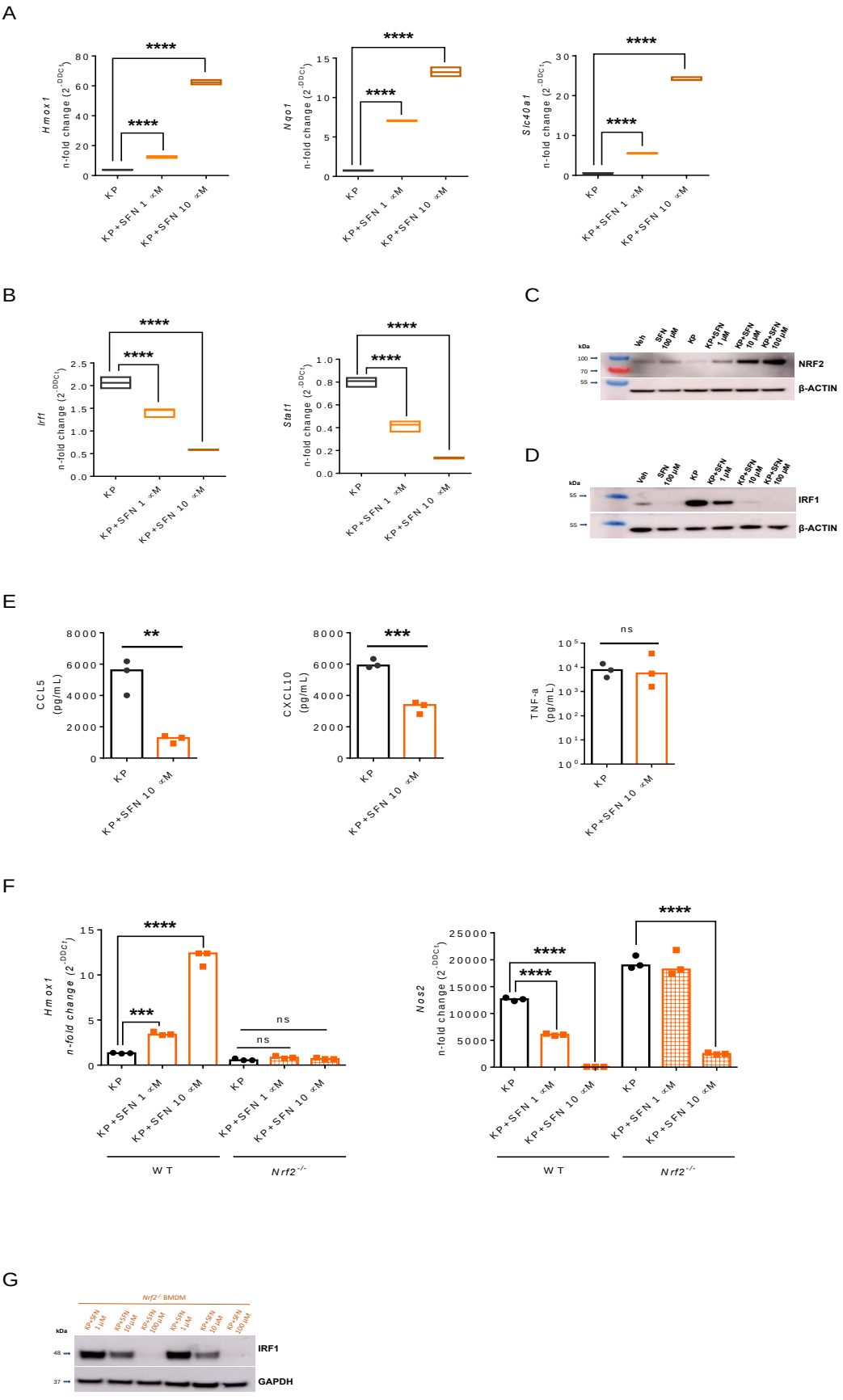
A
Hmox1 n-fold change (2-DDCt)
Nqo1 n-fold change (2-DDCt)
Slc40a1 n-fold change (2-DDCt)
****
KP
KP+SFN 1 μM
KP+SFN 10 μM
B
Irf1 n-fold change (2-DDCt)
Stat1 n-fold change (2-DDCt)
C
Veh
SFN 100 μM
KP
KP+SFN 1 μM
KP+SFN 10 μM
KP+SFN 100 μM
kDa
NRF2
β-ACTIN
D
IRF1
β-ACTIN
E
CCL5 (pg/mL)
CXCL10 (pg/mL)
TNF-a (pg/mL)
**
***
ns
F
Hmox1 n-fold change (2-DDCt)
Nos2 n-fold change (2-DDCt)
WT
Nrf2-/-
G
Nrf2-/- BMDM
IRF1
GAPDH

Figure 21: Sulforaphane phenocopies the effect of heightened RBC disposal in macrophages during *K. pneumoniae* infection even in the absence of NRF2.

(A) NRF2 target genes *Hmox1, Nqo1, Slc40a1* expression, (B) *Irf1* and *Stat1* gene expression in RAW cells incubated with indicated concentrations of sulforaphane (SFN) for 1 h. Following pre-incubation, cells were challenged with vehicle (PBS) or *Klebsiella pneumoniae* (KP, MOI 10:1) for 4 h. Gene expression was evaluated by qPCR analysis. Fold change relative to vehicle (0.07% ethanol)-treated RAW cells. Bar and whisker plot indicate median and 25-75%, n=3 technical replicates per group. **** $p<0.0001$ by two-tailed t test. (C) NRF2 and (D) IRF1 immunoblots in RAW cells challenged with vehicle (PBS), KP, or KP + SFN for 4 h. (E) CCL5, CXCL10, and TNF-α were measured in cell culture supernatant by ELISA 4 h post-infection. n=3 technical replicates per group. **$p<0.01$, ****$p<0.0001$ by two-tailed t test. (F) *Hmox1* and *Nos2* in BMDMs obtained from $Nrf2^{+/+}$ and $Nrf2^{-/-}$ mice challenged with KP or KP + SFN for 4 h. n=3 technical replicates per group, ***$p<0.001$ ****$p<0.0001$ by one-way ANOVA with Tukey's multiple comparisons test. Fold change relative to vehicle (0.07% ethanol)-treated BMDMs. (G) IRF1 immunoblot in $Nrf2^{-/-}$ BMDMs challenged with KP + increasing concentrations of SFN for 4h.

4.2.6 sRBC-mediated STAT1 suppression during *K. pneumoniae* infection requires NRF1 and NRF2 activation

In the absence of NRF2, heme-iron transcriptional responses, as assessed by *Hmox1* and *Slc40a1* expression, are greatly diminished in *K. pneumoniae*-infected $Nrf2^{-/-}$ macrophages challenged with sRBC (Fig. 22A). Though deletion of NRF2 prevented *Stat1* suppression in *K. pneumoniae* + sRBC- treated macrophages, NRF2 deficiency but did not fully restore *Stat1* induction (Fig. 22A). This finding reinforces the notion that NRF2 activation only partially accounts for sRBC-mediated STAT1 suppression during *K. pneumoniae* infection.

As Nuclear factor erythroid 2-related factor 1 (NFE2L1, NRF1) binds to similar cis-regulatory regions of antioxidant response elements as NRF2[140], we sought to determine whether *Nrf1* knockdown further boosts *Stat1* expression observed in *Nrf2*$^{-/-}$ macrophages challenged with *K. pneumoniae* and sRBC. We show that sRBC delivery activates NRF1 target gene Metallothionein 1 (*Mt1*)[141] in *K. pneumoniae*-infected macrophages challenged with sRBC (Fig. 22B). We utilized hemin as a surrogate RBC component in macrophages transfected with *Nrf1* siRNA. We achieved > 80% *Nrf1* knockdown in macrophages with or without *K. pneumoniae* and hemin challenge (Fig. 22C). *Nrf1* silencing reversed hemin-mediated *Stat1* suppression in *K. pneumoniae*-infected macrophages (Fig. 22D). Moreover, *Nrf2*$^{-/-}$ macrophages showed higher *Stat1* transcript compared to wildtype macrophages during *K. pneumoniae* infection but *Nrf1* knockdown further boosted *Stat1* transcript in *Nrf2*$^{-/-}$ macrophages (Fig. 22E), suggesting synergism between NRF1 and NRF2 in control of *Stat1* even in the absence of hemin. Collectively, these data show that while sRBC delivery induces HO-1 and activates NRF1 and NRF2 target genes, STAT1 suppression does not require HO-1 but is mediated, in part, by NRF1 and NRF2.

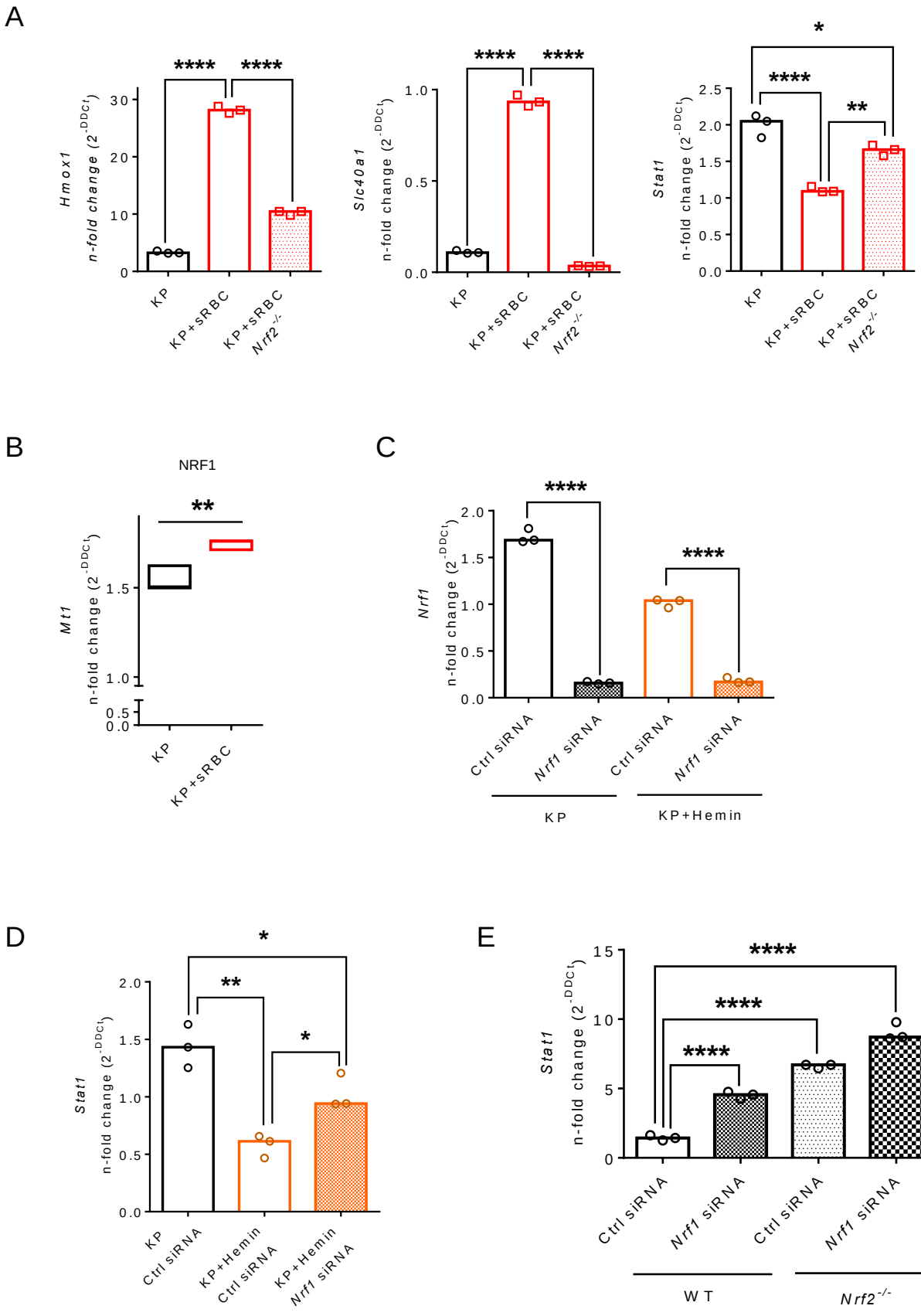
A
Hmox1
n-fold change (2-DDCt)
****
****
KP
KP+sRBC
KP+sRBC Nrf2-/-
Slc40a1
n-fold change (2-DDCt)
****
****
KP
KP+sRBC
KP+sRBC Nrf2-/-
Stat1
n-fold change (2-DDCt)
*
****
**
KP
KP+sRBC
KP+sRBC Nrf2-/-
B
NRF1
Mt1
n-fold change (2-DDCt)
**
KP
KP+sRBC
C
Nrf1
n-fold change (2-DDCt)
****
****
Ctrl siRNA
Nrf1 siRNA
Ctrl siRNA
Nrf1 siRNA
KP
KP+Hemin
D
Stat1
n-fold change (2-DDCt)
*
**
*
KP Ctrl siRNA
KP+Hemin Ctrl siRNA
KP+Hemin Nrf1 siRNA
E
Stat1
n-fold change (2-DDCt)
****
****
****
Ctrl siRNA
Nrf1 siRNA
Ctrl siRNA
Nrf1 siRNA
WT
Nrf2-/-

Figure 22: sRBC-mediated STAT1 suppression during *K. pneumoniae* infection requires NRF1 and NRF2 activation

(A) *Hmox1*, *Slc40a1*, and *Stat1* expression in bone marrow-derived macrophages (BMDMs) obtained from *Nrf2*$^{+/+}$ and *Nrf2*$^{-/-}$ mice challenged with KP or KP + sRBC for 4 h. n = 3 technical replicates per group, **p<0.01, ****p<0.0001 by one-way ANOVA with Tukey's multiple comparisons test. Data is indicative of 2 independent experiments. (B) NRF1 target gene (*Mt1*) expression RAW cells challenged with KP or KP + sRBC for 4 h. n = 3 technical replicates per group, **p<0.01 by two-tailed t test. Data is indicative of 2 independent experiments. (C) *Nrf1* and (D) *Stat1* expression in BMDMs transfected with control siRNA or *Nrf1* siRNA and subsequently challenged with KP or KP + Hemin (50 μM) for 4 h. n = 3 technical replicates per group, *p<0.05, **p<0.01, ****p<0.0001 by one-way ANOVA with Tukey's multiple comparisons test. (E) *Stat1* expression in BMDMs obtained from *Nrf2*$^{+/+}$ and *Nrf2*$^{-/-}$, transfected with control siRNA or *Nrf1* siRNA and subsequently challenged with KP for 4 h. (A) Fold change relative to vehicle (PBS)-treated BMDMs. (C-E) Fold change relative to uninfected control siRNA-transfected BMDMs.

4.3 Discussion

Under homeostasis, CNC-basic leucine zipper (bZIP) transcription factors, NRF1 and NRF2, are constitutively targeted for proteasomal degradation[140,142]. Undue heme exposure dysregulates proteasome activity resulting in cellular protein accumulation[143]. We demonstrate that sRBC delivery evokes NRF1 and NRF2 activity, as evidenced by increased *Mt1* and *Nqo1*, respectively, in infected macrophages. NRF2 has been shown to suppress innate immune response to viral[137] and microbial trigger[135,136]. Here, we uncover an additional role for NRF2 in tempering macrophage *Stat1* expression during *K. pneumoniae* infection. In contrast to NRF2, relatively little is known about NRF1 and its role in immune regulation, as targeted disruption of *Nrf1* results in

murine embryonic lethality due to impaired fetal liver erythropoiesis[144]. Though NRF1 and NRF2 appear to have distinct gene targets[141], NRF1 and NRF2 bind to overlapping antioxidant response element (ARE) sequences as obligate dimers with small musculoaponeurotic fibrosarcoma (sMaf) proteins[145]. Indeed, in contrast to late embryonic lethality (16.5–18.5 days) observed in *Nrf1* mutants[144], compound deficiency in both *Nrf1* and *Nrf2* leads to early lethality between embryonic days 9 and 10[146], indicating shared NRF1 and NRF2 functionality. In this study, we demonstrate that NRF1 and NRF2 synergistically temper *Stat1* during *K. pneumoniae* infection. The mechanism by which NRF1 and NRF2 regulate *Stat1* remains unclear. Though *Stat1* does not appear to contain any known ARE sequences in its promoter region, others have shown that NRF2 can bind and inhibit inflammatory cytokine gene expression in an ARE-independent manner[136]. Thus, NRF1 and NRF2 may directly bind to and block *Stat1* transcription or may induce a yet to be discovered mechanism that represses *Stat1* during *K. pneumoniae* infection.

BACH1, another bZIP transcription factor, heterodimerizes with sMaf proteins to repress *Hmox1* induction. Mice lacking BACH1 show resistance to experimental colitis due to constitutive HO-1 expression[147]. Moreover, HO-1 has well-documented roles in mitigating inflammation in various contexts[133,148–151], although the molecular mechanisms underpinning HO-1's anti-inflammatory properties remain elusive. Though HO-1 can be induced by a variety of stimuli, heme, derived from RBC breakdown, is one of its most potent inducers. We show here, following sRBC delivery, that neither BACH1 nor HO-1 is required for *Stat1* suppression induced by acute sRBC disposal during *K. pneumoniae* infection in macrophages. Furthermore, we show that the mechanism is independent of autocrine type I or II interferon receptor signaling as *Ifngr1*$^{-/-}$ and *Ifnar1*$^{-/-}$ bone marrow-derived macrophages retain ability to induce IRF1 with *K. pneumoniae* infection.

Lastly, STAT3-dependent SOCS3 activation has been shown to attenuate STAT1 activation in response to IL-6[152] and IFNα[153] stimulation. Furthermore, hepcidin-activated JAK2 in ferroportin-expressing macrophages, as occurs following sRBC delivery, phosphorylates STAT3 and may dampen inflammatory response to LPS[128]. Though we observed elevated *Stat3* and *Socs3* in *K. pneumoniae*-infected macrophages following sRBC delivery, pharmacological inhibition of STAT3 activation did not restore IRF1 induction to *K. pneumoniae* in infected macrophages challenged with sRBC. This indicates that STAT3 activation is not the primary mechanism for STAT1 suppression observed in our model, and other mechanisms, notably NRF1 and NRF2 activation, are at play here.

4.4 Methods

Animals

C57BL/6J, (#000664), *Ifnar1*$^{-/-}$ (#32045), *Ifngr1*$^{-/-}$ (#003288), and *Nrf2*$^{-/-}$ (#017009), mice were obtained from the Jackson Laboratory (Bar Harbor, ME). All mice were fed the same chow within the same room of the vivarium for at least 1 week prior to experimentation and animals were housed and maintained in a specific pathogen-free environment and studies were conducted in accordance with the Institutional Animal Care and Use Committee at the University of Pittsburgh.

Cell culture

RAW 264.7 cells (murine macrophage cell line) were obtained from ATCC. RAW cells were cultured in DMEM supplemented with 10% newborn calf serum (NCS) in a humidified

incubator 5% CO_2 at 37ºC. Bone marrow cells were isolated from adult male and female mice and cultured in DMEM supplemented with 20% fetal bovine serum (FBS), 30% L929-conditioned medium (LCM), and 1% penicillin-streptomycin (P/S) for 6–7 days in a humidified incubator 5% CO_2 at 37ºC to allow for differentiation into macrophages as previously described [154].

siRNA transfection

Macrophages were plated at a density of 1 x 10^5 or 2 x 10^5 cells per well of a 12-well tissue culture plate 24 h prior to transfection. On the day of transfection, cells were washed with RPMI 1640, incubated in RPMI containing 2% FBS, and transfected with 50–240 nM of siRNA using HiPerfect transfection reagent (Qiagen, Germany) according to the manufacturer's instructions. siRNAs were purchased from Dharmacon Inc. (now Horizon Discovery Ltd, United Kingdom). Negative pool of four control siRNAs was utilized as control. Experiments were conducted 24–48 h post-transfection and transcription efficiency was determined by qRT-PCR and immunoblot.

Small molecule stimulation

BAY 11-7082 was obtained from Dr. Saumendra N. Sarkar. Sunitinib (#PZ0012) and cycloheximide (#C7698) were purchased from Sigma-Aldrich (St. Louis, MO). Sulforaphane (#10496) was purchased from Cayman Chemical Company (Ann Arbor, MI). BAY 11-7082, sunitinib, and cycloheximide were dissolved in DMSO prior to administration. Final concentration of DMSO administered to cells was ≤ 1%. Sulforaphane was administered in a solution of ethanol, final concentration of sulforaphane administered to cells was 0.07%.

Immunoblot

Macrophages were lysed and protein was extracted as detailed in 4.4. After protein transfer, membranes were incubated with 1:1000 dilution of specific antibodies to phospho-STAT3 (tyr 705, #9131) STAT3 79D7 (#4904), NRF2 D1Z9C (#12721), and IRF1 (#8478) obtained from Cell Signaling Technology (Danvers, MA). Membranes also were incubated with 1:2000 dilution of antibody to β-ACTIN (#4970) obtained from Cell Signaling Technology (Danvers, MA) or 1:1000 dilution of antibody to α-TUBULIN (ab4074) obtained from Abcam (United Kingdom) as loading control. Antibodies to BACH1 (HRP conjugated, sc-271211) and HO-1 (HRP conjugated, sc-390991) were obtained from Santa Cruz Biotechnology (Dallas, TX) and utilized in 1:1000 dilutions.

Quantification and statistical analysis

Results are reported as the median unless otherwise indicated. For comparisons between two groups, a two-tailed t test was undertaken. For comparisons of multiple groups, a one-way ANOVA with Tukey's multiple comparisons test was undertaken. GraphPad Prism software version 6.0 was used for statistical analysis (La Jolla, CA). A *p*-value less than 0.05 was considered significant.

5.0 The porphyrin moiety of heme is necessary and sufficient for NRF1/NRF2 activation and STAT1 suppression

5.1 Rationale

In mammals, circulating erythrocytes are uniquely enucleated cells with no well-defined subcellular metabolic structures[155]. Their membranes are comprised of two domains; (1) a lipid bilayer, composed of nearly equal parts of lipid and protein, and (2) a cytoskeleton composed of a filamentous network of several proteins[156]. Unlike in other mammalian cells, RBC cytoskeleton does not contain the structural protein tubulin and is not involved in cell motility or phagocytosis[156], instead, the cytoskeleton is critical for RBC flexibility and lipid organization[157]. Glycolipids, phosphatidylcholine, and sphingomyelin are found in the outer layer of the lipid domain, whereas phosphatidylinositol, phosphatidylethanolamine, and phosphatidylserine are found in the inner layer of the lipid domain facing the cytoplasm[156]. Redistribution of membrane phospholipids, as occurs with aging or stress[5,158], results in exposure of phosphatidylserine, an "eat-me" signal for macrophages. While it remains to be fully characterized how RBCs are recognized and internalized by macrophages, engulfment of apoptotic or stressed RBC may modulate the immune response through induction of liver X receptor (LXR) signaling in macrophages[159] and may represent a mechanism of immunosuppression in our acute infection model.

In contrast to the hundreds of unique proteins found in the RBC membrane[160], hemoglobin is, by far, the predominant protein encountered in the RBC cytoplasm[161]. Hemoglobin, and in particular, its catabolic products heme and iron, have been shown to exert profound

immunomodulatory effects on immune cells[80,83,162,163]. Thus, we sought to characterize which component of RBC—membrane-associated or intracytoplasmic—was essential for producing the phenotype observed in our two-hit model.

5.2 Results

5.2.1 Heme is the constituent of RBC that mediates STAT1 suppression during *K. pneumoniae* infection.

To determine which component of sRBC mediates suppression of STAT1, macrophages were challenged with vehicle (PBS), sRBC, stroma-free sRBC lysates, and ghost RBC prepared from equivalent number of sRBC with or without *K. pneumoniae* infection. IRF1 expression was utilized as a STAT1 target readout. While *K. pneumoniae* strongly induced IRF-1 expression, sRBC addition suppressed IRF1 expression that was recapitulated by addition of sRBC lysate but not sRBC ghost (Fig. 23A). Hemoglobin is the principal cytoplasmic component of RBC[161] and purified hemoglobin recapitulated sRBC-mediated IRF1 suppression during *K. pneumoniae* infection (Fig. 23B).

The heme moiety of hemoglobin has been implicated as an immunomodulating agent and can trigger[82,164] or dampen[97,165] the immune response. Though heme and hemin have been shown to directly bind to TLR4 and induce proinflammatory cytokine secretion[82,166], hemin alone was a weak activator of STAT1 in macrophages but, as expected, potently induced heme oxygenase-1 (HO-1) (Fig. 23C-D). However, we noted that hemin dose-dependently inhibited *K. pneumoniae*-induced STAT1 phosphorylation, at both its serine and tyrosine sites, in addition to total STAT1

and IRF1 expression (Fig. 23D). Furthermore, CXCL10—but not TNFα—was dose-dependently suppressed by hemin in *K. pneumoniae*-infected macrophages (Fig. 23E), indicating that hemin recapitulates sRBC-mediated STAT1 suppression.

To delineate extracellular versus intracellular heme contribution to STAT1 suppression in our model, RAW macrophages challenged with *K. pneumoniae* and sRBC were incubated in the presence or absence of hemopexin (HPX). HPX is hydrophilic with no known transcellular transport mechanism and would thus chelate extracellular heme but not heme concentrated intracellularly. As expected, sRBC delivery to *K. pneumoniae*-infected macrophages potently induced HO-1 and markedly suppressed STAT1 activation and total STAT1 protein expression (Fig. 23F). However, extracellular heme scavenging by hemopexin failed to restore STAT1 (Fig. 23F) or STAT1-dependent CXCL10 (Fig. 23G) in macrophages challenged with *K. pneumoniae* and sRBC. Collectively, these findings suggest that intracellular heme resulting from sRBC breakdown is responsible for STAT1 suppression during *K. pneumoniae* infection.

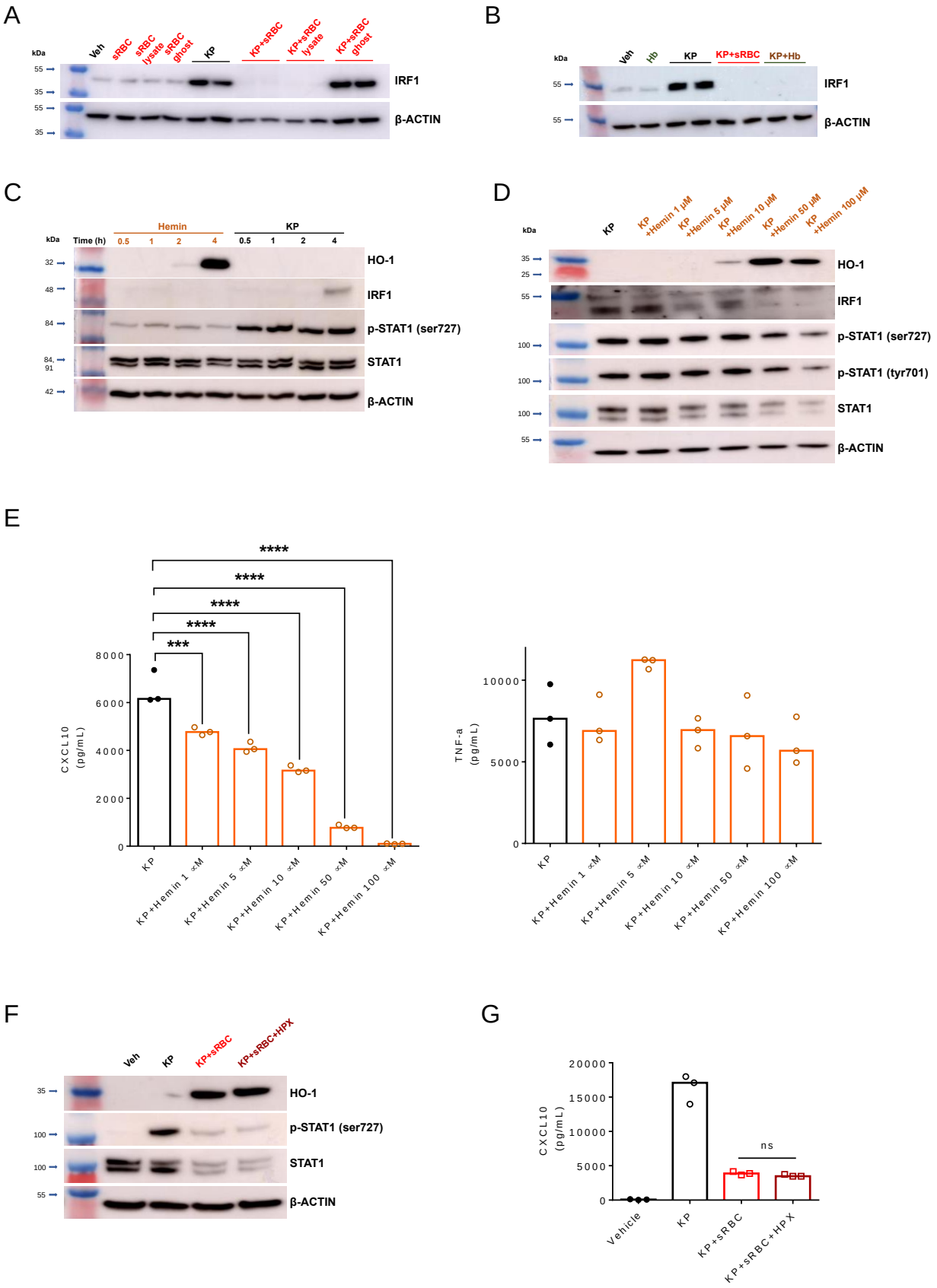
A
kDa
Veh
sRBC
sRBC lysate
sRBC ghost
KP
KP+sRBC
KP+sRBC lysate
KP+sRBC ghost
55
35
IRF1
β-ACTIN
B
Veh
Hb
KP
KP+sRBC
KP+Hb
C
Hemin
KP
Time (h)
0.5
1
2
4
32
48
84
84, 91
42
HO-1
IRF1
p-STAT1 (ser727)
STAT1
β-ACTIN
D
KP
KP +Hemin 1 μM
KP +Hemin 5 μM
KP +Hemin 10 μM
KP +Hemin 50 μM
KP +Hemin 100 μM
35
25
100
HO-1
IRF1
p-STAT1 (ser727)
p-STAT1 (tyr701)
STAT1
β-ACTIN
E
****
****
****
****
***
CXCL10 (pg/mL)
8000
6000
4000
2000
0
KP
KP+Hemin 1 ∝M
KP+Hemin 5 ∝M
KP+Hemin 10 ∝M
KP+Hemin 50 ∝M
KP+Hemin 100 ∝M
TNF-a (pg/mL)
10000
5000
F
Veh
KP
KP+sRBC
KP+sRBC+HPX
HO-1
p-STAT1 (ser727)
STAT1
β-ACTIN
G
CXCL10 (pg/mL)
20000
15000
10000
5000
0
ns
Vehicle
KP
KP+sRBC
KP+sRBC+HPX

Figure 23: Heme is the constituent of RBC that mediates STAT1 suppression during *K. pneumoniae* infection. IRF1 immunoblots in (A) RAW cells challenged with vehicle (PBS), sRBC (30 sRBC:1 Mφ), sRBC lysates obtained from equivalent numbers of sRBC, ghosts obtained from equivalent numbers of sRBC, *Klebsiella pneumoniae* (KP, MOI 10:1), KP + sRBC, KP + sRBC lysate or KP + sRBC ghost for 4 h, and (B) RAW cells challenged with vehicle, purified hemoglobin from equivalent number of lysed RBC (Hb), KP, KP + sRBC or KP + Hb for 4 h. Blot is indicative of two independent experiments. (C) HO-1, IRF1, p-STAT1 (ser727), and STAT1 in RAW cells challenged with hemin (100 μM) or KP at 0.5, 1, 2 or 4 h. (D) HO-1, IRF1, p-STAT1 (ser727), p-STAT1 (tyr 701), and STAT1 in RAW cells challenged with KP and increasing concentrations of hemin for 4 h. (E) CXCL10 and TNF-α were measured in cell culture supernatant by ELISA 4 h post-infection. n=3 technical replicates per group. ***$p<0.001$, ****$p<0.0001$ by one-way ANOVA with Tukey's multiple comparisons test. (F) HO-1, p-STAT1 (ser727), and STAT1 in bone marrow-derived macrophages (BMDM) challenged with vehicle (PBS), KP, KP + sRBC 50:1 or KP + sRBC + hemopexin (HPX, 200 μg/mL) for 4 h. (G) CXCL10 was measured in cell culture supernatant by ELISA 4 h post-infection. n=3 technical replicates per group. Comparisons were made by one-way ANOVA with Tukey's multiple comparisons test.

5.2.2 Depletion of hemoglobin from RBC limits *K. pneumoniae* extrapulmonary dissemination.

Next, we tested whether depletion of hemoglobin from RBC reverses the profound extrapulmonary dissemination induced by sRBC delivery during *K. pneumoniae* intrapulmonary infection. Mice were challenged with either PBS vehicle, washed sRBC, or hemoglobin-depleted ghost RBC prepared from sRBC obtained from the same donor mice. There were no differences in lung bacterial burden in infected mice receiving either vehicle, sRBC or sRBC ghost following bacterial inoculation (Fig. 24A). However, depletion of hemoglobin from sRBC severely limited extrapulmonary dissemination of *K. pneumoniae* to the spleen and liver (Fig. 24B-C). No

significant differences were observed in the blood compartment among the three groups (Fig. 24D). Thus, these findings indicate that hemoglobin contained within RBC is required for reproducing the phenotype.

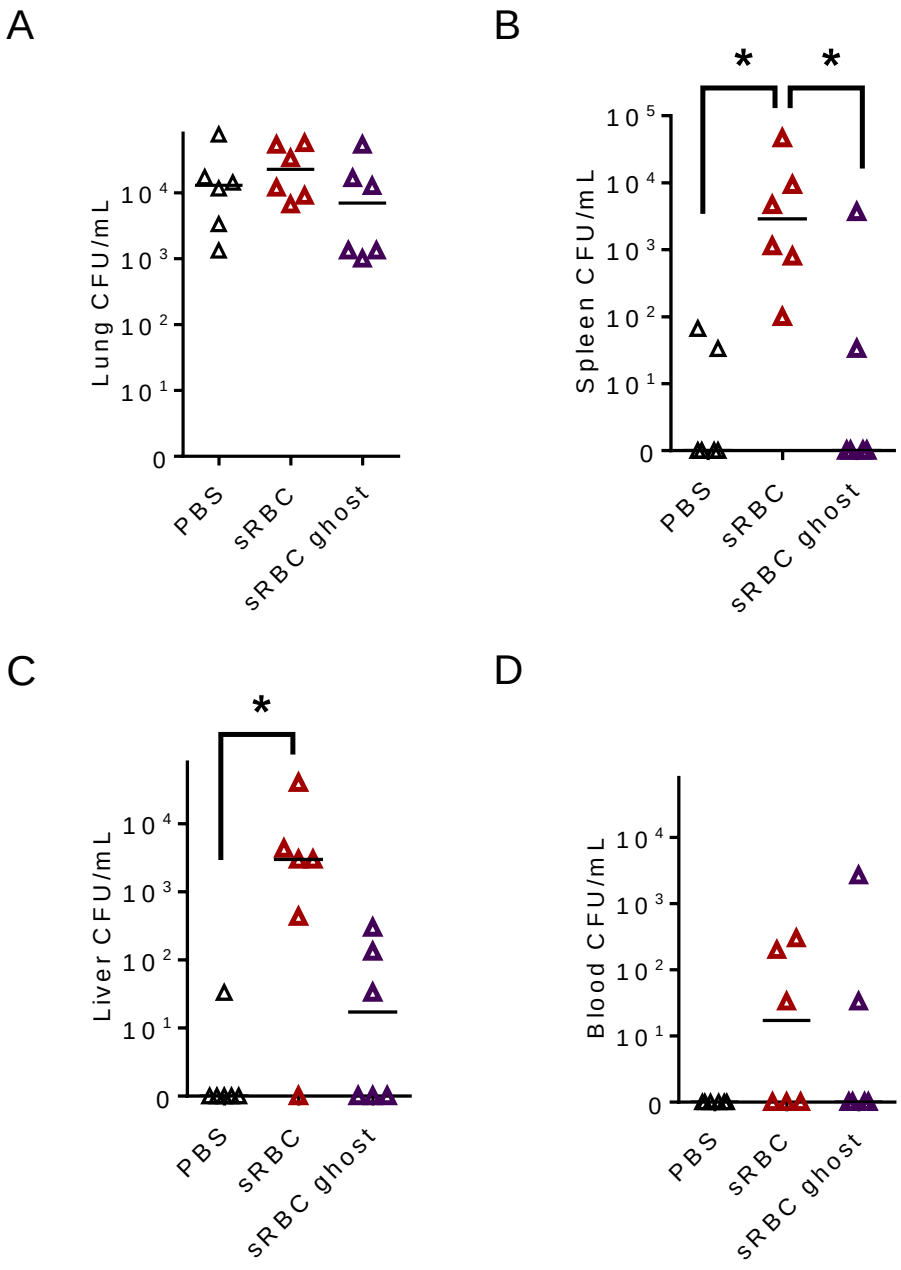

Figure 24: Depletion of hemoglobin from RBC limits *K. pneumoniae* extrapulmonary dissemination.

EntB ybtS K. pneumoniae mutant was instilled intratracheally into C57BL/6 mice (10^3 CFU inoculum) and followed by challenge with PBS vehicle, sRBC or sRBC ghost. Mice were euthanized and tissue harvested 24 h post-infection. Bacterial burden was estimated in (A) lung, (B) spleen, (C) liver homogenates, and blood as CFU per milliliter. Each data point indicates individual mice, n = 6 mice per group. Lines indicate median. *p <0.05 by Kruskal-Wallis test with Dunn's multiple comparisons

5.2.3 Iron is dispensable for sRBC-mediated STAT1 suppression during *K. pneumoniae* infection.

Iron liberated from heme by HO-1 may weaken immunity either by direct iron provision to the pathogen or through dysregulated iron recycling in the host cell. To investigate the contribution of iron to heme-mediated STAT1 suppression during *K. pneumoniae* infection, we utilized iron chelators Deferasirox (DFX) and Deferoxamine (DFO). DFX is lipophilic and can bind intracellular ferric iron in a 2:1 binding ratio (Fig. 25A)[167,168]. DFO, on the other hand, is highly hydrophilic with no known transcellular transport mechanism and binds extracellular ferric iron in a 1:1 binding ratio (Fig. 25A) [169]. Neither chelation of host intracellular iron by DFX nor chelation of extracellular iron available to pathogen by DFO restored STAT1 activation or total STAT1 expression in *K. pneumoniae*-infected macrophages challenged with hemin (Fig. 25B). STAT1-dependent CXCL10 secretion in macrophages challenged with *K. pneumoniae* + hemin was also not rescued by introduction of iron chelators (Fig. 25C). Moreover, transfusion of iron dextran that approximates iron contained in one unit of packed RBC did not recapitulate enhanced extrapulmonary dissemination observed with sRBC delivery in *K. pneumoniae*-infected mice (Fig. S25D-G) or *entB ybtS K. pneumoniae* mutant-infected mice (Fig. 25H-K), indicating that enhanced iron delivery is not the major mechanism for increased extrapulmonary dissemination observed with sRBC delivery.

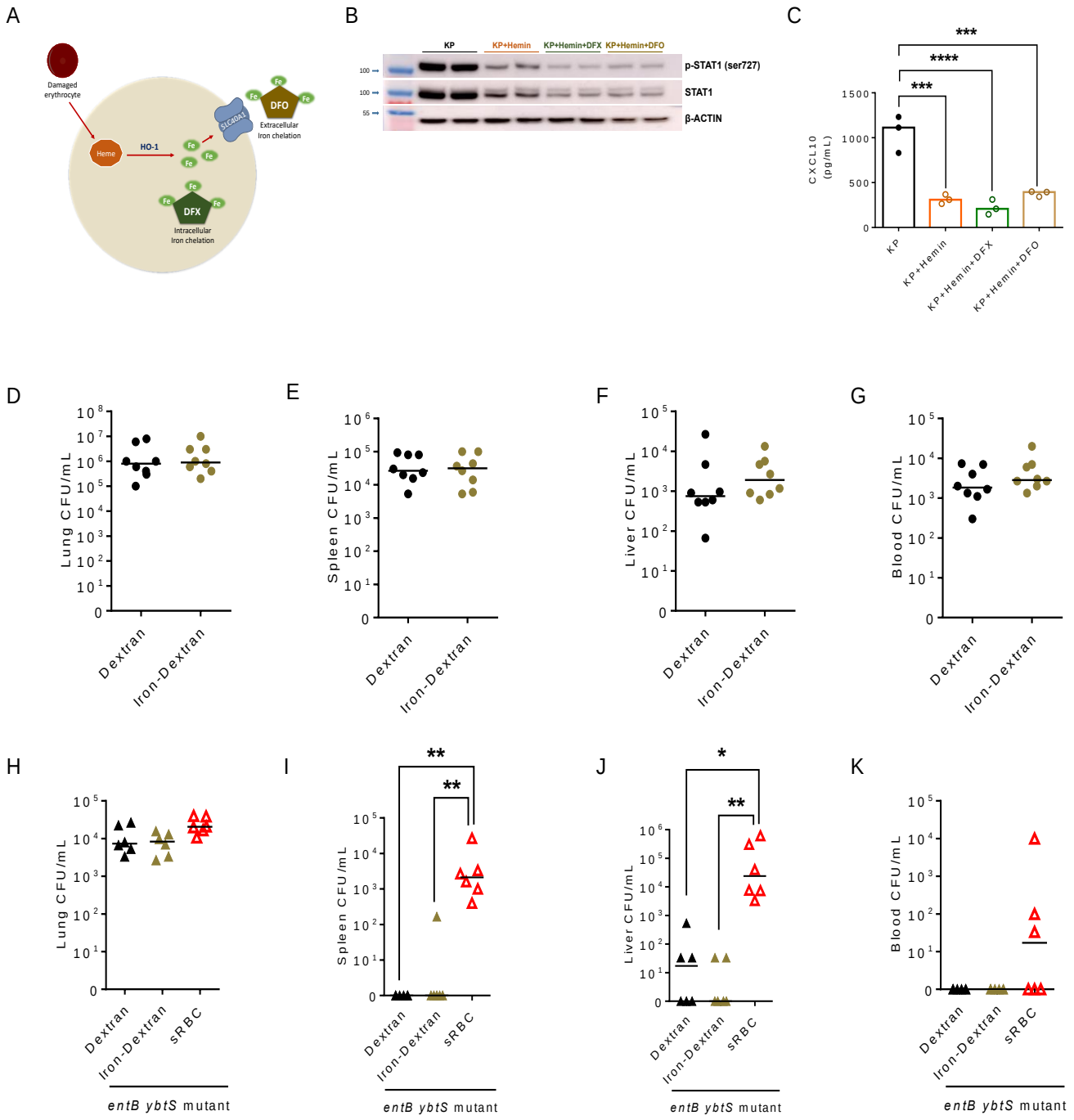

Figure 25: Iron is dispensable for sRBC-mediated STAT1 suppression during *K. pneumoniae* infection.

(A) Schematic depicting mechanism of action of Deferasirox (DFX) and Deferoxamine (DFO). (B) STAT1 immunoblot in BMDMs challenged with *Klebsiella pneumoniae* (KP, MOI 10:1), KP + Hemin (25 µM), KP + Hemin

+ DFX (300 µM), KP + Hemin + DFO (300 µM) for 4 h. All groups contained vehicle (DMSO, ~1%). Blot is indicative of 2 independent experiments. (C) CXCL10 was measured in cell culture supernatant by ELISA 4 h post-infection. n = 3 technical replicates per group, ***p<0.001, ****p<0.0001 by one-way ANOVA with Tukey's multiple comparisons test. (D–G) KP was instilled intratracheally into C57BL/6 mice and followed by transfusion of dextran or iron dextran (total 200 µg iron). Bacterial burden is shown as CFU/mL in (D) lung, (E) spleen, (F) liver homogenates, and (G) blood at 24 hours. Each point indicates individual mice, n=8 per group, line indicates the median, no statistical significance by Mann-Whitney U two-tailed test. (H-K) *EntB ybtS* KP mutant lacking siderophore production was instilled intratracheally into C57BL/6 mice and followed by transfusion of dextran or iron dextran (total 200 µg iron) or sRBC. Bacterial burden is shown as CFU/mL in (H) lung, (I) spleen, (J) liver homogenates, and (K) blood at 24 hours. Each point indicates individual mice. Line indicates median. n=6 per group, *p<0.05, **p<0.01, by Kruskal-Wallis test with Dunn's multiple comparisons.

5.2.4 The porphyrin moiety of heme recapitulates sRBC-mediated NRF1/2 activation and STAT1 suppression during *K. pneumoniae* infection.

Given these findings, we tested whether a metal within the porphyrin ring was necessary for NRF1/2 activation and STAT1 suppression observed in macrophages challenged with *K. pneumoniae* and hemin. We utilized hemin (iron protoporphyrin IX, FePPIX), cobalt-substituted protoporphyrin IX (CoPPIX), and protoporphyrin IX (PPIX) which lacks a metal ion at its center (Fig. 26A). The metalloporphyrins, FePPIX and CoPPIX, activated NRF1 and NRF2 target genes, as assessed by *Mt1* and *Nqo1* induction, respectively (Fig. 26B) and induced *Hmox1* in *K. pneumoniae*-infected macrophages (Fig. 26C). PPIX also activated NRF1 and NRF2 target genes (Fig. 26B) but did not induce *Hmox1* in *K. pneumoniae*-infected macrophages (Fig. 26C). Interestingly, the presence of a metal ion within the porphyrin macrocycle appeared dispensable as all three protoporphyrins—FePPIX, CoPPIX and PPIX—suppressed *Stat1* in *K. pneumoniae*-

infected macrophages (Fig. 26C). STAT1-dependent CXCL10 secretion was also impaired by all three protoporphyrins (Fig. 26D). PPIX dose-dependently degraded BACH1 but, unlike hemin, did not induce HO-1 protein expression in *K. pneumoniae*-infected macrophages (Fig. 26E). As observed with hemin, PPIX dose-dependently suppressed STAT1 activation and total STAT1 protein expression in *K. pneumoniae*-infected macrophages (Fig. 26E). Moreover, FePPIX and PPIX suppressed IRF1 (Fig. 26F) and CXCL10, but not TNFα secretion (Fig. 26G), in *K. pneumoniae*-infected human monocyte-derived macrophages, suggesting that response is conserved in human macrophages. Collectively, these findings indicate that the presence of iron within the porphyrin ring is not essential for STAT1 suppression during *K. pneumoniae* infection.

A

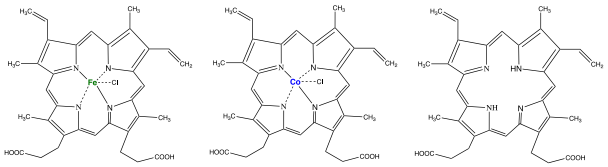
Fe
Co
HN
NH
HOOC
COOH

B

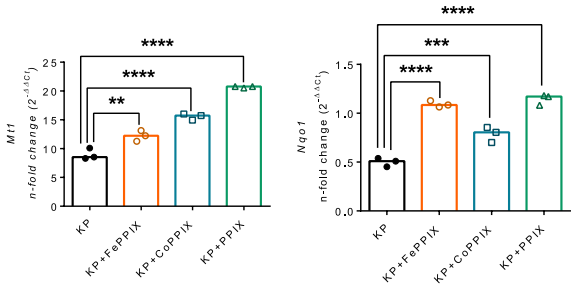
Mt1
n-fold change (2^-ΔΔCt)
Nqo1
KP
KP+FePPIX
KP+CoPPIX
KP+PPIX
****
***
**

C

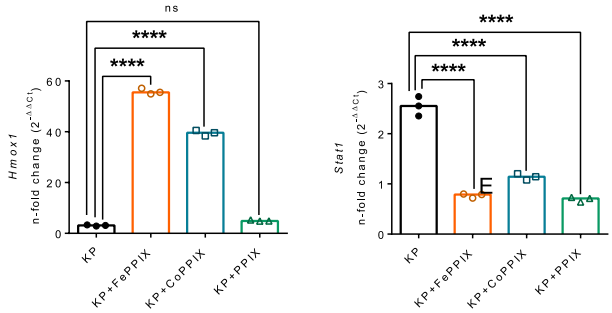
Hmox1
Stat1
n-fold change (2^-ΔΔCt)
ns
****
KP
KP+FePPIX
KP+CoPPIX
KP+PPIX

D

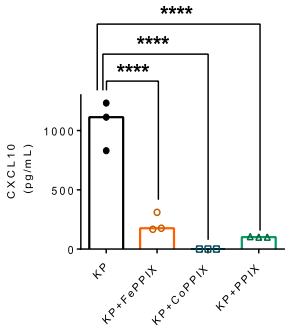
CXCL10
(pg/mL)
****
KP
KP+FePPIX
KP+CoPPIX
KP+PPIX

E

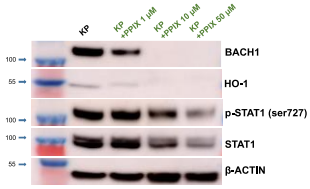
KP
KP +PPIX 1 μM
KP +PPIX 10 μM
KP +PPIX 50 μM
BACH1
HO-1
p-STAT1 (ser727)
STAT1
β-ACTIN

F

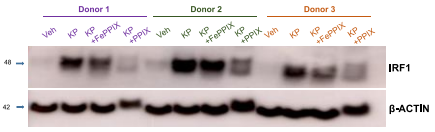
Donor 1
Donor 2
Donor 3
Veh
KP
KP +FePPIX
KP +PPIX
IRF1
β-ACTIN

G

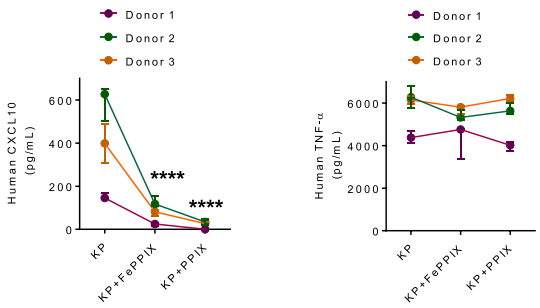
Donor 1
Donor 2
Donor 3
Human CXCL10
(pg/mL)
Human TNF-α
(pg/mL)
****
KP
KP+FePPIX
KP+PPIX

Figure 26: The porphyrin moiety of heme recapitulates sRBC-meduated NRF1/2 activation and STAT1 suppression during *K. pneumoniae* infection.

(A) Chemical structures of hemin (iron protoporphyrin IX, FePPIX), cobalt protoporphyrin IX (CoPPIX), and protoporphyrin IX (PPIX). (B) NRF1 target gene (*Mt1*) expression and NRF2 target gene (*Nqo1*) expression in BMDMs challenged with *K. pneumoniae* (KP), KP + FePPIX (50 μM), KP + CoPPIX (50 μM), KP + PPIX (50 μM) for 4 h. (C) *Hmox1* and *Stat1* gene expression, (D) CXCL10 secretion in BMDMs challenged with KP, KP + FePPIX (50 μM), KP + CoPPIX (50 μM), KP + PPIX (50 μM) for 4 h. (B–C) Fold change relative to vehicle (PBS)-treated BMDMs. (B-D) n = 3 technical replicates per group, **p<0.01, ***p<0.001, ****p<0.0001. (E) BACH1, HO-1, p-STAT1, total STAT1, and β-ACTIN immunoblot in BMDMs challenged with KP and increasing concentrations of PPIX. (F) IRF1 and β-ACTIN immunoblot in human monocyte-derived macrophages (HMDM) challenged with vehicle (PBS), KP, KP + FePPIX (25 μM) or KP + PPIX (25 μM) for 4 h. (G) CXCL10 and TNFα secretion from HMDMs in (I). n = 3 donors, ****p<0.0001 by two-way ANOVA with Tukey's multiple comparisons test.

5.2.5 Non-iron porphyrin recapitulates sRBC-induced *K. pneumoniae* extrapulmonary dissemination.

Lastly, we tested whether porphyrin lacking iron recapitulates extrapulmonary dissemination seen with sRBC delivery in *K. pneumoniae*-infected mice. Mice were intratracheally instilled with *K. pneumoniae* and challenged an hour later with vehicle, CoPPIX 5 mg/kg or CoPPIX 25 mg/kg. No differences in bacterial burden in the lung (Fig. 27A) or spleen (Fig. 27B) were observed among the three groups 24 h post-*K. pneumoniae* instillation. Notably, we observed increased extrapulmonary dissemination to the liver, the primary organ that supports rapid RBC removal during RBC damage[19], in *K. pneumoniae*-infected mice challenged with CoPPIX 25 mg/kg (Fig. 27C). Though there was a trend towards dose-dependent increase in blood bacterial

burden of *K. pneumoniae*-infected mice challenged with CoPPIX, this did not achieve statistical significance (Fig. 27D). Taken together, these findings reinforce the notion that iron is dispensable for STAT1 suppression and extrapulmonary bacterial proliferation observed with sRBC delivery to *K. pneumoniae*-infected mice.

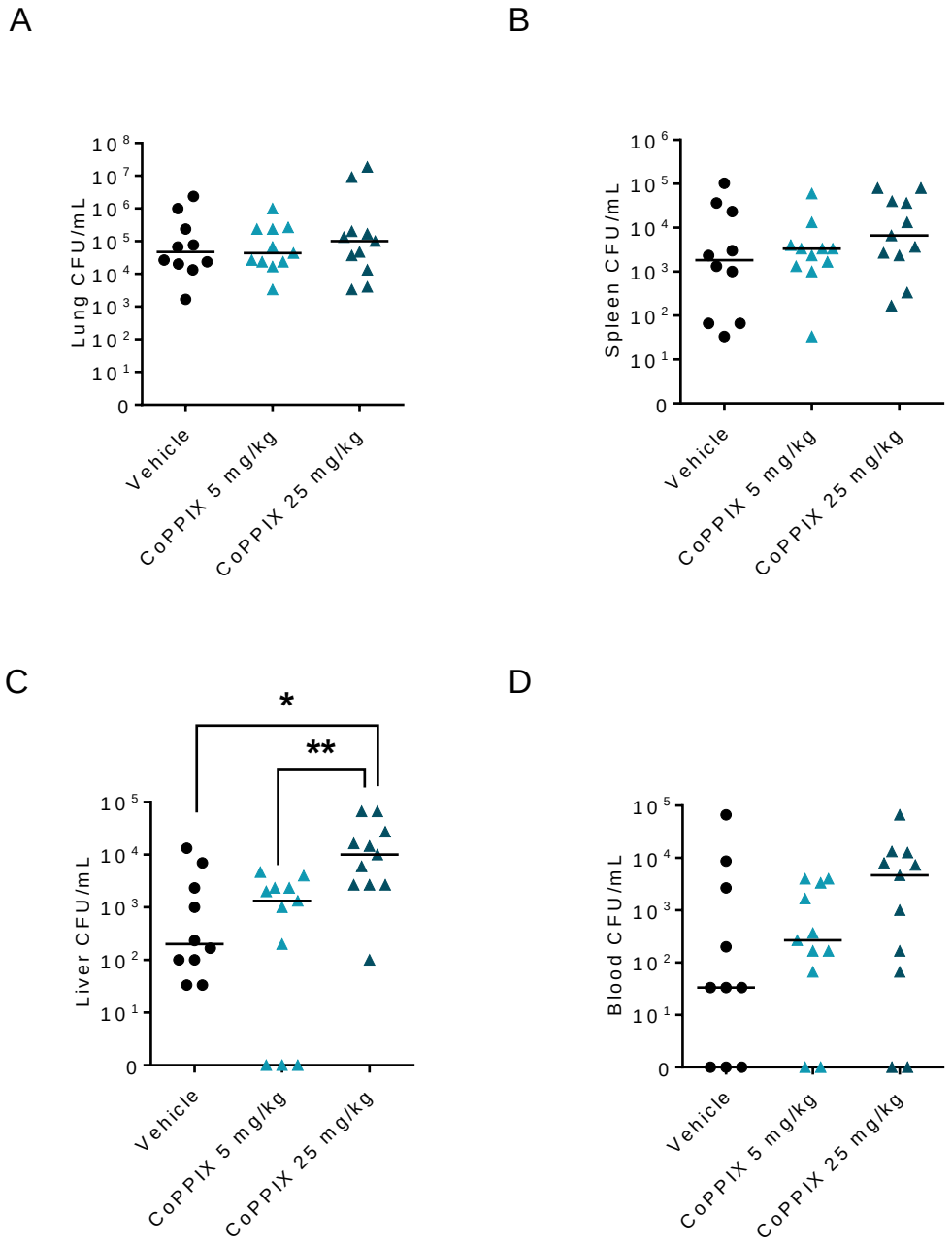

Figure 27: Non-iron porphyrin recapitulates sRBC-induced *K. pneumoniae* extrapulmonary dissemination.

K. pneumoniae (KP) was instilled intratracheally into C57BL/6 mice and followed by intraperitoneal challenge with vehicle (2.5% DMSO) or CoPP (5 mg/kg, 25 mg/kg) 1 h post-KP instillation. Bacterial burden was obtained from (A) lung, (B) spleen, (C) liver tissue homogenates, and (D) blood of mice 24 h following KP infection and reported as

CFU/mL. Each point indicates individual mice, n = 10–11 mice per group combined from two independent studies. Line indicates median. *p<0.05, **p<0.01 by Kruskal-Wallis test with Dunn's multiple comparisons.

5.3 Discussion

Excess heme handling by macrophages occurs as a consequence of several pathologies where there is increased circulation of damaged RBC precipitating 'on-demand' mononuclear phagocytic uptake—including hemoglobinopathies[170,171], RBC membrane disorders[20], severe infections [21,22,77,97], and transfusion of storage-damaged RBC [95]. Though iron acquisition from the host during infection has been regarded as an important mechanism of enhanced pathogenicity, we present the novel finding that heme, in particular its porphyrin moiety, suppresses a critical transcription factor STAT1 and impairs host defense.

Owing to its potent pro-oxidant activity and studies implicating iron overload in disruption of interferon signaling[172,173], it came as a surprise that iron appeared dispensable for NRF1 and NRF2 activation, and subsequent STAT1 suppression. Our findings indicate that CoPPIX and PPIX lacking a metal ion recapitulate heme-mediated NRF1 and NRF2 activation in macrophages during *K. pneumoniae* infection. PPIX potently suppressed STAT1 and its downstream effectors, IRF1 and CXCL10, in both mouse and human macrophages. Furthermore, CoPPIX—which, unlike FePPIX, does not yield iron that is of benefit to the pathogen—enhanced bacterial proliferation in the liver during *K. pneumoniae* infection, affirming that provision of a readily available source of iron is not the primary mechanism for enhanced *K. pneumoniae* pathogenicity following sRBC delivery.

Cellular heme levels are tightly controlled[174] as perturbations in heme homeostasis may underlie the pathophysiology of many life-threatening hematological disorders affecting millions of people worldwide. The primary source of heme in the mammal is the RBC and the primary cell responsible for clearing damaged RBC from circulation is the macrophage. The macrophage is also at the forefront of mucosal immunity, yet the impact of intracellular heme perturbations on macrophage effector function remains poorly understood. Here, we show that heme, due to its porphyrin ring, activates NRF1/NRF2 target genes and impairs macrophage STAT1 expression during infection. Our findings demonstrate that the detrimental effects of excess heme extend beyond its propensity as an alarmin[175] and establish a previously unknown link between cellular heme metabolism and regulation of immune response with important implications for infection and inflammation.

5.4 Methods

Human subjects

Peripheral whole blood (30 mL) was obtained from healthy adult volunteers. All subjects underwent venipuncture after informed written consent and ethnicities and gender were identified by self-reporting. Male and female subjects were included. Following collection, monocytes were isolated from whole blood as previously described[176], and utilized in the *in vitro* study in a de-identified manner. The Institutional Review Board of the University of Pittsburgh approved the study (#IRB0410173).

Purification of mouse hemoglobin

The process for purification of hemoglobin from RBC has been previously described[177]. Briefly, initial sample was loaded in a chelating sepharose fast flow resin charged with Zn^{2+} and equilibrated in 20 mM Tris, 500 mM NaCl, pH 8.3. Column was washed with 20 mM Tris, 500 mM NaCl, pH 8.3 (Flowthrough sample #1). Column was washed with 200 mM Tris, pH 8.3 (Flowthrough sample#2). Column was washed with 20 mM Tris, pH 8.3 and then washed with 20 mM Tris, 15 mM EDTA, pH 8.3 (Hb after IMAC small sample). Sample was concentrated and washed with PBS using a 50 kDa filter (final estimated EDTA concentration < 22 nM). Calculated hemoglobin concentration was 4.7 mM (93.5% oxyHb, 6.5% metHb).

sRBC ghost preparation

For RBC ghost preparation, leukoreduced stressed RBC was centrifuged at 800 *g* for 10 minutes, washed 3 times with cold PBS, and lysed with 20 mOsm phosphate buffer. Lysed RBC was centrifuged at 30,000 *g* for 30 minutes at 4^{o}C and RBC ghost pellets were washed 3 times with 20 mOsm phosphate buffer. RBC ghosts were reconstituted in a volume of PBS equivalent to the sRBC transfusate[178].

In vitro K. pneumoniae stimulation

RAW cells or BMDMs were cultured as described in 4.4. Media was replaced and opsonized live *K. pneumoniae* serotype 2 (MOI 10:1, log phase) was introduced. *K. pneumoniae* was opsonized by incubating with 20% bovine serum for 30 minutes at 4^{o}C. Where indicated, hemin, CoPPIX or PPIX were introduced concurrently. Hemin, CoPPIX, and PPIX were dissolved in dimethyl sulfoxide (DMSO) and further diluted in PBS to achieve desired experimental

concentrations (final DMSO concentration = 0.25%). At indicated time (usually 4 h post-KP infection), media was collected, spun at 10,000 *g* for 10 min at 4ºC, and cytokine release was evaluated in resulting supernatant. Macrophages were washed with PBS and lysed to examine gene and protein expression via qRT-PCR and western blot, respectively.

Deferoxamine, deferasirox, hemopexin treatment

Deferoxamine mesylate salt (Cat #D9533) was obtained from Sigma-Aldrich (St. Louis, MO) and reconstituted in sterile PBS. Deferasirox (Cat #16753) was obtained from Cayman Chemical (Ann Arbor, MI) and reconstituted in DMSO (final DMSO concentration = 0.56%). Hemopexin, purified from human plasma, (Cat #16-16-080513) was obtained from Athens Research & Technology (Athens, GA) and reconstituted in sterile PBS.

CoPPIX administration

Male and female mice were intratracheally instilled with *K. pneumoniae*, serotype 2 ATCC 43816, as described in section 2.4. One hour following bacterial instillation, mice were injected intraperitoneally with vehicle (2.5 % DMSO), cobalt protoporphyrin IX (CoPPIX) 5 mg/kg or CoPPIX 25 mg/kg. Bacterial burden was evaluated 24 h post-*K. pneumoniae* infection.

Quantification and statistical analysis

Results are reported as the median unless otherwise indicated. For in vivo comparisons between two groups, a nonparametric Mann-Whitney test was undertaken. For in vivo comparisons of multiple groups, Kruskal-Wallis with Dunn's multiple comparisons test was undertaken. For in vitro comparisons between two groups, a two-tailed t test was undertaken. For

in vitro comparisons of multiple groups, a one-way ANOVA with Tukey's multiple comparisons test was undertaken. For comparisons between groups under multiple experimental conditions, a two-way ANOVA was undertaken. GraphPad Prism software version 6.0 was used for statistical analysis (La Jolla, CA). A *p*- value less than 0.05 was considered significant.

6.0 Future Perspectives

6.1 Heme-induced immunosuppression: More than NRF1 & NRF2?

While NRF1 and NRF2 appear to synergistically mediate *Stat1* suppression observed in infected macrophages challenged with heme, it is likely that other mechanisms act in concert with the aforementioned transcription factors to exert heme's immunosuppressive effects during infection. Heme binds to the nuclear receptors, REV-ERBα (encoded by nuclear receptor subfamily 1, group D, member 1, *NR1D1*) and REV-ERBβ (encoded by nuclear receptor subfamily 1, group D, member 2, *NR1D2*), resulting in enhanced stability of the proteins and recruitment of nuclear receptor co-repressor (NCoR)[179] with subsequent repression of enhancer-directed transcription in macrophages[180]. Activation of REV-ERBα in primary human monocyte-derived macrophages represses proinflammatory transcriptional response to LPS[181], and mouse macrophages lacking both REV-ERBα and REV-ERBβ show increased inflammatory response to injury in vivo[182]. Interestingly, this transcriptomic response to injury in macrophages requires complex integration and co-localization of NRF2 (and other transcription factors, including NF-κB) with REV- ERBα/REV-ERBβ[182]. Thus, in response to complex and diverse stimuli (as occurs in tissue environments), macrophages integrate multiple signals to yield transcriptomic profiles that are often qualitatively distinct from the sum of each individual polarizing signal[182] and warrants further investigation.

Furthermore, heme promotes dimerization of the RNA-binding protein, DiGeorge Critical Region 8 (DGCR8), an essential cofactor for RNase III enzyme, Drosha, in the microRNA (miRNA) maturation pathway[183]. While DGCR8 dimerization alone is insufficient for accurate

pri-miRNA processing, heme-bound DGCR8 has been shown to correct erroneous binding events and heme is critical for DGCR8 activation and microprocessor fidelity[184]. Notably, T cells deficient in DGCR8 show increased STAT1 phosphorylation following IFNγ stimulation, compared to wildtype-stimulated T cells[185]. Enhanced interferon signaling in the absence of DGCR8 activity was due to loss of miR-29a and miR29b[185], suggesting that DGCR8 activation and subsequent miRNA production negatively regulates STAT1 signaling in T cells. Whether or not DGCR8 alters interferon signaling in macrophages during infection remains to be determined.

6.2 Host-pathogen interplay: What's bug got to do with it?

Of note, the immunosuppressive effects observed with sRBC delivery are most profound when the pathogen is viable and pathogen death seems to reverse sRBC-mediated IRF1 suppression (Fig. 28A). The mechanism appears distinct from pathogen-induced hemolysis, as sRBC lysate incubated with heat-killed *K. pneumoniae* does not cause IRF1 suppression (Fig. 28A). Furthermore, neither FePPIX nor CoPPIX appear to suppress IRF1 induction or STAT1 activation in LPS-stimulated macrophages (Fig. 28B), suggesting that live pathogen, rather than purified bacterial ligand or killed bacterial preparation, actively interacts with porphyrin moiety to suppress macrophage interferon response. Two potential mechanisms may account for this phenomenon. First, Gram-negative bacteria like *K. pneumoniae* share the same steps for heme synthesis, from precursor δ-aminolevulinic acid (ALA) to eventual FePPIX, with eukaryotes[186]. While the contribution of heme synthesis to bacterial pathogenesis has been largely unexplored[186], evidence suggests that some pathogenic bacteria rely on heme biosynthesis to cause disease[187].

Thus, it is conceivable that *K. pneumoniae* incorporates excess porphyrin into its heme biosynthetic pathway to boost virulent gene expression and thereby necessitates pathogen viability.

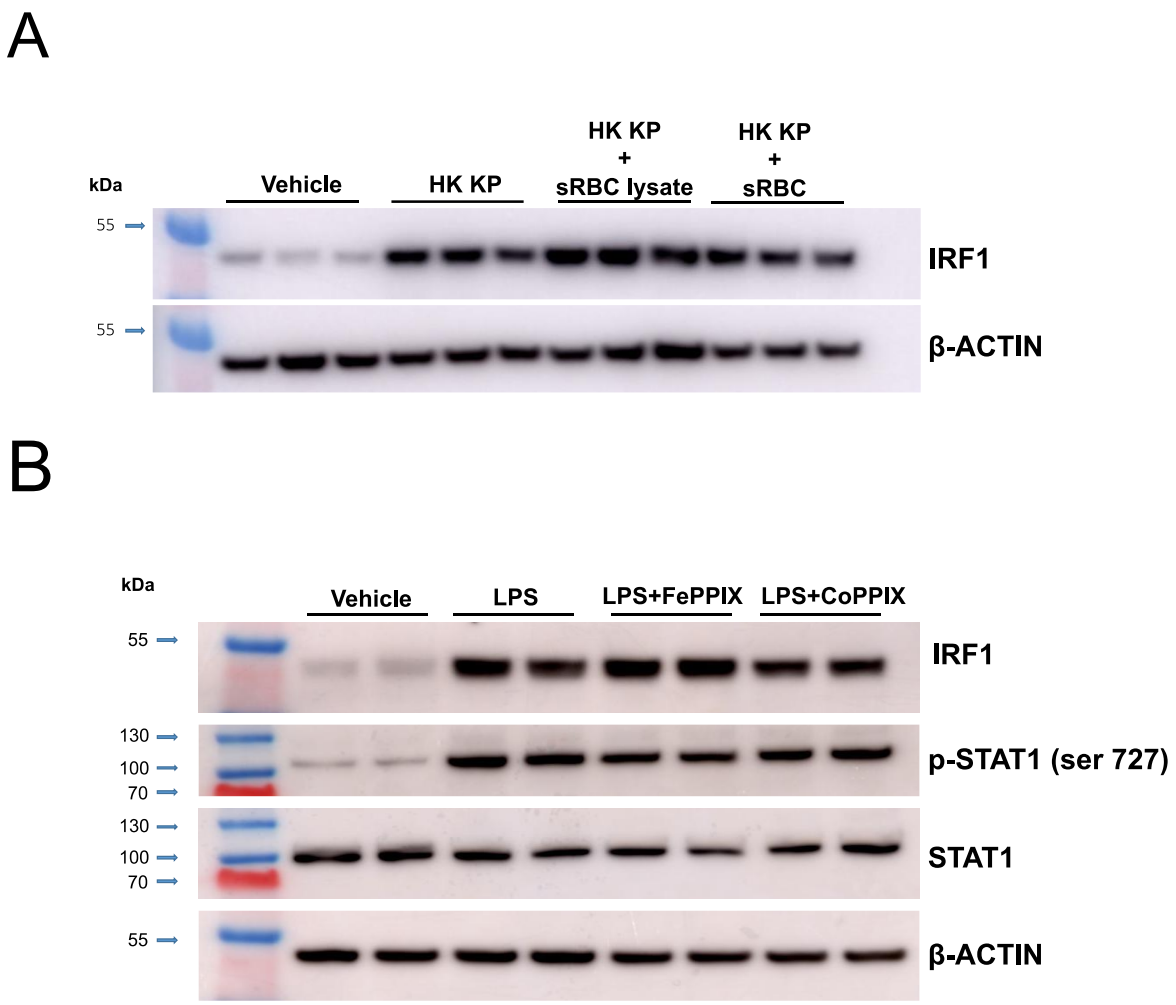

Figure 28: Role of pathogen viability in heme-induced immunosuppression.

(A) IRF1 immunoblot in RAW cells challenged with vehicle (PBS), heat-killed *K. pneumoniae* (HK KP), HK KP + sRBC 50:1 or HK KP + equivalent number of lysed sRBC for 4 h. (B) IRF1, p-STAT1, and STAT1 in RAW cells incubated with LPS (1 μg/mL), LPS + FePPIX (100 μM) or LPS + CoPPIX (100 μM) for 4 h.

Second, supernatant (obtained from macrophages cultured with live *K. pneumoniae* and sRBC) recapitulates IRF1 suppression observed with whole pathogen (Fig. 29 A-B). Likewise, incubation of macrophages with supernatant obtained from live *K. pneumoniae*, but not heat-killed *K. pneumoniae*, cultured with hemoglobin recapitulates IRF1 suppression observed with whole pathogen (Fig. 29C).

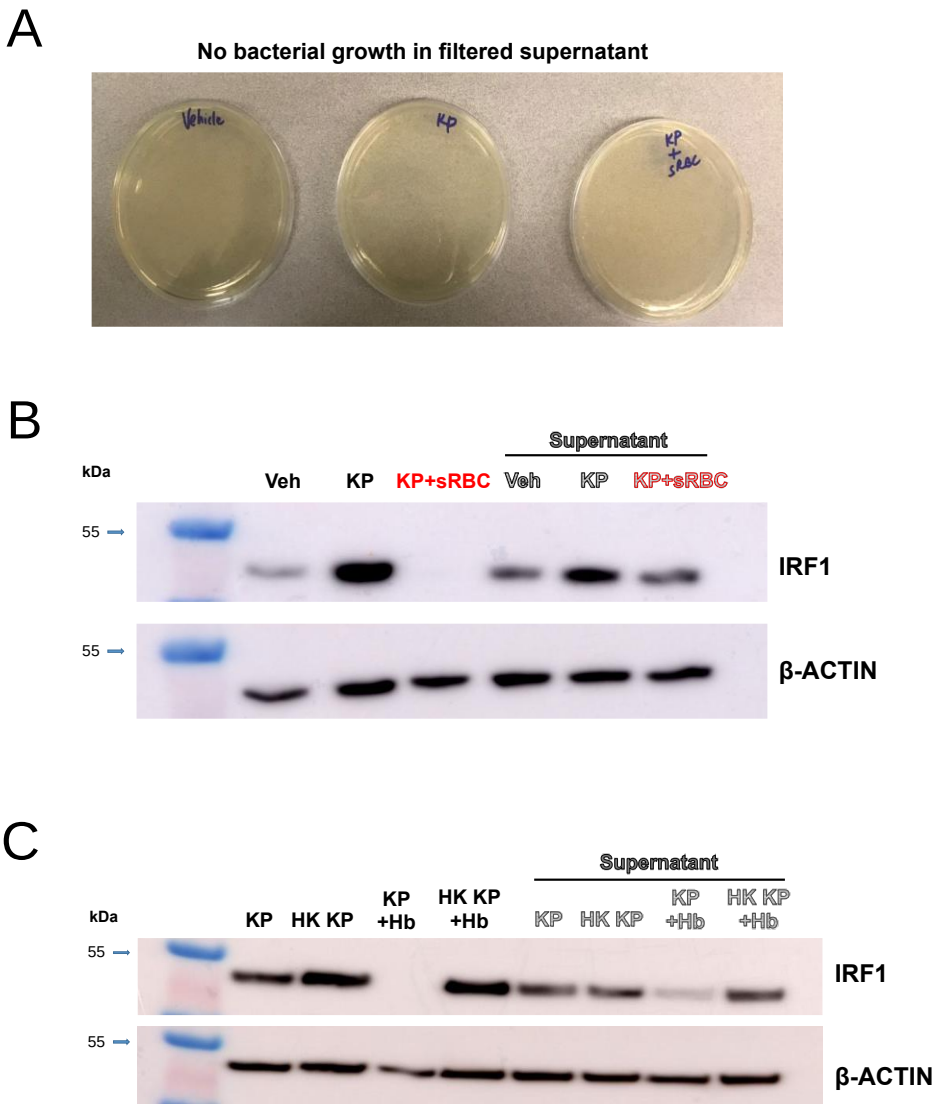

Figure 29: Role of bacteria-derived soluble factor in heme-induced immunosuppression.

RAW cells were challenged with vehicle (PBS), *K. pneumoniae* (KP, MOI 10:1) or KP + sRBC (50 sRBC:1 Mφ). 4 h later, supernatant was isolated from aforementioned experimental groups, filtered through 0.22 μm filter unit, and cultured on tryptic soy agar plates (A). (B) IRF1 immunoblot in RAW cells from aforementioned groups or naïve RAW cells challenged with supernatant for 4 h. (C) IRF1 immunoblot in RAW cells challenged with KP (MOI 10:1, heat-killed KP (HK KP, MOI 10:1), KP + hemoglobin (Hb, 100 μM), HK KP + Hb or supernatant obtained from the aforementioned groups for 4 h.

Like other Gram-negatives, *K. pneumoniae* has been shown to secrete outer membrane vesicles (OMVs)—spherical bilayered structures with diameters ranging from 20–200 nm—into the extracellular milieu[188]. Besides associated proteins and siderophores, OMVs from *K. pneumoniae* are predominantly comprised of LPS and capsular polysaccharide[189]. In fact, we have shown that depletion of LPS in cell-free supernatants obtained from *K. pneumoniae* culture blunts macrophage cytokine production to cell-free *K. pneumoniae* supernatant[37]. While *K. pneumoniae* doesn't appear to have an extensive secretome, it is conceivable that interaction with hemoglobin, specifically the porphyrin moiety of heme, results in secretion of a novel soluble, transferrable factor that modulates the immune response to infection. Indeed, an antibacterial type VI secretion system that is "silent" in basic medium but is induced by stimuli such as antibiotics[190] or iron availability[191] has been described in *K. pneumoniae*, suggesting that heme availability may modulate secretion of novel effector factors by *K. pneumoniae* and warrants further investigation.

6.3 Bench to bedside: Immunosuppression in sepsis

Sepsis is a severe, life-threatening infection characterized by organ dysfunction and a dysregulated host response[192], and a condition that was declared in 2017 by the World Health Organization as a global health priority[193]. Two critical gaps exist in our understanding of sepsis immunology—(1) identification of factors within the host that impair immunity and (2) delineation of organ-specific alterations that occur in the course of sepsis[194]. Although macrophages in the liver are the primary cells that support rapid clearance of stressed, damaged red cells[19], remarkably little is known about whether this competing physiologic stressor weakens macrophage function during infection, thereby impairing host defense and contributing to immunosuppression. Our

findings reveal that (1) imposing an additional physiologic stressor targeting the mononuclear phagocyte system during infection results in an immunosuppressive phenotype, and (2) the immunosuppression encountered during severe infection in our model is due to excess heme handling in the liver.

Though infection originates in the lungs in our model, we identify alterations in the liver, the primary organ that responds to fluctuations in RBC integrity[19], as pivotal to the impaired immunity caused by stressed erythrophagocytosis during severe bacterial infection. As is typical of immune dysfunction in sepsis[195], we demonstrate that stressed erythrophagocytosis induces systemic hyperinflammation with concurrent organ-specific immunosuppression during severe bacterial infection. Of broad significance, states of intracellular heme-iron excess are associated with increased risk of infection, a finding that has been attributed to iron overload, but growing evidence implicates heme as an important regulator of macrophage function and invites the possibility that heme is also involved in altered host immunity. In pathologic states of intracellular heme excess, our findings indicate the ability to mount optimal STAT1 responses is impaired (Fig. 30) and unmasks a previously unknown mechanism linking cellular heme metabolism and regulation of immune response with important implications for infection and inflammation.

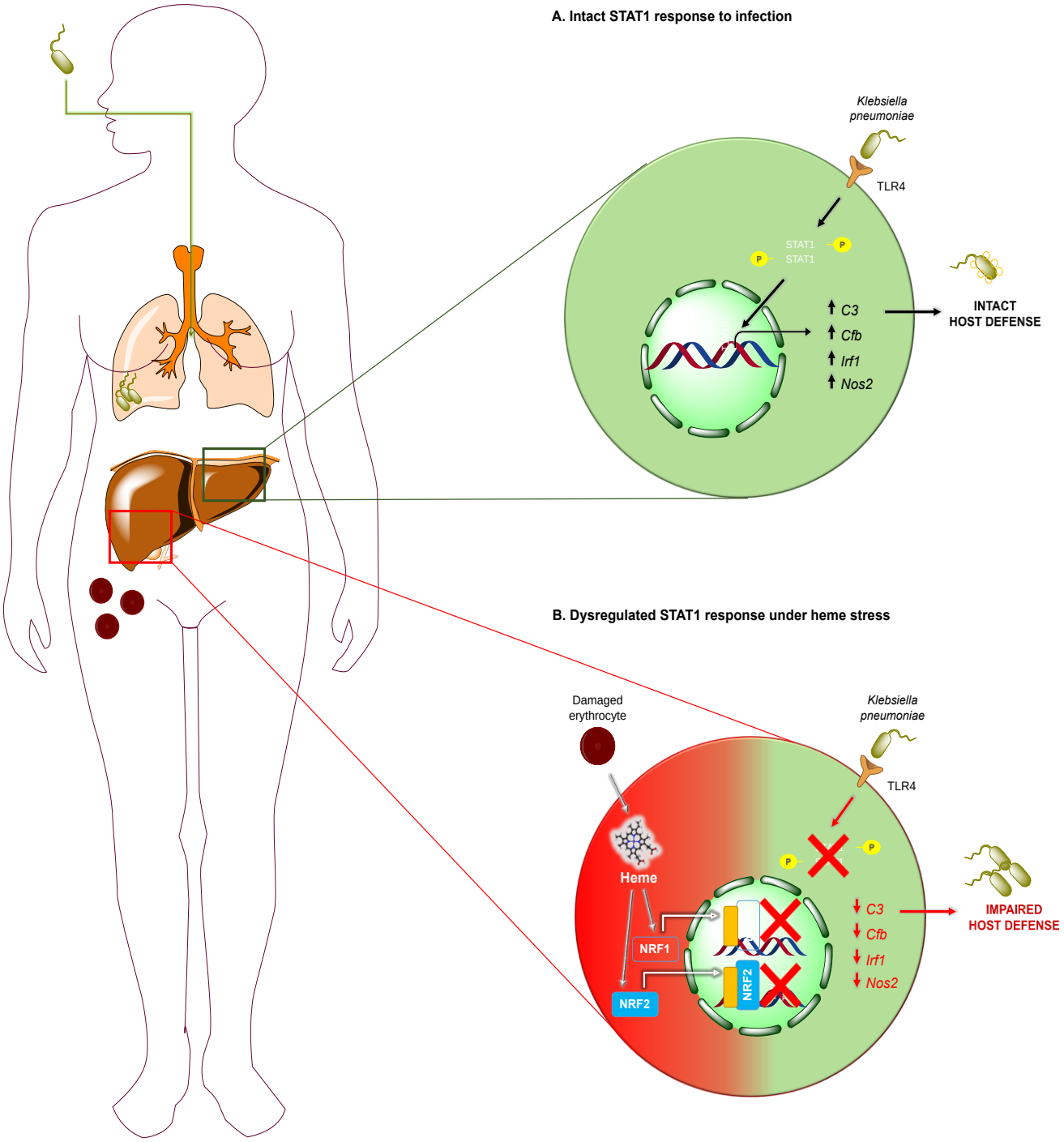

Figure 30: Role of heme-induced immunosuppression during sepsis.

Severe acute lower respiratory tract infection remains a major cause of sepsis worldwide and *K. pneumoniae* is a common cause of hospital-acquired pneumonia culminating in sepsis. In immunocompetent hosts (A), STAT1

activation upregulates complement component 3 (*C3*), complement factor B (*Cfb*), interferon regulatory factor 1 (*Irf1*), and nitric oxide synthase 2 (*Nos2*), and ultimately results in adequate containment of infection. (B) Increased circulation of damaged or stressed RBC (sRBC) precipitates mononuclear phagocytic uptake and disrupts heme-iron homeostasis. Excess intracellular heme stabilizes NRF1 and NRF2, resulting in suppression of STAT1 responses, and worsened immunity during bacterial infection.

Appendix A

Table 1: Innate immune gene expression in livers of mice following sRBC delivery.

Publicly available InnateDB dataset (under the aegis of International Molecular Exchange Consortium, Nucleic Acids Research) was used to identify genes with documented roles in innate immunity in RNA-seq obtained from livers of *K. pneumoniae* (KP) + sRBC-challenged mice 24 h post-KP infection. Dataset last accessed February 26, 2018.

Name	Chromosome	Region	Max group mean	Log_2 fold change	Fold change	P-value	FDR p-value	Bonferroni
Abca1	4	complement(53030787..53159895)	130.93	1.84	3.58	1.18E-12	6.87E-11	5.77E-08
Abcg1	17	31057698..31115777	2.11	-1.42	-2.68	5.50E-13	3.32E-11	2.68E-08
Ace	11	105967945..105989964	0.65	-2.06	-4.18	2.74E-11	1.30E-09	1.33E-06
Aco1	4	40143081..40198338	28.09	-1.02	-2.03	6.97E-10	2.67E-08	3.39E-05
Adrb2	18	complement(62177817..62179959)	7.39	3.33	10.08	0	0	0
Ahr	12	complement(35497974..35535038)	6.28	-1.01	-2.01	5.88E-10	2.29E-08	2.86E-05
Aimp1	3	complement(132660499..132684370)	12.25	0.65	1.57	3.25E-05	0.00052	1
Amacr	15	10981756..10996624	17.22	-0.79	-1.73	7.28E-06	0.000138	0.35
Angpt1	15	complement(42424727..42676977)	0.15	-1.12	-2.17	0.00168	0.02	1
Anpep	7	complement(79821803..79861059)	8.94	-0.81	-1.75	8.25E-07	1.89E-05	0.04

Table 1 continued

Anxa2	9	69453620..69491795	9.12	1.62	3.07	3.33E-16	2.81E-14	1.62E-11
Arg1	10	complement(24915208..24927470)	719.06	0.71	1.64	0.000342	0.00423	1
Arhgap15	2	43748824..44395953	0.17	-0.83	-1.78	0.00485	0.04	1
Arl5b	2	15049395..15082456	3.8	-0.66	-1.58	0.000141	0.00194	1
Atf4	15	80255184..80257540	62.84	0.85	1.8	1.43E-07	3.83E-06	0.00699
Atm	9	complement(53439149..53536740)	1.7	-1.14	-2.2	3.58E-12	1.95E-10	1.74E-07
Azi2	9	118040499..118069794	10.58	0.59	1.5	0.000224	0.00291	1
Bcl10	3	145922804..145934356	8.75	0.96	1.94	1.08E-09	4.08E-08	5.28E-05
Bcl2	1	complement(106538178..106714274)	0.29	-1.16	-2.23	1.86E-05	0.000318	0.91
Bcl2l1	2	complement(152780668..152831728)	6.25	0.89	1.86	1.96E-08	6.07E-07	0.00096
Birc2	9	complement(7818227..7837064)	27.58	1.51	2.86	2.61E-14	1.82E-12	1.27E-09
Birc3	9	complement(7848699..7873186)	11	1.28	2.43	1.98E-10	8.32E-09	9.62E-06
Bnip3	7	complement(138890836..138909519)	85.51	0.93	1.91	3.11E-07	7.81E-06	0.02
Bnip3l	14	complement(66985239..67008877)	19.47	0.71	1.63	3.43E-06	6.96E-05	0.17
C1qa	4	complement(136895917..136898803)	20.53	-1.59	-3	0	0	0
C1qb	4	complement(136880129..136886187)	23.72	-1.35	-2.55	0	0	0
C1qc	4	complement(136889804..136893065)	10.97	-1.66	-3.17	0	0	0
C5ar1	7	complement(16246743..16259540)	1.74	0.97	1.95	6.91E-05	0.00103	1

Table 1 continued

C8a	4	complement(104815679..104876398)	170.44	-0.76	-1.7	2.98E-05	0.000482	1
C8b	4	104766317..104804548	81.54	-0.59	-1.5	0.000639	0.00726	1
C8g	2	complement(25498651..25501719)	85.34	-0.7	-1.62	1.86E-05	0.000317	0.91
C9	15	6445327..6498751	143.03	-0.73	-1.66	7.88E-05	0.00115	1
Camp	9	complement(109847379..109849617)	1.46	6.54	93.29	7.99E-12	4.13E-10	3.89E-07
Casp1	9	5298517..5307265	2.12	-1.14	-2.21	4.20E-06	8.35E-05	0.2
Casp12	9	5345430..5373032	0.72	-0.82	-1.77	0.000114	0.01	1
Ccl17	8	94810453..94812036	0.47	3.5	11.32	3.78E-05	0.000595	1
Ccl2	11	82035571..82037453	126.46	3.08	8.46	0	0	0
Ccl5	11	complement(83525778..83530518)	4.7	2.81	7	0	0	0
Ccr7	11	complement(99144196..99155077)	0.36	1.64	3.12	0.000353	0.00435	1
Cd14	18	complement(36725074..36726736)	173.14	3.7	12.97	0	0	0
Cd180	13	102693558..102739629	0.3	-1.65	-3.14	7.12E-07	1.65E-05	0.03
Cd200	16	complement(45382135..45409053)	0.53	1.47	2.78	8.89E-08	2.46E-06	0.00433
Cd22	7	complement(30865402..30880342)	0.16	-1.16	-2.23	0.000797	0.00881	1
Cd300e	11	complement(115051917..115062177)	2.07	-1.02	-2.02	9.43E-07	2.13E-05	0.05
Cd300lf	11	complement(115116214..115133992)	1.55	1.75	3.37	7.77E-16	6.30E-14	3.79E-11
Cd36	5	complement(17781690..17888801)	14.48	0.78	1.71	0.000289	0.00364	1
Cd47	16	49855618..49915010	12.45	0.66	1.58	1.35E-05	0.000239	0.66

Table 1 continued

Cd48	1	171682009..171705258	4.05	-0.83	-1.78	2.17E-05	0.000363	1
Cd5l	3	87357881..87371073	50.01	-1.58	-2.98	0	0	0
Cd63	10	128908919..128912816	18.66	3.32	9.98	0	0	0
Cdkn1a	17	29090979..29100722	18.54	3.48	11.14	0	0	0
Cebpa	7	35119293..35121928	39.71	-0.59	-1.51	0.000366	0.0045	1
Cebpd	16	15887286..15891031	8.54	1.3	2.46	1.11E-07	3.01E-06	0.00541
Cebpe	14	complement(54710363..54712174)	1.24	-1.75	-3.36	9.04E-07	2.05E-05	0.04
Cfb	17	complement(34856374..34862518)	1208.14	0.78	1.72	3.25E-05	0.00052	1
Cfp	X	complement(20925454..20931555)	10.43	-0.61	-1.52	9.41E-05	0.00135	1
Cish	9	107296026..107302784	2.16	0.74	1.67	1.66E-05	0.000287	0.81
Clec1b	6	129397297..129409335	0.9	-0.79	-1.73	0.000703	0.00788	1
Clec4d	6	123262111..123275265	4.07	1.89	3.7	5.55E-16	4.58E-14	2.70E-11
Clec4e	6	complement(123281789..123289870)	4.71	2.33	5.04	0	0	0
Clec4n	6	123229843..123247021	5.02	1.44	2.71	6.25E-13	3.76E-11	3.05E-08
Clec9a	6	129408862..129424763	0.38	-2.04	-4.11	6.89E-09	2.31E-07	0.00034
Cnot8	11	58104153..58118594	7.6	-0.68	-1.6	9.18E-06	0.00017	0.45
Crp	1	172698055..172833031	188.51	-1.35	-2.56	3.64E-09	1.27E-07	0.00018
Cryab	9	50752758..50756633	0.82	-1.14	-2.2	0.000466	0.00554	1
Csf1r	18	61105572..61132149	9.36	-0.73	-1.66	5.33E-06	0.000104	0.26
Csk	9	complement(57626647..57645653)	7.54	-0.81	-1.75	3.51E-07	8.71E-06	0.02
Ctnnal1	4	complement(56810935..56865188)	0.71	0.59	1.5	0.000808	0.0089	1

Table 1 continued

Ctss	3	95526786..95556403	28.84	-0.62	-1.54	3.63E-05	0.000574	1
Cxcl1	5	90891241..90893115	370.82	1.57	2.96	1.42E-08	4.53E-07	0.00069
Cxcl11	5	complement(92359544..92365485)	0.61	-1.68	-3.21	3.15E-07	7.89E-06	0.02
Cxcl12	6	117168535..117181367	16.05	-0.93	-1.91	8.73E-08	2.41E-06	0.00425
Cxcl13	5	95956951..95961068	23.47	1.07	2.1	8.92E-05	0.00128	1
Cxcl14	13	complement(56288647..56296551)	2.93	1.7	3.26	6.24E-07	1.46E-05	0.03
Cxcl16	11	complement(70453983..70459984)	3.42	-0.61	-1.53	0.000146	0.00199	1
Cxcl2	5	90903871..90905938	61.87	4.48	22.35	0	0	0
Cxcl5	5	90759360..90761624	3.09	3.09	8.5	3.68E-12	1.99E-10	1.79E-07
Cxcr6	9	123806477..123811754	0.55	-0.84	-1.79	0.00494	0.04	1
Dcn	10	97479500..97518162	72.16	0.98	1.98	3.90E-09	1.35E-07	0.00019
Ddx21	10	complement(62580248..62602298)	11.46	0.67	1.59	4.93E-06	9.69E-05	0.24
Ddx3x	X	13280970..13294052	62.5	0.66	1.58	0.000307	0.00384	1
Dhcr24	4	106561038..106589113	99.23	-1.07	-2.1	9.22E-09	3.02E-07	0.00045
Dhx58	11	complement(100694884..100704271)	13.04	0.77	1.7	3.76E-05	0.000593	1
Dok3	13	complement(55523235..55528538)	1.72	0.76	1.69	0.00487	0.04	1
Duox2	2	complement(122279247..122298165)	0.29	5.18	36.3	0	0	0
Dusp1	17	complement(26505590..26508519)	7.22	1.35	2.56	1.77E-09	6.49E-08	8.61E-05
Dusp10	1	184013302..184075636	1.93	1.06	2.09	2.15E-06	4.53E-05	0.1
Dusp16	6	complement(134715468..134792625)	7.07	1.4	2.64	2.00E-15	1.55E-13	9.73E-11

Table 1 continued

E2f1	2	complement(154559407..154569892)	0.22	-1.5	-2.83	0.000221	0.00288	1
Edn1	13	42301270..42307989	2.39	3.06	8.31	0	0	0
Eif4ebp1	8	27260329..27276674	14.92	0.85	1.8	5.73E-07	1.35E-05	0.03
Ern1	11	complement(106394650..106487852)	3.6	-1.33	-2.51	2.78E-13	1.73E-11	1.36E-08
Ets1	9	32636221..32757820	4.58	0.94	1.91	2.81E-09	1.00E-07	0.000014
F2rl1	13	complement(95511732..95525240)	0.16	1.88	3.67	0.000111	0.00155	1
Fancc	13	complement(63304709..63497278)	1.29	1.25	2.38	1.48E-08	4.70E-07	0.000072
Fcrl5	3	87435773..87500678	0.04	-2.14	-4.41	0.00537	0.05	1
Flt4	11	49609263..49652739	1.39	-1.1	-2.14	5.53E-07	1.31E-05	0.03
Foxa2	2	complement(148042877..148046969)	4.38	-0.84	-1.8	1.75E-06	3.74E-05	0.09
Fpr1	17	complement(17876471..17883940)	11.06	0.66	1.58	0.00111	0.01	1
Fstl1	16	37776873..37836514	2.23	1.06	2.09	3.78E-10	1.53E-08	1.84E-05
Gas6	8	complement(13465374..13494490)	38.48	-0.74	-1.67	1.36E-05	0.00024	0.66
Gata6	18	11052510..11085635	2.55	1.19	2.28	1.33E-10	5.75E-09	6.47E-06
Gbp2	3	142620602..142638008	93.61	1.38	2.59	2.64E-07	6.71E-06	0.01
Gbp6	5	complement(105270702..105293698)	22.63	-0.69	-1.61	0.000497	0.00586	1
Gja1	10	56377300..56390419	6.38	1.73	3.33	0	0	0
Glrx	13	75839868..75850151	17.22	1.18	2.27	1.33E-11	6.62E-10	6.49E-07
Gm4955	1	complement(173468485..173491041)	0.83	-0.87	-1.82	0.00123	0.01	1
Gpsm1	2	26315515..26348237	0.22	1.12	2.18	0.000365	0.00449	1

Table 1 continued

Gsk3b	16	38089001..38246084	2.91	0.92	1.9	3.73E-09	1.29E-07	0.00018
H2-Aa	17	complement(34282744..34287827)	9.23	-1.09	-2.12	9.07E-12	4.64E-10	4.42E-07
H2-Ab1	17	34263209..34269418	7.99	-0.85	-1.8	2.63E-07	6.68E-06	0.01
Hace1	10	45577829..45712345	0.45	0.81	1.75	4.97E-06	9.75E-05	0.24
Hc	2	complement(34983331..35061438)	141.43	-0.93	-1.91	1.06E-06	2.36E-05	0.05
Hdac11	6	91156665..91174692	3.89	-1.15	-2.22	1.56E-09	5.77E-08	7.62E-05
Hif1a	12	73901375..73947530	41.55	2.37	5.17	0	0	0
Hmgb2	8	57511907..57515999	3.49	1.76	3.38	0	0	0
Hmgb3	X	71555918..71560676	5.63	1.01	2.01	1.22E-09	4.55E-08	5.92E-05
Hmgn2	4	complement(133964738..133968650)	7.33	1.18	2.26	9.86E-12	5.00E-10	4.80E-07
Hmox1	8	75093621..75100589	107.62	1.79	3.46	0	0	0
Hrg	16	22951072..22961656	159.6	-0.59	-1.5	0.00141	0.01	1
Hsp90aa1	12	complement(110690605..110702728)	59.94	0.68	1.61	0.00195	0.02	1
Hspa14_1	2	complement(3488850..3512814)	2.42	0.94	1.91	4.36E-10	1.74E-08	2.13E-05
Hspa1a	17	complement(34969190..34972156)	1.16	-1.99	-3.96	4.57E-06	9.02E-05	0.22
Hspa1b	17	complement(34956436..34959238)	6.54	-3.82	-14.17	0	0	0
Icam1	9	21015960..21028797	64.94	1.13	2.18	6.75E-06	0.000129	0.33
Icosl	10	78069360..78079525	0.92	0.85	1.8	0.00108	0.01	1
Idi1	13	8885501..8892451	103.21	-1.16	-2.24	1.58E-08	4.99E-07	0.00077
Ifit2	19	34550694..34576419	7.13	-0.92	-1.89	0.00188	0.02	1

Table 1 continued

Ifitm2	7	complement(140954837..140955987)	483.03	0.78	1.71	1.15E-05	0.000206	0.56
Ifrd1	12	complement(40201567..40248504)	11	1.77	3.4	0	0	0
Igf1	10	87858265..87937042	29.84	0.64	1.56	0.00091	0.00989	1
Igtp	11	58199556..58207591	101.35	-2.24	-4.73	0	0	0
Il10	1	131019845..131024974	3.22	2.77	6.81	0	0	0
Il12b	11	44400063..44414033	0.67	2.98	7.92	2.13E-14	1.50E-12	1.04E-09
Il15	8	complement(82331632..82403222)	0.36	-1.84	-3.59	1.35E-07	3.62E-06	0.00659
Il19	1	complement(130932656..131040115)	0.09	2.7	6.48	0.00302	0.03	1
Il1a	2	complement(129299610..129309972)	16.43	2.42	5.35	0	0	0
Il1b	2	complement(129364570..129371139)	25.63	2.23	4.68	0	0	0
Il1r1	1	40225080..40317257	76.78	1.64	3.12	1.90E-11	9.24E-10	9.26E-07
Il1r2	1	40074079..40125231	3.46	1.71	3.27	1.78E-08	5.54E-07	0.00087
Il1rap	16	26581704..26730117	6.78	-0.91	-1.88	2.29E-09	8.27E-08	0.00011
Il1rl2	1	40324610..40367562	0.09	1.23	2.34	0.000663	0.00749	1
Il20rb	9	complement(100457719..100486788)	3.03	4.25	19.04	0	0	0
Il23a	10	complement(128296140..128298084)	0.38	3	7.99	2.18E-07	5.63E-06	0.01
Il33	19	29925114..29960718	6.33	2.48	5.59	0	0	0
Il6	5	30013114..30019981	1.66	2.55	5.85	6.68E-09	2.24E-07	0.00033
Il6st	13	112464070..112510086	16.97	-0.63	-1.54	0.000563	0.00653	1
Irak2	6	113638467..113695026	6	0.89	1.86	1.71E-06	3.68E-05	0.08

Table 1 continued

Irak3	10	complement(120141648..120202130)	8.72	1.75	3.36	2.31E-10	9.60E-09	1.13E-05
Irak4	15	94543643..94581815	1.91	-0.6	-1.51	0.000211	0.00277	1
Irf1	11	53770014..53778374	17.39	-1.19	-2.28	7.96E-11	3.55E-09	3.88E-06
Irf2	8	46739732..46847458	1.88	-0.91	-1.87	2.57E-06	5.35E-05	0.13
Irf3	7	44997648..45002848	8.12	-0.85	-1.8	5.40E-08	1.54E-06	0.00263
Irf5	6	29526625..29541871	3.66	-0.88	-1.84	2.02E-07	5.25E-06	0.00982
Irf8	8	120736358..120756694	2.43	-0.72	-1.64	8.01E-06	0.00015	0.39
Irgm1	11	complement(48861968..48871683)	30.45	-1.02	-2.03	2.77E-07	7.01E-06	0.01
Isg15	4	complement(156199424..156200818)	106.1	0.82	1.76	0.000195	0.00258	1
Itgam_1	7	128062640..128118491	6.75	0.69	1.61	0.000543	0.00631	1
Itgax	7	128129547..128150657	0.69	-0.78	-1.72	0.00375	0.03	1
Itgb3	11	104608000..104670476	3.37	0.77	1.71	0.000105	0.00148	1
Jmjd6	11	complement(116837432..116843449)	4.58	0.96	1.94	1.50E-10	6.46E-09	7.32E-06
Jun	4	complement(95049034..95052222)	14.06	0.98	1.97	0.000626	0.00714	1
Kcnj8	6	complement(142564837..142571614)	11.17	2.32	4.99	0	0	0
Kdm4a	4	complement(118136957..118180043)	5.92	0.74	1.67	4.33E-06	8.61E-05	0.21
Kdr	5	complement(75932827..75978458)	2.75	-2.88	-7.36	0	0	0
Lair1	7	complement(4003402..4063204)	1.06	-0.68	-1.6	0.000611	0.007	1
Lcn2	2	complement(32384633..32388252)	1578.46	1.93	3.82	0	0	0

Table 1 continued

Lgals9	11	complement(78962974..78984946)	93.2	0.77	1.7	1.05E-05	0.000192	0.51
Lrrk2	15	91673175..91816120	0.43	-0.62	-1.54	0.00135	0.01	1
Lst1	17	complement(35185095..35188439)	6.77	-2.01	-4.03	2.45E-12	1.37E-10	1.19E-07
Lum	10	97565501..97572703	2.05	-0.89	-1.85	7.63E-05	0.00112	1
Ly6g	15	75155240..75159126	0.37	1.57	2.97	0.000378	0.00462	1
Ly86	13	37345345..37419036	2.55	-1.59	-3.01	2.50E-09	8.99E-08	0.00012
Mafb	2	complement(160363703..160367065)	3.85	-1.62	-3.07	0	0	0
Malt1	18	65430963..65478823	3.63	1.55	2.92	0	0	0
Map2k6	11	110399122..110525522	0.35	-1.73	-3.33	5.93E-06	0.000114	0.29
Map3k1	13	complement(111746428..111808993)	4.48	0.71	1.63	3.07E-05	0.000495	1
Map3k14	11	complement(103219762..103267472)	1.35	1.01	2.01	2.37E-09	8.53E-08	0.00012
Map3k5	10	19934472..20142753	3.93	-0.81	-1.75	1.72E-06	3.69E-05	0.08
Map3k8	18	complement(4331327..4353015)	3.59	1.44	2.72	2.22E-16	1.88E-14	1.08E-11
Mapk8	14	complement(33377898..33447158)	2.41	0.74	1.67	9.79E-07	2.21E-05	0.05
Mapkapk2	1	complement(131053700..131097826)	24.57	0.6	1.51	0.000116	0.00162	1
Mavs	2	131234063..131248025	11.64	-2.1	-4.28	0	0	0
Mbl1	14	41151456..41158959	172.53	-0.75	-1.69	9.15E-06	0.000169	0.45
Mertk	2	128698956..128802894	2.96	-1	-2	3.21E-08	9.62E-07	0.00156
Mfn2	4	complement(147873599..147904704)	7.51	-0.64	-1.56	2.87E-05	0.000468	1
Mid1	X	169685199..170005736	1.32	1.42	2.67	4.30E-10	1.73E-08	2.1E-05

Table 1 continued

Mid2	X	140664599..140767715	0.67	0.68	1.6	0.00025	0.00322	1
Mmp12	9	7344381..7369499	0.44	2.92	7.58	0	0	0
Mmp7	9	7692090..7699585	1.04	1.21	2.31	0.0037	0.03	1
Mmp9	2	164940780..164955850	1.02	1.43	2.69	2.69E-07	6.83E-06	0.01
Mov10	3	complement(104794836..104818563)	3.05	-1.32	-2.5	2.66E-13	1.65E-11	1.29E-08
Mrc1	2	14229392..14332057	3.74	-2.26	-4.78	0	0	0
Mst1r	9	107906873..107920383	0.43	3.33	10.07	0	0	0
Muc1	3	89229057..89233381	0.23	1.01	2.01	0.00437	0.04	1
Myc	15	61985341..61990374	2.19	1.86	3.63	1.22E-15	9.70E-14	5.95E-11
Nampt	12	32820335..32853369	144.34	2.16	4.48	0	0	0
Nfkbia	12	complement(55489411..55492647)	72.3	1.47	2.77	2.22E-16	1.88E-14	1.08E-11
Nfkbib	7	complement(28758251..28767512)	6.79	0.69	1.62	0.0011	0.01	1
Nfkbie	17	45555716..45563169	4.07	0.72	1.65	0.000332	0.00412	1
Nfkbiz	16	complement(55811375..55838899)	16.72	2.02	4.07	0	0	0
Nlrc5	8	94434356..94527272	6.01	-0.9	-1.86	5.16E-07	1.23E-05	0.03
Nlrp12	7	complement(3218784..3249740)	9.38	1.03	2.05	3.97E-06	7.94E-05	0.19
Nlrp1a	11	complement(71092236..71144704)	0.1	-2.47	-5.55	5.49E-07	0.000013	0.03
Nlrp3	11	59541568..59566956	1.79	1.06	2.08	4.44E-06	8.79E-05	0.22
Nlrp6	7	140920902..140929192	11.53	0.61	1.52	0.000383	0.00467	1
Nos2	11	78920787..78960254	0.98	3.29	9.76	0	0	0
Nox4	7	87246096..87398710	1.25	-1.92	-3.8	0	0	0

Table 1 continued

Noxa1	2	complement(25085667..25095149)	0.28	-1.88	-3.67	0.000754	0.00838	1
Nr1h3	2	complement(91184061..91202834)	27.62	-1.16	-2.24	9.87E-14	6.47E-12	4.81E-09
Nr1h4	10	complement(89454234..89533585)	25.49	-0.97	-1.96	1.90E-08	5.90E-07	0.00093
Nr4a3	4	48045153..48086447	0.04	1.45	2.72	0.0046	0.04	1
Nras	3	103058285..103067914	7.44	0.65	1.57	2.07E-05	0.000349	1
Numbl	7	27258433..27282144	0.14	1.64	3.11	3.64E-08	1.08E-06	0.00177
Oas1b	5	120812635..120824163	1.06	-1.3	-2.47	5.29E-06	0.000103	0.26
Olfm4	14	80000302..80021930	0.27	3.46	10.98	1.85E-08	5.77E-07	0.0009
Orai1	5	123015074..123030456	2.06	-0.82	-1.77	3.53E-05	0.000559	1
Osm	11	4236420..4241026	0.4	2.4	5.29	3.14E-08	9.43E-07	0.00153
Pard3	8	127063893..127612286	2.68	-0.97	-1.95	1.25E-08	4.02E-07	0.00061
Pglyrp1	7	18871331..18890459	1.23	1.74	3.33	5.59E-07	1.33E-05	0.03
Pklr	3	89136142..89146784	13.13	-1.41	-2.65	1.42E-06	3.09E-05	0.07
Plaur	7	24462484..24475968	5.21	2.36	5.12	0	0	0
Plec	15	complement(76170974..76232574)	11.92	1.21	2.31	6.12E-11	2.77E-09	2.98E-06
Plscr1	9	92249750..92272278	62.49	1.72	3.3	1.49E-08	4.73E-07	0.00073
Pml	9	complement(58218076..58249786)	3.1	-0.86	-1.81	4.62E-07	1.12E-05	0.02
Ppargc1a	5	complement(51454250..51567726)	0.38	-0.95	-1.94	0.00121	0.01	1
Ppargc1b	18	complement(61298136..61400431)	0.22	-1.06	-2.09	0.00382	0.03	1
Prdm1	10	complement(44437177..44528501)	0.36	1.47	2.77	1.04E-06	2.33E-05	0.05

Table 1 continued

Prkra	2	complement(76629898..76648015)	3.21	-0.76	-1.7	0.000042	0.000656	1
Prkx	X	complement(77761411..77796278)	1.99	1.04	2.05	1.90E-11	9.23E-10	9.24E-07
Prmt1	7	complement(44975989..44986568)	2.69	0.84	1.79	9.78E-07	0.000022	0.05
Prtn3	10	79874476..79883174	3.67	-4.88	-29.4	0	0	0
Pstpip1	9	56089962..56128888	0.52	1.08	2.12	3.39E-05	0.00054	1
Ptafr	4	132564067..132582683	3.13	1.3	2.47	6.96E-11	3.14E-09	3.39E-06
Ptges	2	complement(30889471..30929863)	1.32	4.12	17.37	0	0	0
Ptgs2	1	150100031..150108227	1.49	4.24	18.83	1.11E-16	9.61E-15	5.41E-12
Ptk2b	14	complement(66153257..66281052)	2.09	-0.8	-1.74	1.12E-06	0.000025	0.05
Ptpn2	18	complement(67665511..67724595)	13.43	1.56	2.95	0	0	0
Ptprc	1	complement(138062861..138175708)	4.43	-0.68	-1.6	2.54E-05	0.000419	1
Ptx3	3	66219910..66225805	0.43	4.71	26.18	2.73E-12	1.52E-10	1.33E-07
Pura	18	36281097..36289723	3.73	-1.16	-2.23	3.60E-12	1.96E-10	1.75E-07
Pydc3	1	173673675..173698392	0.71	-1.14	-2.2	1.16E-05	0.000208	0.56
Pyhin1	1	173630917..173647928	2.37	-0.64	-1.56	0.00147	0.02	1
Rad23a	8	complement(84834019..84840665)	3.45	-0.71	-1.63	3.25E-05	0.00052	1
Ranbp9	13	complement(43402673..43480973)	9.99	0.93	1.9	8.15E-09	2.69E-07	0.0004
Reg3g	6	complement(78466269..78468872)	14.66	6.92	120.7	0	0	0
Rel	11	complement(23736847..23770970)	1.11	0.77	1.7	3.99E-05	0.000626	1

Table 1 continued

Rela	19	5637483..5648130	9.11	0.69	1.61	5.29E-05	0.000809	1
Relb	7	complement(19606217..19629438)	4.25	1.23	2.35	1.45E-06	3.16E-05	0.07
Rest	5	77265491..77286432	4.73	0.65	1.57	4.16E-05	0.00065	1
Rftn1	17	complement(49992257..50190674)	0.78	0.74	1.67	0.00024	0.00311	1
Rhbdf2	11	complement(116598165..116627019)	5.18	0.99	1.99	7.88E-09	2.61E-07	0.00038
Rnf125	18	20944625..20983848	36.27	1.83	3.57	0	0	0
Rnf135	11	80183851..80199757	3.95	-1.3	-2.46	3.03E-12	1.67E-10	1.48E-07
Rnf5	17	complement(34601091..34603690)	5.75	-0.97	-1.96	2.01E-07	5.23E-06	0.00979
Rorc	3	94372794..94398276	7.29	-1.2	-2.3	9.36E-07	2.12E-05	0.05
Rps6ka4	19	complement(6829085..6840601)	3.25	0.79	1.73	1.57E-06	3.39E-05	0.08
Rsad2	12	complement(26442753..26456452)	22.15	1.14	2.21	3.35E-05	0.000535	1
Rusc1	3	complement(89083981..89093311)	1.29	0.87	1.82	0.00127	0.01	1
S100a8	3	90668978..90670035	71.02	1.43	2.69	1.48E-09	5.50E-08	7.23E-05
S100a9	3	complement(90692632..90695721)	124.23	1.59	3.02	9.50E-13	5.57E-11	4.63E-08
Scamp5	9	complement(57441328..57468024)	3.02	0.59	1.51	0.00357	0.03	1
Sele	1	164048234..164057677	5.92	2.9	7.47	0	0	0
Selk	14	29968308..29975074	60.93	0.75	1.68	3.81E-06	7.65E-05	0.19
Sema3a	5	13125414..13602565	0.19	2.44	5.43	4.77E-15	3.60E-13	2.33E-10
Serpine1	5	complement(137061504..137072268)	254.92	4.04	16.47	0	0	0

Table 1 continued

Sftpa1	14	41131782..41136452	0.65	1.2	2.3	4.21E-05	0.000656	1
Sigirr	7	complement(141091175..141100572)	5.2	-1.64	-3.12	0	0	0
Siglec1	2	complement(131069220..131086765)	1.19	-1	-2	5.47E-05	0.000836	1
Skp2	15	complement(9111985..9155425)	0.23	-0.98	-1.97	0.000192	0.00254	1
Slamf1	1	171767127..171801184	0.13	1.81	3.51	2.48E-05	0.000409	1
Slamf7	1	complement(171632403..171653035)	0.84	0.68	1.61	0.00292	0.03	1
Slamf8	1	complement(172581758..172590568)	2.87	-2.72	-6.59	0	0	0
Slc11a1	1	74375195..74386062	5.43	0.64	1.55	8.21E-05	0.00119	1
Slx4	16	complement(3979105..4003770)	0.58	0.63	1.54	0.00126	0.01	1
Smarca2	19	26605050..26778322	4.73	-1.66	-3.16	0	0	0
Socs1	16	complement(10783808..10785536)	17.42	2.91	7.53	0	0	0
Socs2	10	complement(95385362..95417180)	2.83	1.4	2.64	0.00032	0.000514	1
Socs3	11	complement(117966079..117970047)	58.61	1.46	2.76	1.53E-14	1.10E-12	7.46E-10
Socs5	17	87107679..87137583	1	-1	-2	1.08E-06	2.42E-05	0.05
Socs6	18	complement(88665224..88927481)	3.05	0.97	1.96	8.75E-11	3.88E-09	4.26E-06
Sphk1	11	116530925..116536674	1.07	3.38	10.42	0	0	0
Sppl3	5	115011137..115098790	2.59	0.7	1.63	5.56E-06	0.000108	0.27
Src	2	157418444..157471862	0.63	0.89	1.85	0.000267	0.0034	1
Srebf1	11	complement(60199089..60222581)	10.99	-0.98	-1.98	2.27E-08	6.98E-07	0.00111

Table 1 continued

Stat1	1	52119440..52161865	40.53	-1.68	-3.21	0	0	0
Stat3	11	complement(100885098..100939540)	37.93	1.19	2.28	1.50E-11	7.41E-10	7.33E-07
Stmn1	4	134468320..134473843	0.79	-1.48	-2.79	3.59E-06	7.26E-05	0.18
Tank	2	61578585..61654171	3.99	0.86	1.82	4.37E-08	1.27E-06	0.00213
Tbk1	10	complement(121546455..121586794)	20.5	0.93	1.91	1.22E-09	4.55E-08	5.92E-05
Tet2	3	complement(133463679..133545139)	1.23	1	1.99	3.90E-09	1.35E-07	0.00019
Tgtp1	11	complement(48985327..48994172)	66.48	-2.05	-4.14	2.43E-14	1.71E-12	1.18E-09
Thbs1	2	118111876..118127133	4.81	1.47	2.77	8.22E-05	0.00119	1
Thrb	14	17660960..18038088	2.99	-0.69	-1.61	4.09E-05	0.000639	1
Ticam2	18	complement(46559155..46574533)	0.21	-1.36	-2.57	4.89E-05	0.000753	1
Tifa	3	127789805..127832164	165.14	1.65	3.14	1.90E-11	9.23E-10	9.23E-07
Tlr1	5	complement(64924679..64933563)	2.09	-1.08	-2.11	6.44E-08	1.82E-06	0.00314
Tlr11	14	50357914..50363663	0.07	-2.23	-4.7	0.000651	0.00737	1
Tlr13	X	106143204..106160493	2.26	1	2	5.57E-09	1.88E-07	0.00027
Tlr4	4	66827584..66930284	0.94	-0.7	-1.62	0.00122	0.01	1
Tlr5	1	182954788..182976044	0.32	-1.07	-2.1	0.000695	0.0078	1
Tlr7	X	complement(167304929..167330558)	0.9	0.87	1.82	2.68E-05	0.000439	1
Tlr8	X	complement(167242696..167264329)	0.38	-1.15	-2.22	0.000636	0.00723	1
Tlr9	9	106222598..106226883	0.16	-1.14	-2.2	0.0023	0.02	1
Tmed7	18	complement(46560235..46597535)	20.11	0.67	1.59	0.000114	0.0016	1

Table 1 continued

Tnf	17	complement(35199381..35202007)	5.8	0.68	1.6	0.00575	0.05	1
Tnfaip3	10	complement(19000910..19015657)	44.46	3.34	10.12	0	0	0
Tnfrsf12a	17	complement(23675447..23677449)	32.21	2.41	5.33	0	0	0
Tnfrsf18	4	156026164..156028895	0.74	1.41	2.65	1.68E-06	0.000036	0.08
Tnfrsf9	4	150914562..150946102	1.91	3.9	14.94	0	0	0
Tnfsf11	14	complement(78277445..78308043)	0.04	3.64	12.46	0.004	0.04	1
Tnfsf9	17	57105385..57107757	0.92	3.14	8.84	2.82E-14	1.96E-12	1.37E-09
Tnip1	11	complement(54910785..54962917)	9.14	1.62	3.07	0	0	0
Tnip3	6	65525313..65634040	0.9	-0.69	-1.62	0.00296	0.03	1
Tpst1	5	130073326..130135729	4.53	-0.69	-1.62	4.80E-06	9.44E-05	0.23
Traf1	2	complement(34941750..34961772)	0.45	1.18	2.26	1.33E-05	0.000235	0.65
Traf6	2	101678429..101701669	2.93	0.99	1.98	2.97E-11	1.40E-09	1.45E-06
Trat1	16	complement(48734690..48771956)	5.81	4.83	28.54	0	0	0
Trem1	17	48232768..48246924	1.33	1.55	2.92	2.50E-08	7.63E-07	0.00122
Trib2	12	complement(15791727..15816877)	2.84	2.45	5.48	0	0	0
Trim13	14	61598226..61605946	2.13	1.56	2.94	9.39E-11	4.13E-09	4.57E-06
Trim21	7	complement(102557921..102565486)	4.72	-0.98	-1.97	2.09E-08	6.45E-07	0.00102
Trim45	3	100922202..100936920	0.12	-0.96	-1.95	0.00396	0.04	1
Trim47	11	complement(116105752..116127210)	2.98	0.9	1.87	0.000011	0.000199	0.54

Table 1 continued

Trim6	7	104218793..104235152	0.31	2.47	5.54	5.78E-14	3.89E-12	2.82E-09
Trim62	4	128883580..128911328	0.13	0.89	1.86	0.00543	0.05	1
Trim65	11	complement(116121846..116131128)	0.66	-1.75	-3.37	3.90E-10	1.57E-08	1.9E-05
Trp63	16	25683763..25892102	0.17	4.99	31.85	0	0	0
Trpm2	10	complement(77907722..77970563)	0.53	-1.3	-2.46	2.50E-10	1.03E-08	1.22E-05
Tsc22d3	X	complement(140539528..140600659)	12.64	-1.94	-3.84	0	0	0
Tufm	7	126487361..126490731	19.42	-0.75	-1.68	7.80E-07	0.000018	0.04
Tyk2	9	complement(21104069..21127346)	3.31	-0.88	-1.84	5.30E-08	1.52E-06	0.00258
Uchl1	5	66676091..66687234	0.74	2.07	4.19	4.86E-09	1.66E-07	0.00024
Ulk1	5	complement(110784488..110810097)	3.41	0.63	1.54	0.000283	0.00359	1
Usp2	9	44067021..44095627	1.29	-2.18	-4.54	1.75E-10	7.43E-09	8.53E-06
Vdr	15	complement(97854425..97910630)	0.05	3.18	9.06	3.79E-06	7.62E-05	0.18
Vegfa	17	complement(46016993..46032377)	19.25	0.64	1.56	0.000127	0.00176	1
Vps45	3	complement(95999832..96058466)	1.24	-0.61	-1.52	0.00124	0.01	1
Wdfy1	1	complement(79702262..79776143)	1.59	0.6	1.52	0.00011	0.00155	1
Wdr62	7	complement(30240138..30280419)	0.14	-1.47	-2.77	0.000127	0.00176	1
Wfdc12	2	complement(164189231..164190608)	0.28	2.81	7.01	0.000138	0.0019	1
Wnt9b	11	complement(103727364..103749821)	0.18	-3.75	-13.46	4.66E-12	2.49E-10	2.27E-07

Table 1 continued

Xbp1	11	5520659..5525893	161.77	1.2	2.29	4.20E-11	1.94E-09	2.05E-06
Xrcc6	15	81987835..82040085	2.09	-0.98	-1.97	3.41E-09	1.20E-07	0.00017
Zbtb20	16	42875881..43642602	3.64	-0.76	-1.69	4.43E-05	0.000687	1
Zc3h12a	4	complement(125118423..125127840)	7.8	2.36	5.15	0	0	0
Zfp36	7	complement(28376784..28380253)	10.13	0.6	1.51	0.000415	0.00502	1

Appendix B

Table 2: Key Resources Table

REAGENT or RESOURCE	SOURCE	IDENTIFIER
Antibodies		
Phospho-STAT1 (ser727)	Cell Signaling Technology	Cat# 9177
Phospho-STAT1 (tyr 701)	Cell Signaling Technology	Cat# 9167
STAT1	Cell Signaling Technology	Cat# 14994
IRF1	Cell Signaling Technology	Cat# 8478
β-ACTIN	Cell Signaling Technology	Cat# 4970
BACH1, HRP conjugated	Santa Cruz Biotechnology	sc-271211
HO-1, HRP conjugated	Santa Cruz Biotechnology	sc-390991
α-TUBULIN	Abcam	ab4074
Bacterial Strains		
Klebsiella pneumoniae, serotype 2	American Type Culture Collection	ATCC 43816
K. pneumoniae parent strain (wild type)	Bachman MA et al., 2012	KPPR1; Rifampin derivative of ATCC 43816
entB ybtS K. pneumoniae (mutant strain)	Bachman MA et al., 2012	VK089; KPPR1 *entB ybtS*
Chemicals, Peptides, and Recombinant Proteins		
Hemin from bovine	ThermoFisher Scientific	Cat# H9309
Hemoglobin	This paper	N/A
Protoporphyrin IX cobalt chloride	Sigma-Aldrich	Cat# C1900
Protoporphyrin IX	Sigma-Aldrich	Cat# P8293
Hemopexin, Human Plasma	Athens Research & Technology	Cat# 16-16-080513
Sulforaphane	Cayman Chemical	Cat# 10496
Deferasirox	Cayman Chemical	Cat# 16753
Deferoxamine	Sigma-Aldrich	Cat#D9533
Critical Commercial Assays		
Mouse CCL5/RANTES DuoSet ELISA	R&D Systems	Cat# DY478

Table 2 continued

Mouse CXCL10/IP-10 DuoSet ELISA	R&D Systems	Cat# DY466
Mouse TNFα DuoSet ELISA	R&D Systems	Cat# DY410
Human CXCL10/IP-10 DuoSet ELISA	R&D Systems	Cat# DY266
Human TNFα DuoSet ELISA	R&D Systems	Cat# DY210
Deposited Data		
RNA seq	This paper	GEO #: GSE144902
Experimental Models: Cell Lines		
RAW 264.7	American Type Culture Collection	ATCC TIB-71
Experimental Models: Organisms/Strains		
Mouse: C57BL/6J	The Jackson Laboratory	#000664
Mouse: *Ifnar1*$^{-/-}$	The Jackson Laboratory	#32045
Mouse: *Ifngr1*$^{-/-}$	The Jackson Laboratory	#003288
Mouse: *Tlr4*$^{-/-}$	The Jackson Laboratory	#029015
Mouse: *Stat1*$^{-/+}$	The Jackson Laboratory	#012606
Mouse: *Nrf2*$^{-/-}$	The Jackson Laboratory	#017009
Oligonucleotides		
Complement component *C3*	Applied Biosystems	Mm01232779_m1
Complement factor b *Cfb*	Applied Biosystems	Mm00433909_m1
Heme oxygenase 1 *Hmox1*	Applied Biosystems	Mm00516004_m1
Interferon regulatory factor 1 *Irf1*	Applied Biosystems	Mm01288580_m1
Interferon regulatory factor 1 *Irf3*	Applied Biosystems	Mm00516784_m1
Interferon regulatory factor 1 *Irf8*	Applied Biosystems	Mm00492567_m1
Inducible nitric oxide synthase *Nos2*	Applied Biosystems	Mm00440502_m1
Ferroportin-1 *Slc40a1*	Applied Biosystems	Mm01254822_m1
NF-κB subunit p65 *Rela*	Applied Biosystems	Mm00501346_m1
Suppressor of cytokine signaling 1 *Socs1*	Applied Biosystems	Mm01342740_g1
Suppressor of cytokine signaling 1 *Socs3*	Applied Biosystems	Mm00545913_s1

Table 2 continued

Signal transducer and activator of transcription 1 *Stat1*	Applied Biosystems	Mm01257286_m1
Signal transducer and activator of transcription 1 *Stat3*	Applied Biosystems	Mm01219775_m1
Glyceraldedyde 3-phosphate dehydrogenase *Gapdh*	Applied Biosystems	Mm99999915_g1
18S	Applied Biosystems	Hs99999901_s1
Software and Algorithms		
GraphPad Prism (version 6.07; June 12, 2015)	GraphPad Software Inc.	www.graphpad.com
BaseSpace Correlation Engine	Illumina	www.illumina.com
ImageJ	National Institutes of Health	www.imagej.nih.gov
Other		
Innate immunity database	InnateDB	www.innatedb.com

Bibliography

1. Ganz, T. Macrophages and systemic iron homeostasis. *J Innate Immun* **4,** 446–453 (2012).
2. Higgins, J. M. & Mahadevan, L. Physiological and pathological population dynamics of circulating human red blood cells. *Proc. Natl. Acad. Sci. USA* **107,** 20587–20592 (2010).
3. Muckenthaler, M. U., Rivella, S., Hentze, M. W. & Galy, B. A red carpet for iron metabolism. *Cell* **168,** 344–361 (2017).
4. Bratosin, D. *et al.* Cellular and molecular mechanisms of senescent erythrocyte phagocytosis by macrophages. A review. *Biochimie* **80,** 173–195 (1998).
5. Freikman, I. & Fibach, E. Distribution and shedding of the membrane phosphatidylserine during maturation and aging of erythroid cells. *Biochim. Biophys. Acta* **1808,** 2773–2780 (2011).
6. Beppu, M., Mizukami, A., Nagoya, M. & Kikugawa, K. Binding of anti-band 3 autoantibody to oxidatively damaged erythrocytes. Formation of senescent antigen on erythrocyte surface by an oxidative mechanism. *J. Biol. Chem.* **265,** 3226–3233 (1990).
7. Arese, P., Turrini, F. & Schwarzer, E. Band 3/complement-mediated recognition and removal of normally senescent and pathological human erythrocytes. *Cell Physiol. Biochem.* **16,** 133–146 (2005).
8. Mebius, R. E. & Kraal, G. Structure and function of the spleen. *Nat. Rev. Immunol.* **5,** 606–616 (2005).
9. Kohyama, M. *et al.* Role for Spi-C in the development of red pulp macrophages and splenic iron homeostasis. *Nature* **457,** 318–321 (2009).
10. Nairz, M., Theurl, I., Swirski, F. K. & Weiss, G. "Pumping iron"-how macrophages handle iron at the systemic, microenvironmental, and cellular levels. *Pflugers Arch.* **469,** 397–418 (2017).
11. Harrison, P. M. & Arosio, P. The ferritins: molecular properties, iron storage function and cellular regulation. *Biochim. Biophys. Acta* **1275,** 161–203 (1996).
12. Knutson, M. D., Oukka, M., Koss, L. M., Aydemir, F. & Wessling-Resnick, M. Iron release from macrophages after erythrophagocytosis is up-regulated by ferroportin 1

overexpression and down-regulated by hepcidin. *Proc. Natl. Acad. Sci. USA* **102,** 1324–1328 (2005).

13. Nicolas, G. *et al.* Lack of hepcidin gene expression and severe tissue iron overload in upstream stimulatory factor 2 (USF2) knockout mice. *Proc. Natl. Acad. Sci. USA* **98,** 8780–8785 (2001).
14. Pigeon, C. *et al.* A new mouse liver-specific gene, encoding a protein homologous to human antimicrobial peptide hepcidin, is overexpressed during iron overload. *J. Biol. Chem.* **276,** 7811–7819 (2001).
15. Hurrell, R. & Egli, I. Iron bioavailability and dietary reference values. *Am. J. Clin. Nutr.* **91,** 1461S–1467S (2010).
16. Hod, E. A. *et al.* Transfusion of human volunteers with older, stored red blood cells produces extravascular hemolysis and circulating non-transferrin-bound iron. *Blood* **118,** 6675–6682 (2011).
17. Hentze, M. W., Muckenthaler, M. U., Galy, B. & Camaschella, C. Two to tango: regulation of Mammalian iron metabolism. *Cell* **142,** 24–38 (2010).
18. Prestia, K. *et al.* Transfusion of stored blood impairs host defenses against Gram-negative pathogens in mice. *Transfusion* **54,** 2842–2851 (2014).
19. Theurl, I. *et al.* On-demand erythrocyte disposal and iron recycling requires transient macrophages in the liver. *Nat. Med.* **22,** 945–951 (2016).
20. Gallagher, P. G. Red cell membrane disorders. *Hematology Am Soc Hematol Educ Program* 13–18 (2005). doi:10.1182/asheducation-2005.1.13
21. Piagnerelli, M. *et al.* Alterations of red blood cell shape and sialic acid membrane content in septic patients. *Crit. Care Med.* **31,** 2156–2162 (2003).
22. Baskurt, O. K., Gelmont, D. & Meiselman, H. J. Red blood cell deformability in sepsis. *Am. J. Respir. Crit. Care Med.* **157,** 421–427 (1998).
23. Scott, M. D., Rouyer-Fessard, P., Ba, M. S., Lubin, B. H. & Beuzard, Y. Alpha- and beta-haemoglobin chain induced changes in normal erythrocyte deformability: comparison to beta thalassaemia intermedia and Hb H disease. *Br. J. Haematol.* **80,** 519–526 (1992).
24. Kato, G. J. & Taylor, J. G. Pleiotropic effects of intravascular haemolysis on vascular homeostasis. *Br. J. Haematol.* **148,** 690–701 (2010).
25. Hod, E. A. *et al.* Transfusion of red blood cells after prolonged storage produces harmful

effects that are mediated by iron and inflammation. *Blood* **115,** 4284–4292 (2010).

26. Dixon, S. J. *et al.* Ferroptosis: an iron-dependent form of nonapoptotic cell death. *Cell* **149,** 1060–1072 (2012).
27. Ashurst, J. V. & Dawson, A. in *StatPearls* (StatPearls Publishing, 2020).
28. Swartz, E. & Rohde, P. A. Klebsiella (Friedländer's bacillus) infections in an Army hospital. *Am. J. Clin. Pathol.* **16,** 88–97 (1946).
29. Bellani, G. *et al.* Epidemiology, patterns of care, and mortality for patients with acute respiratory distress syndrome in intensive care units in 50 countries. *JAMA* **315,** 788–800 (2016).
30. Vincent, J.-L. *et al.* International study of the prevalence and outcomes of infection in intensive care units. *JAMA* **302,** 2323–2329 (2009).
31. Martin, R. M. & Bachman, M. A. Colonization, Infection, and the Accessory Genome of Klebsiella pneumoniae. *Front. Cell Infect. Microbiol.* **8,** 4 (2018).
32. Podschun, R. & Ullmann, U. Klebsiella spp. as nosocomial pathogens: epidemiology, taxonomy, typing methods, and pathogenicity factors. *Clin. Microbiol. Rev.* **11,** 589–603 (1998).
33. Carvalhaes, C. G., Cayô, R. & Gales, A. C. Klebsiella pneumoniae carbapenemase-producing Klebsiella pneumoniae in the intensive care unit: a real challenge to physicians, scientific community, and society. *Shock* **39 Suppl 1,** 32–37 (2013).
34. Kollef, K. E. *et al.* Predictors of 30-day mortality and hospital costs in patients with ventilator-associated pneumonia attributed to potentially antibiotic-resistant gram-negative bacteria. *Chest* **134,** 281–287 (2008).
35. Domenico, P., Salo, R. J., Cross, A. S. & Cunha, B. A. Polysaccharide capsule-mediated resistance to opsonophagocytosis in Klebsiella pneumoniae. *Infect. Immun.* **62,** 4495–4499 (1994).
36. Merino, S., Camprubí, S., Albertí, S., Benedí, V. J. & Tomás, J. M. Mechanisms of Klebsiella pneumoniae resistance to complement-mediated killing. *Infect. Immun.* **60,** 2529–2535 (1992).
37. Olonisakin, T. F. *et al.* CD36 Provides Host Protection Against Klebsiella pneumoniae Intrapulmonary Infection by Enhancing Lipopolysaccharide Responsiveness and Macrophage Phagocytosis. *J. Infect. Dis.* **214,** 1865–1875 (2016).

38. Lewis, A. J., Lee, J. S. & Rosengart, M. R. Translational sepsis research: spanning the divide. *Crit. Care Med.* **46,** 1497–1505 (2018).
39. Siu, L. K., Lin, J.-C., Gomez, E., Eng, R. & Chiang, T. Virulence and plasmid transferability of KPC Klebsiella pneumoniae at the Veterans Affairs Healthcare System of New Jersey. *Microb Drug Resist* **18,** 380–384 (2012).
40. Pan, Y.-J. *et al.* Genetic analysis of capsular polysaccharide synthesis gene clusters in 79 capsular types of Klebsiella spp. *Sci. Rep.* **5,** 15573 (2015).
41. Ofek, I. *et al.* Genetic exchange of determinants for capsular polysaccharide biosynthesis between Klebsiella pneumoniae strains expressing serotypes K2 and K21a. *Infect. Immun.* **61,** 4208–4216 (1993).
42. Kabha, K. *et al.* Relationships among capsular structure, phagocytosis, and mouse virulence in Klebsiella pneumoniae. *Infect. Immun.* **63,** 847–852 (1995).
43. Vinogradov, E. *et al.* Structures of lipopolysaccharides from Klebsiella pneumoniae. Eluicidation of the structure of the linkage region between core and polysaccharide O chain and identification of the residues at the non-reducing termini of the O chains. *J. Biol. Chem.* **277,** 25070–25081 (2002).
44. Raetz, C. R. H., Reynolds, C. M., Trent, M. S. & Bishop, R. E. Lipid A modification systems in gram-negative bacteria. *Annu. Rev. Biochem.* **76,** 295–329 (2007).
45. Llobet, E. *et al.* Deciphering tissue-induced Klebsiella pneumoniae lipid A structure. *Proc. Natl. Acad. Sci. USA* **112,** E6369-78 (2015).
46. Rollenske, T. *et al.* Cross-specificity of protective human antibodies against Klebsiella pneumoniae LPS O-antigen. *Nat. Immunol.* **19,** 617–624 (2018).
47. Follador, R. *et al.* The diversity of Klebsiella pneumoniae surface polysaccharides. *Microb. Genom.* **2,** e000073 (2016).
48. Regué, M. *et al.* A second outer-core region in Klebsiella pneumoniae lipopolysaccharide. *J. Bacteriol.* **187,** 4198–4206 (2005).
49. Ganz, T. Iron and infection. *Int J Hematol* **107,** 7–15 (2017).
50. Archibald, F. *Lactobacillus plantarum* , an organism not requiring iron. *FEMS Microbiol. Lett.* **19,** 29–32 (1983).
51. Wooldridge, K. G. & Williams, P. H. Iron uptake mechanisms of pathogenic bacteria. *FEMS Microbiol. Rev.* **12,** 325–348 (1993).

52. Holden, V. I., Breen, P., Houle, S., Dozois, C. M. & Bachman, M. A. Klebsiella pneumoniae Siderophores Induce Inflammation, Bacterial Dissemination, and HIF-1α Stabilization during Pneumonia. *MBio* **7,** (2016).
53. Bachman, M. A. *et al.* Klebsiella pneumoniae yersiniabactin promotes respiratory tract infection through evasion of lipocalin 2. *Infect. Immun.* **79,** 3309–3316 (2011).
54. Bachman, M. A., Miller, V. L. & Weiser, J. N. Mucosal lipocalin 2 has pro-inflammatory and iron-sequestering effects in response to bacterial enterobactin. *PLoS Pathog.* **5,** e1000622 (2009).
55. Bengoechea, J. A. & Sa Pessoa, J. Klebsiella pneumoniae infection biology: living to counteract host defences. *FEMS Microbiol. Rev.* **43,** 123–144 (2019).
56. Takeuchi, O. & Akira, S. Pattern recognition receptors and inflammation. *Cell* **140,** 805–820 (2010).
57. Athamna, A. *et al.* Lectinophagocytosis of encapsulated Klebsiella pneumoniae mediated by surface lectins of guinea pig alveolar macrophages and human monocyte-derived macrophages. *Infect. Immun.* **59,** 1673–1682 (1991).
58. Zanoni, I. *et al.* CD14 controls the LPS-induced endocytosis of Toll-like receptor 4. *Cell* **147,** 868–880 (2011).
59. Lee, J. S. *et al.* TLR-4 pathway mediates the inflammatory response but not bacterial elimination in E. coli pneumonia. *Am. J. Physiol. Lung Cell Mol. Physiol.* **289,** L731-8 (2005).
60. van de Wetering, J. K., van Golde, L. M. G. & Batenburg, J. J. Collectins: players of the innate immune system. *Eur. J. Biochem.* **271,** 1229–1249 (2004).
61. Casals, C., Campanero-Rhodes, M. A., García-Fojeda, B. & Solís, D. The role of collectins and galectins in lung innate immune defense. *Front. Immunol.* **9,** 1998 (2018).
62. Ganz, T. Defensins: antimicrobial peptides of innate immunity. *Nat. Rev. Immunol.* **3,** 710–720 (2003).
63. Zhao, Y. *et al.* Thrombospondin-1 restrains neutrophil granule serine protease function and regulates the innate immune response during Klebsiella pneumoniae infection. *Mucosal Immunol.* **8,** 896–905 (2015).
64. Charles A Janeway, J., Travers, P., Walport, M. & Shlomchik, M. J. The complement system and innate immunity. (2001).

65. Tzouvelekis, L. S. *et al.* KPC-producing, multidrug-resistant Klebsiella pneumoniae sequence type 258 as a typical opportunistic pathogen. *Antimicrob. Agents Chemother.* **57,** 5144–5146 (2013).
66. Sukhbaatar, N. & Weichhart, T. Iron regulation: macrophages in control. *Pharmaceuticals (Basel)* **11,** (2018).
67. Soares, M. P. & Hamza, I. Macrophages and iron metabolism. *Immunity* **44,** 492–504 (2016).
68. Cairo, G., Recalcati, S., Mantovani, A. & Locati, M. Iron trafficking and metabolism in macrophages: contribution to the polarized phenotype. *Trends Immunol.* **32,** 241–247 (2011).
69. Nemeth, E. *et al.* IL-6 mediates hypoferremia of inflammation by inducing the synthesis of the iron regulatory hormone hepcidin. *J. Clin. Invest.* **113,** 1271–1276 (2004).
70. Wrighting, D. M. & Andrews, N. C. Interleukin-6 induces hepcidin expression through STAT3. *Blood* **108,** 3204–3209 (2006).
71. Pietrangelo, A. *et al.* STAT3 is required for IL-6-gp130-dependent activation of hepcidin in vivo. *Gastroenterology* **132,** 294–300 (2007).
72. Nemeth, E. *et al.* Hepcidin regulates cellular iron efflux by binding to ferroportin and inducing its internalization. *Science* **306,** 2090–2093 (2004).
73. Goetz, D. H. *et al.* The neutrophil lipocalin NGAL is a bacteriostatic agent that interferes with siderophore-mediated iron acquisition. *Mol. Cell* **10,** 1033–1043 (2002).
74. Cellier, M. F., Courville, P. & Campion, C. Nramp1 phagocyte intracellular metal withdrawal defense. *Microbes Infect.* **9,** 1662–1670 (2007).
75. Ganz, T. Hepcidin--a peptide hormone at the interface of innate immunity and iron metabolism. *Curr. Top. Microbiol. Immunol.* **306,** 183–198 (2006).
76. Reiter, C. D. *et al.* Cell-free hemoglobin limits nitric oxide bioavailability in sickle-cell disease. *Nat. Med.* **8,** 1383–1389 (2002).
77. Larsen, R. *et al.* A central role for free heme in the pathogenesis of severe sepsis. *Sci. Transl. Med.* **2,** 51ra71 (2010).
78. Schaer, D. J., Buehler, P. W., Alayash, A. I., Belcher, J. D. & Vercellotti, G. M. Hemolysis and free hemoglobin revisited: exploring hemoglobin and hemin scavengers as a novel class of therapeutic proteins. *Blood* **121,** 1276–1284 (2013).

79. Kaca, W., Roth, R. I. & Levin, J. Hemoglobin, a newly recognized lipopolysaccharide (LPS)-binding protein that enhances LPS biological activity. *J. Biol. Chem.* **269,** 25078–25084 (1994).
80. Bodet, C., Chandad, F. & Grenier, D. Hemoglobin and LPS act in synergy to amplify the inflammatory response. *J. Dent. Res.* **86,** 878–882 (2007).
81. Fernandez, P. L. *et al.* Heme amplifies the innate immune response to microbial molecules through spleen tyrosine kinase (Syk)-dependent reactive oxygen species generation. *J. Biol. Chem.* **285,** 32844–32851 (2010).
82. Figueiredo, R. T. *et al.* Characterization of heme as activator of Toll-like receptor 4. *J. Biol. Chem.* **282,** 20221–20229 (2007).
83. Martins, R. & Knapp, S. Heme and hemolysis in innate immunity: adding insult to injury. *Curr. Opin. Immunol.* **50,** 14–20 (2018).
84. Vallelian, F. *et al.* Revisiting the putative role of heme as a trigger of inflammation. *Pharmacol. Res. Perspect.* **6,** e00392 (2018).
85. Cortés, G. *et al.* Molecular analysis of the contribution of the capsular polysaccharide and the lipopolysaccharide O side chain to the virulence of Klebsiella pneumoniae in a murine model of pneumonia. *Infect. Immun.* **70,** 2583–2590 (2002).
86. March, C. *et al.* Role of bacterial surface structures on the interaction of Klebsiella pneumoniae with phagocytes. *PLoS One* **8,** e56847 (2013).
87. Smith, M. R. & Wood, W. B. Studies on the mechanism of recovery in pneumonia due to friedlader's bacillus : iii. the role of "surface phagocytosis" in the destruction of the microorganisms in the lung. *J. Exp. Med.* **86,** 257–266 (1947).
88. Areschoug, T. & Gordon, S. Scavenger receptors: role in innate immunity and microbial pathogenesis. *Cell Microbiol.* **11,** 1160–1169 (2009).
89. Suzuki, H. *et al.* A role for macrophage scavenger receptors in atherosclerosis and susceptibility to infection. *Nature* **386,** 292–296 (1997).
90. Peiser, L. *et al.* The class A macrophage scavenger receptor is a major pattern recognition receptor for Neisseria meningitidis which is independent of lipopolysaccharide and not required for secretory responses. *Infect. Immun.* **70,** 5346–5354 (2002).
91. Peiser, L., Gough, P. J., Kodama, T. & Gordon, S. Macrophage class A scavenger receptor-mediated phagocytosis of Escherichia coli: role of cell heterogeneity, microbial strain, and

culture conditions in vitro. *Infect. Immun.* **68,** 1953–1963 (2000).

92. Arredouani, M. S. *et al.* The macrophage scavenger receptor SR-AI/II and lung defense against pneumococci and particles. *Am. J. Respir. Cell Mol. Biol.* **35,** 474–478 (2006).
93. Van Berkel, T. J., Van Velzen, A., Kruijt, J. K., Suzuki, H. & Kodama, T. Uptake and catabolism of modified LDL in scavenger-receptor class A type I/II knock-out mice. *Biochem. J.* **331 (Pt 1),** 29–35 (1998).
94. Thelen, T. *et al.* The class A scavenger receptor, macrophage receptor with collagenous structure, is the major phagocytic receptor for Clostridium sordellii expressed by human decidual macrophages. *J. Immunol.* **185,** 4328–4335 (2010).
95. Rapido, F. *et al.* Prolonged red cell storage before transfusion increases extravascular hemolysis. *J. Clin. Invest.* **127,** 375–382 (2017).
96. Ward, C. G., Hammond, J. S. & Bullen, J. J. Effect of iron compounds on antibacterial function of human polymorphs and plasma. *Infect. Immun.* **51,** 723–730 (1986).
97. Martins, R. *et al.* Heme drives hemolysis-induced susceptibility to infection via disruption of phagocyte functions. *Nat. Immunol.* **17,** 1361–1372 (2016).
98. Shankar-Sinha, S. *et al.* The Klebsiella pneumoniae O antigen contributes to bacteremia and lethality during murine pneumonia. *Infect. Immun.* **72,** 1423–1430 (2004).
99. Thomas, C. A. *et al.* Protection from lethal gram-positive infection by macrophage scavenger receptor-dependent phagocytosis. *J. Exp. Med.* **191,** 147–156 (2000).
100. Canton, J., Neculai, D. & Grinstein, S. Scavenger receptors in homeostasis and immunity. *Nat. Rev. Immunol.* **13,** 621–634 (2013).
101. Baranova, I. N. *et al.* Role of human CD36 in bacterial recognition, phagocytosis, and pathogen-induced JNK-mediated signaling. *J. Immunol.* **181,** 7147–7156 (2008).
102. Osei-Hwedieh, D. O. *et al.* Sickle Cell Trait Increases Red Blood Cell Storage Hemolysis and Post-Transfusion Clearance in Mice. *EBioMedicine* **11,** 239–248 (2016).
103. Quinton, L. J. *et al.* Hepatocyte-specific mutation of both NF-κB RelA and STAT3 abrogates the acute phase response in mice. *J. Clin. Invest.* **122,** 1758–1763 (2012).
104. Meraz, M. A. *et al.* Targeted disruption of the Stat1 gene in mice reveals unexpected physiologic specificity in the JAK-STAT signaling pathway. *Cell* **84,** 431–442 (1996).
105. Poe, S. L. *et al.* STAT1-regulated lung MDSC-like cells produce IL-10 and efferocytose apoptotic neutrophils with relevance in resolution of bacterial pneumonia. *Mucosal*

Immunol. **6,** 189–199 (2013).

106. Youssef, L. A. *et al.* Increased erythrophagocytosis induces ferroptosis in red pulp macrophages in a mouse model of transfusion. *Blood* **131,** 2581–2593 (2018).
107. Kagan, V. E. *et al.* Oxidized arachidonic and adrenic PEs navigate cells to ferroptosis. *Nat. Chem. Biol.* **13,** 81–90 (2017).
108. Akilesh, H. M. *et al.* Chronic TLR7 and TLR9 signaling drives anemia via differentiation of specialized hemophagocytes. *Science* **363,** (2019).
109. Alam, J., Shibahara, S. & Smith, A. Transcriptional activation of the heme oxygenase gene by heme and cadmium in mouse hepatoma cells. *J. Biol. Chem.* **264,** 6371–6375 (1989).
110. Marro, S. *et al.* Heme controls ferroportin1 (FPN1) transcription involving Bach1, Nrf2 and a MARE/ARE sequence motif at position -7007 of the FPN1 promoter. *Haematologica* **95,** 1261–1268 (2010).
111. Vodovotz, Y. *et al.* The hepatocyte as a microbial product-responsive cell. *J Endotoxin Res* **7,** 365–373 (2001).
112. Zhou, Z., Xu, M.-J. & Gao, B. Hepatocytes: a key cell type for innate immunity. *Cell Mol Immunol* **13,** 301–315 (2016).
113. Crispe, I. N. Hepatocytes as immunological agents. *J. Immunol.* **196,** 17–21 (2016).
114. Dupuis, S. *et al.* Impaired response to interferon-alpha/beta and lethal viral disease in human STAT1 deficiency. *Nat. Genet.* **33,** 388–391 (2003).
115. Stockwell, B. R. *et al.* Ferroptosis: A regulated cell death nexus linking metabolism, redox biology, and disease. *Cell* **171,** 273–285 (2017).
116. Sano, H. *et al.* Critical role of galectin-3 in phagocytosis by macrophages. *J. Clin. Invest.* **112,** 389–397 (2003).
117. Schneider, W. M., Chevillotte, M. D. & Rice, C. M. Interferon-stimulated genes: a complex web of host defenses. *Annu. Rev. Immunol.* **32,** 513–545 (2014).
118. Moore, T. A., Perry, M. L., Getsoian, A. G., Newstead, M. W. & Standiford, T. J. Divergent role of gamma interferon in a murine model of pulmonary versus systemic Klebsiella pneumoniae infection. *Infect. Immun.* **70,** 6310–6318 (2002).
119. Ivin, M. *et al.* Natural killer cell-intrinsic type I IFN signaling controls Klebsiella pneumoniae growth during lung infection. *PLoS Pathog.* **13,** e1006696 (2017).
120. Lin, Y.-C. *et al.* Activation of IFN-γ/STAT/IRF-1 in hepatic responses to Klebsiella

pneumoniae infection. *PLoS One* **8,** e79961 (2013).

121. Barrat, F. J., Crow, M. K. & Ivashkiv, L. B. Interferon target-gene expression and epigenomic signatures in health and disease. *Nat. Immunol.* **20,** 1574–1583 (2019).
122. Ohmori, Y. & Hamilton, T. A. Requirement for STAT1 in LPS-induced gene expression in macrophages. *J. Leukoc. Biol.* **69,** 598–604 (2001).
123. Toshchakov, V. *et al.* TLR4, but not TLR2, mediates IFN-beta-induced STAT1alpha/beta-dependent gene expression in macrophages. *Nat. Immunol.* **3,** 392–398 (2002).
124. Jacobs, A. T. & Ignarro, L. J. Lipopolysaccharide-induced expression of interferon-beta mediates the timing of inducible nitric-oxide synthase induction in RAW 264.7 macrophages. *J. Biol. Chem.* **276,** 47950–47957 (2001).
125. Rhee, S. H., Jones, B. W., Toshchakov, V., Vogel, S. N. & Fenton, M. J. Toll-like receptors 2 and 4 activate STAT1 serine phosphorylation by distinct mechanisms in macrophages. *J. Biol. Chem.* **278,** 22506–22512 (2003).
126. Tenoever, B. R. *et al.* Multiple functions of the IKK-related kinase IKKepsilon in interferon-mediated antiviral immunity. *Science* **315,** 1274–1278 (2007).
127. Kawai, T. & Akira, S. Signaling to NF-kappaB by Toll-like receptors. *Trends Mol. Med.* **13,** 460–469 (2007).
128. De Domenico, I. *et al.* Hepcidin mediates transcriptional changes that modulate acute cytokine-induced inflammatory responses in mice. *J. Clin. Invest.* **120,** 2395–2405 (2010).
129. Zenke-Kawasaki, Y. *et al.* Heme induces ubiquitination and degradation of the transcription factor Bach1. *Mol. Cell. Biol.* **27,** 6962–6971 (2007).
130. Sun, J. *et al.* Hemoprotein Bach1 regulates enhancer availability of heme oxygenase-1 gene. *EMBO J.* **21,** 5216–5224 (2002).
131. Alcaraz, M. J., Fernández, P. & Guillén, M. I. Anti-inflammatory actions of the heme oxygenase-1 pathway. *Curr. Pharm. Des.* **9,** 2541–2551 (2003).
132. Otterbein, L. E. *et al.* Carbon monoxide has anti-inflammatory effects involving the mitogen-activated protein kinase pathway. *Nat. Med.* **6,** 422–428 (2000).
133. Paine, A., Eiz-Vesper, B., Blasczyk, R. & Immenschuh, S. Signaling to heme oxygenase-1 and its anti-inflammatory therapeutic potential. *Biochem. Pharmacol.* **80,** 1895–1903 (2010).
134. Boyle, J. J. *et al.* Heme induces heme oxygenase 1 via Nrf2: role in the homeostatic

macrophage response to intraplaque hemorrhage. *Arterioscler. Thromb. Vasc. Biol.* **31,** 2685–2691 (2011).

135. Thimmulappa, R. K. *et al.* Nrf2 is a critical regulator of the innate immune response and survival during experimental sepsis. *J. Clin. Invest.* **116,** 984–995 (2006).
136. Kobayashi, E. H. *et al.* Nrf2 suppresses macrophage inflammatory response by blocking proinflammatory cytokine transcription. *Nat. Commun.* **7,** 11624 (2016).
137. Olagnier, D. *et al.* Nrf2 negatively regulates STING indicating a link between antiviral sensing and metabolic reprogramming. *Nat. Commun.* **9,** 3506 (2018).
138. Venugopal, R. & Jaiswal, A. K. Nrf1 and Nrf2 positively and c-Fos and Fra1 negatively regulate the human antioxidant response element-mediated expression of NAD(P)H:quinone oxidoreductase1 gene. *Proc. Natl. Acad. Sci. USA* **93,** 14960–14965 (1996).
139. Chorley, B. N. *et al.* Identification of novel NRF2-regulated genes by ChIP-Seq: influence on retinoid X receptor alpha. *Nucleic Acids Res.* **40,** 7416–7429 (2012).
140. Yang, K., Huang, R., Fujihira, H., Suzuki, T. & Yan, N. N-glycanase NGLY1 regulates mitochondrial homeostasis and inflammation through NRF1. *J. Exp. Med.* **215,** 2600–2616 (2018).
141. Ohtsuji, M. *et al.* Nrf1 and Nrf2 play distinct roles in activation of antioxidant response element-dependent genes. *J. Biol. Chem.* **283,** 33554–33562 (2008).
142. Hayes, J. D. & Dinkova-Kostova, A. T. The Nrf2 regulatory network provides an interface between redox and intermediary metabolism. *Trends Biochem. Sci.* **39,** 199–218 (2014).
143. Vallelian, F. *et al.* Proteasome inhibition and oxidative reactions disrupt cellular homeostasis during heme stress. *Cell Death Differ.* **22,** 597–611 (2015).
144. Chan, J. Y. *et al.* Targeted disruption of the ubiquitous CNC-bZIP transcription factor, Nrf-1, results in anemia and embryonic lethality in mice. *EMBO J.* **17,** 1779–1787 (1998).
145. Biswas, M. & Chan, J. Y. Role of Nrf1 in antioxidant response element-mediated gene expression and beyond. *Toxicol. Appl. Pharmacol.* **244,** 16–20 (2010).
146. Leung, L., Kwong, M., Hou, S., Lee, C. & Chan, J. Y. Deficiency of the Nrf1 and Nrf2 transcription factors results in early embryonic lethality and severe oxidative stress. *J. Biol. Chem.* **278,** 48021–48029 (2003).
147. Harusato, A. *et al.* BTB and CNC homolog 1 (Bach1) deficiency ameliorates TNBS colitis

in mice: role of M2 macrophages and heme oxygenase-1. *Inflamm. Bowel Dis.* **19,** 740–753 (2013).

148. Yachie, A. *et al.* Oxidative stress causes enhanced endothelial cell injury in human heme oxygenase-1 deficiency. *J. Clin. Invest.* **103,** 129–135 (1999).
149. Otterbein, L. E. *et al.* Exogenous administration of heme oxygenase-1 by gene transfer provides protection against hyperoxia-induced lung injury. *J. Clin. Invest.* **103,** 1047–1054 (1999).
150. Vijayan, V., Wagener, F. A. D. T. G. & Immenschuh, S. The macrophage heme-heme oxygenase-1 system and its role in inflammation. *Biochem. Pharmacol.* **153,** 159–167 (2018).
151. Kapturczak, M. H. *et al.* Heme oxygenase-1 modulates early inflammatory responses: evidence from the heme oxygenase-1-deficient mouse. *Am. J. Pathol.* **165,** 1045–1053 (2004).
152. Croker, B. A. *et al.* SOCS3 negatively regulates IL-6 signaling in vivo. *Nat. Immunol.* **4,** 540–545 (2003).
153. Ho, H. H. & Ivashkiv, L. B. Role of STAT3 in type I interferon responses. Negative regulation of STAT1-dependent inflammatory gene activation. *J. Biol. Chem.* **281,** 14111–14118 (2006).
154. Pineda-Torra, I., Gage, M., de Juan, A. & Pello, O. M. Isolation, Culture, and Polarization of Murine Bone Marrow-Derived and Peritoneal Macrophages. *Methods Mol. Biol.* **1339,** 101–109 (2015).
155. Anderson, H. L., Brodsky, I. E. & Mangalmurti, N. S. The evolving erythrocyte: red blood cells as modulators of innate immunity. *J. Immunol.* **201,** 1343–1351 (2018).
156. Smith, J. E. Erythrocyte membrane: structure, function, and pathophysiology. *Vet. Pathol.* **24,** 471–476 (1987).
157. Hereditary Spherocytosis and Hereditary Elliptocytosis | The Online Metabolic and Molecular Bases of Inherited Disease | OMMBID | McGraw-Hill Medical. at <https://ommbid.mhmedical.com/content.aspx?bookId=2709&sectionId=225553991>
158. Boas, F. E., Forman, L. & Beutler, E. Phosphatidylserine exposure and red cell viability in red cell aging and in hemolytic anemia. *Proc. Natl. Acad. Sci. USA* **95,** 3077–3081 (1998).
159. A-Gonzalez, N. *et al.* Apoptotic cells promote their own clearance and immune tolerance

through activation of the nuclear receptor LXR. *Immunity* **31,** 245–258 (2009).

160. Gautier, E.-F. *et al.* Absolute proteome quantification of highly purified populations of circulating reticulocytes and mature erythrocytes. *Blood Adv.* **2,** 2646–2657 (2018).
161. Beutler, E. in *Williams Hematology* (McGraw-Hill, 2010).
162. Fortes, G. B. *et al.* Heme induces programmed necrosis on macrophages through autocrine TNF and ROS production. *Blood* **119,** 2368–2375 (2012).
163. Finn, A. V. *et al.* Hemoglobin directs macrophage differentiation and prevents foam cell formation in human atherosclerotic plaques. *J. Am. Coll. Cardiol.* **59,** 166–177 (2012).
164. Graça-Souza, A. V., Arruda, M. A. B., de Freitas, M. S., Barja-Fidalgo, C. & Oliveira, P. L. Neutrophil activation by heme: implications for inflammatory processes. *Blood* **99,** 4160–4165 (2002).
165. Cunnington, A. J., de Souza, J. B., Walther, M. & Riley, E. M. Malaria impairs resistance to Salmonella through heme- and heme oxygenase-dependent dysfunctional granulocyte mobilization. *Nat. Med.* **18,** 120–127 (2011).
166. Lin, S. *et al.* Heme activates TLR4-mediated inflammatory injury via MyD88/TRIF signaling pathway in intracerebral hemorrhage. *J. Neuroinflammation* **9,** 46 (2012).
167. National Center for Biotechnology Information, P. D. Deferasirox, CID = 214348. https://pubchem.ncbi.nlm.nih.gov/compound/Deferasirox. Accessed November 15, 2019. *PubChem Database* at <https://pubchem.ncbi.nlm.nih.gov/compound/Deferasirox>
168. Glickstein, H. *et al.* Action of chelators in iron-loaded cardiac cells: Accessibility to intracellular labile iron and functional consequences. *Blood* **108,** 3195–3203 (2006).
169. Liddell, J. R. *et al.* Lipophilic adamantyl- or deferasirox-based conjugates of desferrioxamine B have enhanced neuroprotective capacity: implications for Parkinson disease. *Free Radic. Biol. Med.* **60,** 147–156 (2013).
170. Williamson, D. The unstable haemoglobins. *Blood Rev* **7,** 146–163 (1993).
171. Ware, R. E., de Montalembert, M., Tshilolo, L. & Abboud, M. R. Sickle cell disease. *Lancet* **390,** 311–323 (2017).
172. Oexle, H. *et al.* Pathways for the regulation of interferon-gamma-inducible genes by iron in human monocytic cells. *J. Leukoc. Biol.* **74,** 287–294 (2003).
173. Dlaska, M. & Weiss, G. Central role of transcription factor NF-IL6 for cytokine and iron-mediated regulation of murine inducible nitric oxide synthase expression. *J. Immunol.* **162,**

6171–6177 (1999).

174. Ponka, P. Cell biology of heme. *Am. J. Med. Sci.* **318,** 241–256 (1999).
175. Soares, M. P. & Bozza, M. T. Red alert: labile heme is an alarmin. *Curr. Opin. Immunol.* **38,** 94–100 (2016).
176. Pinilla-Vera, M. *et al.* Full spectrum of LPS activation in alveolar macrophages of healthy volunteers by whole transcriptomic profiling. *PLoS One* **11,** e0159329 (2016).
177. Elmer, J., Harris, D. & Palmer, A. F. Purification of hemoglobin from red blood cells using tangential flow filtration and immobilized metal ion affinity chromatography. *J. Chromatogr. B, Analyt. Technol. Biomed. Life Sci.* **879,** 131–138 (2011).
178. Dodge, J. T., Mitchell, C. & Hanahan, D. J. The preparation and chemical characteristics of hemoglobin-free ghosts of human erythrocytes. *Arch. Biochem. Biophys.* **100,** 119–130 (1963).
179. Raghuram, S. *et al.* Identification of heme as the ligand for the orphan nuclear receptors REV-ERBalpha and REV-ERBbeta. *Nat. Struct. Mol. Biol.* **14,** 1207–1213 (2007).
180. Lam, M. T. Y. *et al.* Rev-Erbs repress macrophage gene expression by inhibiting enhancer-directed transcription. *Nature* **498,** 511–515 (2013).
181. Gibbs, J. E. *et al.* The nuclear receptor REV-ERBα mediates circadian regulation of innate immunity through selective regulation of inflammatory cytokines. *Proc. Natl. Acad. Sci. USA* **109,** 582–587 (2012).
182. Eichenfield, D. Z. *et al.* Tissue damage drives co-localization of NF-κB, Smad3, and Nrf2 to direct Rev-erb sensitive wound repair in mouse macrophages. *Elife* **5,** (2016).
183. Faller, M., Matsunaga, M., Yin, S., Loo, J. A. & Guo, F. Heme is involved in microRNA processing. *Nat. Struct. Mol. Biol.* **14,** 23–29 (2007).
184. Partin, A. C. *et al.* Heme enables proper positioning of Drosha and DGCR8 on primary microRNAs. *Nat. Commun.* **8,** 1737 (2017).
185. Steiner, D. F. *et al.* MicroRNA-29 regulates T-box transcription factors and interferon-γ production in helper T cells. *Immunity* **35,** 169–181 (2011).
186. Choby, J. E. & Skaar, E. P. Heme synthesis and acquisition in bacterial pathogens. *J. Mol. Biol.* **428,** 3408–3428 (2016).
187. Hammer, N. D. *et al.* Two heme-dependent terminal oxidases power Staphylococcus aureus organ-specific colonization of the vertebrate host. *MBio* **4,** (2013).

188. Lee, J. C. *et al.* Klebsiella pneumoniae secretes outer membrane vesicles that induce the innate immune response. *FEMS Microbiol. Lett.* **331,** 17–24 (2012).
189. Cahill, B. K., Seeley, K. W., Gutel, D. & Ellis, T. N. Klebsiella pneumoniae O antigen loss alters the outer membrane protein composition and the selective packaging of proteins into secreted outer membrane vesicles. *Microbiol Res* **180,** 1–10 (2015).
190. Liu, L. *et al.* Identification and Characterization of an Antibacterial Type VI Secretion System in the Carbapenem-Resistant Strain Klebsiella pneumoniae HS11286. *Front. Cell Infect. Microbiol.* **7,** 442 (2017).
191. Brunet, Y. R., Bernard, C. S., Gavioli, M., Lloubès, R. & Cascales, E. An epigenetic switch involving overlapping fur and DNA methylation optimizes expression of a type VI secretion gene cluster. *PLoS Genet.* **7,** e1002205 (2011).
192. Venet, F. & Monneret, G. Advances in the understanding and treatment of sepsis-induced immunosuppression. *Nat. Rev. Nephrol.* **14,** 121–137 (2018).
193. Reinhart, K. *et al.* Recognizing Sepsis as a Global Health Priority - A WHO Resolution. *N. Engl. J. Med.* **377,** 414–417 (2017).
194. Rubio, I. *et al.* Current gaps in sepsis immunology: new opportunities for translational research. *Lancet Infect. Dis.* **19,** e422–e436 (2019).
195. Hotchkiss, R. S., Monneret, G. & Payen, D. Sepsis-induced immunosuppression: from cellular dysfunctions to immunotherapy. *Nat. Rev. Immunol.* **13,** 862–874 (2013).